This is to certify that the
dissertation entitled

Thermodynamic and Kinetic Characterization of Solute Transfer in Reversed-Phase Liquid Chromatography

presented by

Samuel Barnett Howerton

has been accepted towards fulfillment
of the requirements for the

Ph.D. degree in Chemistry – Environmental Toxicology

Victoria McGuffin
Major Professor's Signature

11/19/2003
Date

DATE DUE	DATE DUE	DATE DUE

THERMODYNAMIC AND KINETIC CHARACTERIZATION OF SOLUTE TRANSFER IN REVERSED-PHASE LIQUID CHROMATOGRAPHY

By

Samuel Barnett Howerton

A Dissertation

Submitted to
Michigan State University
in partial fulfillment of the requirements
for the degree of

DOCTOR OF PHILOSOPHY

Department of Chemistry

2003

ABSTRACT

THERMODYNAMIC AND KINETIC CHARACTERIZATION OF SOLUTE TRANSFER IN REVERSED-PHASE LIQUID CHROMATOGRAPHY

By

Samuel Barnett Howerton

Reversed-phase liquid chromatography is a technique by which complex mixtures of solutes are separated from one another based upon their affinities for a polar mobile phase and a nonpolar stationary phase. This thesis discusses the use of functions derived from the theoretical description of retention developed by Giddings, as well as instrumentation, the thermodynamics and kinetics of retention are measured and quantitated in tandem.

In order to validate the data treatment procedure, a series of simulations was carried out to study the effect of the integration limit, the number of points across the profile, and noise. Statistical moment analysis and the exponential modified Gaussian model (EMG) were compared, and the data indicated that the EMG model was more robust and resulted in smaller errors for simulated and experimental data.

Using the conclusions drawn from the simulation studies, the thermodynamics and kinetics of solute transfer for a series of polycyclic aromatic hydrocarbons (PAHs) were studied as a function of ring number, annelation (i.e., degree of ring fusion), planarity, temperature, pressure and bonding phase density using octadecylsilica (ODS). The data from this study indicated that an increase in ring number results in more negative changes in molar enthalpy

(ΔH_{sm}) and molar volume (ΔV_{sm}). For a series of isomers, highly annelated solutes exhibited less negative changes in molar enthalpy and molar volume than the more linear solutes. Nonplanar solutes demonstrated changes in molar enthalpy and molar volume that are less negative than would be expected based upon ring number alone. These data indicated that the condensed PAHs, as well as the nonplanar PAHs, interacted with the first few carbons near the distal terminus, and that the more linear solutes, as well as the solutes with more rings, interacted with the more ordered regions of the ODS closer to the proximal terminus. In addition, the rate constants demonstrated that the rates of transfer decreased with increasing ring number and decreasing annelation. The enthalpic and volume barriers were found to be very large. These barriers increased as a function of ring number, but decreased with increasing annelation.

In addition to the parent PAHs, a series of nitrogen containing polycyclic aromatic hydrocarbons (NPAHs) were studied as a function of temperature, pressure and mobile phase (i.e. protic or aprotic). The thermodynamics for the NPAHs were similar to the PAHs. However, the rate constants varied dramatically as a function of mobile phase. Comparisons between methanol and acetonitrile demonstrated changes in the rate constants ranging from two to four orders of magnitude. These differences are attributed to the interaction between the nitrogen and the silica support.

In addition to the studies using octadecylsilica, the retention mechanism of soil was also explored. Furthermore, the qualitative analysis of PAH contaminated samples was studied using selective fluorescence quenching.

To all those who believed in me, even when I did not;

especially my mother and father.

ACKNOWLEDGEMENTS

And now my charms are all o'erthrown
And what strength I have's mine own
Which is most faint; now t'is true
I must here be released by you

But release me from my bands
With the help of your good hands
Gentle breath of yours my sails
Must fill, or else my project fails,
Which was to please. Now I want
Spirits to enforce, art to enchant
And my ending is despair,
Unless I be relieved by prayer

Which pierces so that it assaults
Mercy itself and frees all faults
As you from your crimes would pardon'd be
Let your indulgence set me free.

-William Shakespeare, "The Tempest"

It seems fitting that the last words I pen for this dissertation are for those people who have made my work possible. As I sit here, contemplating where I have been, and where I am going, I think back to the old adage that no man is an island. I certainly am not, and the people listed below have helped me in ways that mere words can never convey.

I extend my profound thanks to my advisor Professor Victoria McGuffin for molding me into a better scientist and thinker. Her desire to explore the fundamental nature of the universe will stay with me forever, driving me to always wonder why the world is the way that it is. I would also like to thank to my committee members Drs. Boyd, Voice, Jackson, Garrett, and Bruening. With their help and viewpoints, I was able to see beyond the traditional boundaries of analytical science.

Then there are my friends...those individuals, who against better judgment actively engaged the world of Sam. First and foremost there are my peers. Dr. Thomas Cullen, a steadfast friend who, through humor, reminds me that while chemistry is important, it is not the only thing to live for. He is a paragon not only of virtue, but also of dedication to excellence. Dr. John Goodpaster, who despite my constant abuse and pestering, demonstrated the greatest work ethic I have ever seen in a human being. He taught me not only how to be productive in a sleep deprived state, but how to ask for help when I needed it most. Dr. Peter Krouskop, for reminding me on a daily basis what it is that I am fighting for and the type of man I am striving to become. Without a doubt, he is one of the most moral men I have met, and the world would be better served if more were like

him. And

grown pa

distancy a

would ha

An

express

provided

ultimately

been by

not doub

To

be found

course is

boldness

desperat

To

your love

finately

sent to yo

Fi

Though

Though it

have learn

him. And finally Carl Newman...who is, by definition, indefinable to me. He has shown patience and understanding where few others would, tolerating my flights of fancy and my overwhelming bouts of cynicism. Without his humor this process would have been worse.

And to my soul mates, Charlotte and Raven. There are no words that can express my love for each of you. Your support over the years has always provided a beacon for me, reminding me of who I was, where I came from, and ultimately where I want to go. Through the good and the bad, you have always been by my side, looking out for me when no one else would, or could. I have not doubt that I am better man for having you as my friends.

To Tiffany, my time with you has taught me many lessons that will never be found in books; the greatest among these to have no regrets. And though my course is different from yours, I will always remember our times together with fondness. You have reminded me what it is to be human, though I try so desperately not to be.

To my family, those who have shaped me into the man that I am. Without your love and words of comfort my time in graduate school would have been infinitely worse. All that I am, all that this document represents, is due in no small part to your guidance throughout my life.

Finally to all the others whose names are obscured in my memory. Though unnamed, your aid is not unnoticed. To each of you I say thank you. Though it is hard to imagine, my world has been impacted by each of you and I have learned and adapted from your lessons.

TABLE OF CONTENTS

LIST OF TABLES

Table 8.4: Co
for
de
dis

LIST OF FIGURES

Figure 8.3

Figure 8.4

Figure 8.5

Figure 8.

Figure 8.

Chapter 1: Introduction and Background

Over the past fifty years, analytical science has undergone dramatic changes as new techniques and new instrumentation have been developed. While many of these advances have become commonplace in both industrial and academic laboratories, fundamental studies of these systems have often lagged behind the applications themselves. One technique that has been widely used, but inadequately described, is liquid chromatography.

In this dissertation, the fundamental molecular processes that govern solute retention in synthetic and natural materials are studied. These processes are quantitated using thermodynamic and kinetic theories that describe the entire retention event.

This chapter presents a description of the solutes that were used throughout the studies, thermodynamic and kinetic theory, as well as a review of previous investigations of reversed-phase liquid chromatography.

1.1 Polycyclic Aromatic Hydrocarbons (PAHs)

1.1.1 Classification and Structure

Polycyclic aromatic hydrocarbons are a class of solutes that belong to the larger family of chemicals known as hydrophobic organic compounds. PAHs are comprised of two, or more, aromatic rings and are differentiated as a function of ring number, annelation, and planarity. The ring number describes the number of fused rings that comprise the PAH. Alternant/nonalternant character describes

the two subclasses of PAHs. A traditional way to differentiate the alternant PAHs from the nonalternant is by using a labeling scheme. In this scheme, a single carbon is chosen as the starting point and labeled. The remaining exterior carbons are alternatively labeled, skipping an atom between the labels (Figure 1.1). Alternant PAHs possess a structure in which no two adjacent carbons are labeled or unlabeled. By contrast, nonalternant PAHs contain two adjacently labeled or unlabeled carbons. Examples of alternant PAHs are anthracene and pyrene. Examples of nonalternant PAHs are acenaphthylene and fluoranthene. The structures of these PAHs can be found in Figure 1.2.

One consequence of alternant/nonalternant character is the difference in the spectral responses of individual PAHs. All PAHs have high-energy π-bonding orbitals and low energy π^*-antibonding orbitals that allow for the absorption of visible or ultraviolet light [1]. However, the fluorescence emission of alternant PAHs is characterized by vibrational fine structure. By contrast, nonalternant PAHs have very broad spectral features in their fluorescence emission (Figure 1.3) [1,2]. The presence or lack of fine structure is determined by the redistribution of the electrons when the PAHs are excited. As demonstrated by Goodpaster et al., the excited states of alternant PAHs have a high degree of symmetry relative to the ground state, wherein the excitation relocates electrons within the π system [3]. By contrast, the excitation of nonalternant PAHs results in a redistribution of the electrons between π and σ bonds within the molecule when it is excited. These spectral responses are important for the qualitative

A

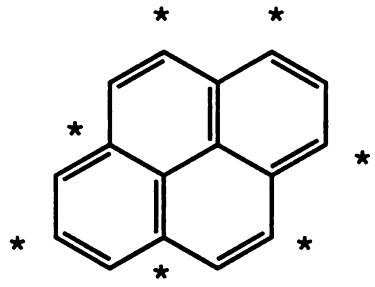

B

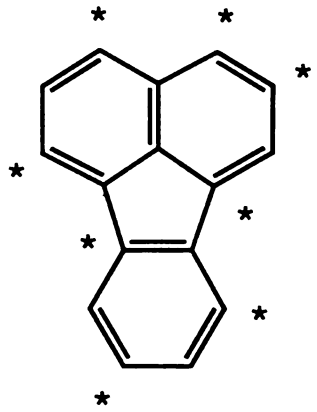

Figure 1.1: Examples of A) alternant and B) nonalternant PAH structures with labeled atoms

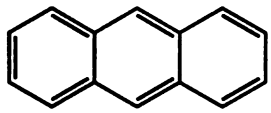

Anthracene

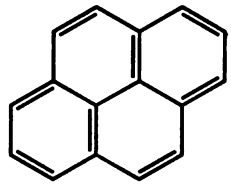

Pyrene

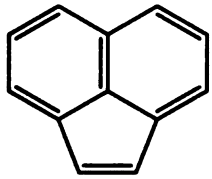

Acenaphthylene

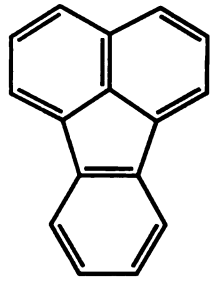

Fluoranthene

Figure 1.2: Structures of alternant and nonalternant PAHs

Figure 1.3: Fluorescence (emission) spectra of alternant and nonalternant PAHs

Figure 1.3

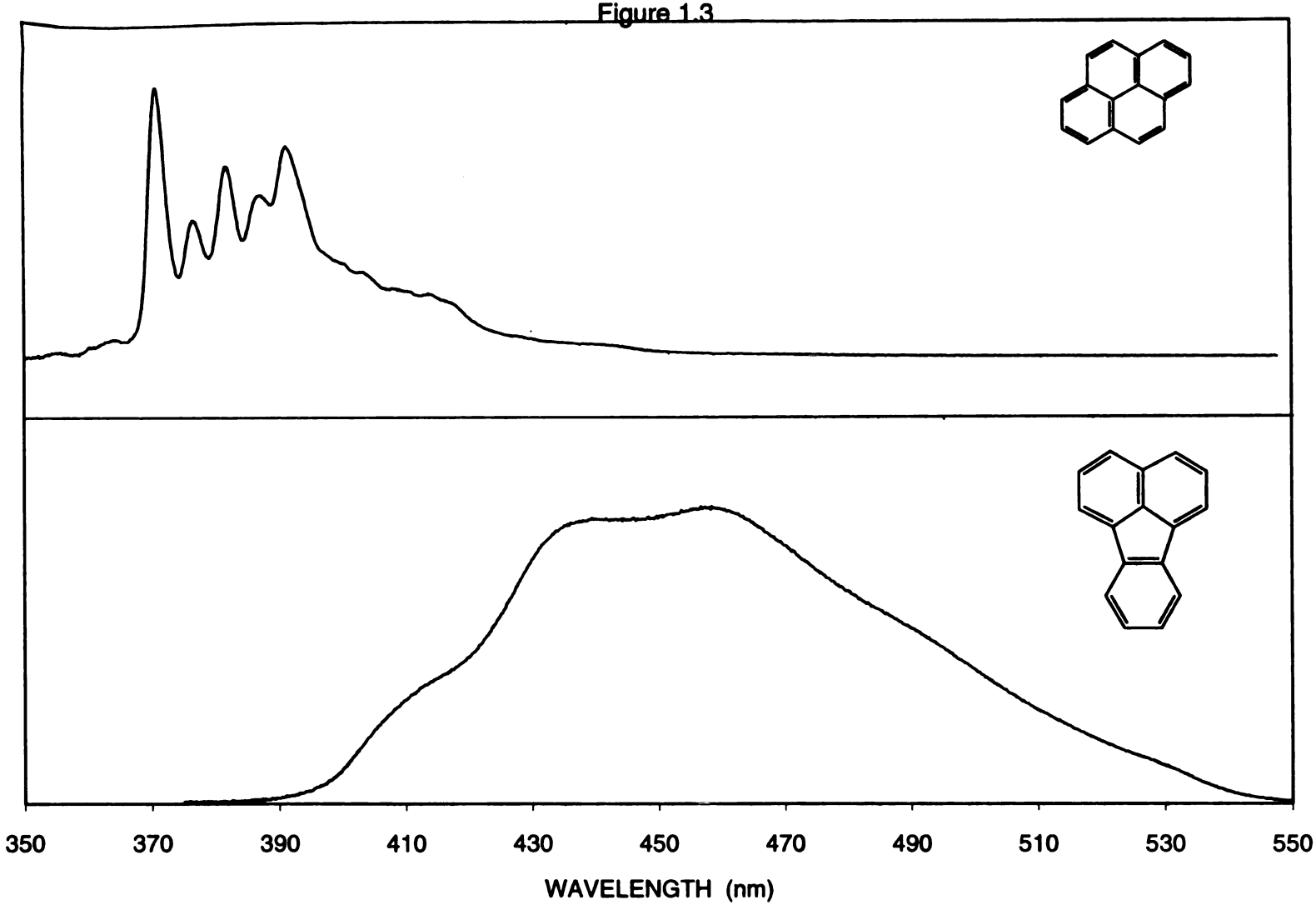

identification of alternant and nonalternant molecules as demonstrated in Chapter 8.

In addition to classification based upon alternant/nonalternant character, PAHs can also be differentiated based upon their annelation structure. Annelation is a descriptor of the degree of fusion between the rings of a given PAH. Annelation is divided into three categories: linearly fused, ortho-fused, and peri-fused. Linearly fused PAHs are identified as having all of the rings along a single axis. Ortho-fused PAHs are compounds in which two rings have two, and only two, atoms in common [4]. Peri-fused PAHs are compounds in which one ring contains two, and only two, atoms in contact with each of two or more rings of a contiguous series of rings [4]. Examples of linearly fused, ortho-fused, and peri-fused PAHs are shown in Figure 1.4. Since the number of isomers increases with ring number, the ortho- and peri-fused descriptors may describe several isomers for any given ring number.

Similar to the alternant/nonalternant character, the type of annelation affects the spectroscopic behavior of the PAH. Linearly fused isomers exhibit fluorescence emissions that are shifted to longer wavelengths than ortho-fused isomers, which are in turn shifted to longer wavelengths than peri-fused isomers [5,6].

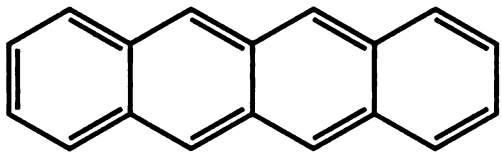

Linearly-fused

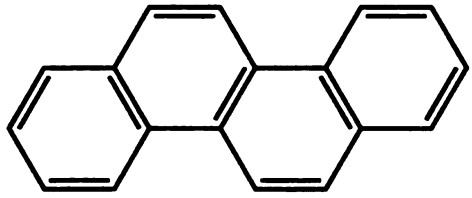

Ortho-fused

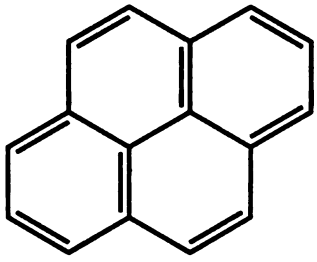

Peri-fused

***Figure* 1.4**: Structures of linearly fused, ortho-fused and peri-fused PAHs

1.1.2 Origin and Formation

Polycyclic aromatic hydrocarbons can be formed through natural or anthropogenic processes. In general, any process that involves the heating of carbon-containing compounds will form PAHs [7]. Natural processes that lead to PAH formation include volcanic activity and forest fires, as well as subsurface events that result in the creation of fossil fuels. Anthropogenic processes that lead to PAH formation include the production and processing of fossil fuels, as well as the combustion of wood and petroleum products [1].

Although PAHs can originate from a variety of sources, different structures are formed preferentially under certain conditions. For instance, nonalternant PAHs tend to form at lower temperatures, where an increase in reaction time yields an increase in the number of nonaromatic rings [8]. By contrast, alternant PAHs, as well as PAHs with a large number of rings, require long periods of high temperature exposure to form. PAH structure is important because it affects the chemical stability of a PAH. Blumer reports that peri-fused PAHs are more stable than ortho-fused isomers, which are more stable than their linear isomers (Figure 1.4) [7].

1.1.3 Biological and Chemical Significance

As a class, PAHs are important for study because of their biological and chemical significance. While single doses of PAHs have low to moderate acute toxicity, many PAHs have been shown to elicit mutagenic and carcinogenic events in mammalian cells (Tables 1.1 and 1.2) [9-11]. These events include

Table 1.1: Sample values for acute toxicity of selected polycyclic aromatic hydrocarbons

Solute	Species	Route of administration	LD_{50} (mg/kg) [a]
Naphthalene	Mouse	Oral	533
Anthracene	Mouse	Oral	18000
Phenanthrene	Mouse	Oral	1000
Pyrene	Mouse	Intraperitoneal	678
Chrysene	Mouse	Intraperitoneal	>320
Benzo[*a*]pyrene	Mouse	Oral	>1600

[a] LD_{50} – Dose at which 50% of the test population dies [11]

Table 1.2: Carcinogenicity of polycyclic aromatic hydrocarbons in mammals

Solute	Carcinogenicty (weight of evidence)	Species	Route of administration (# of positive/negative studies)	
			Subcutaneous	Dermal
Naphthalene	Questionable	Mouse	NA[a]	1/2
Anthracene	Negative	Mouse	0/1	0/6
Phenanthrene	Questionable	Mouse	0/3	1/3
Pyrene	Questionable	Mouse	NA[a]	1/7
Chrysene	Positive	Mouse	3/3	11/9
Benzo[*a*]pyrene	Positive	Mouse	5/0	26/0

[a] NA – no data available [11]

both initiation and propagation of carcinogenesis and mutagenesis at low doses. For example, benzo[*a*]pyrene has been shown to form DNA adducts resulting in potent carcinogenesis [12,13]. In vitro, most PAHs are converted via intermediate epoxides into phenols, diols, and tetrols. This conversion allows the metabolized PAH to be excreted. PAHs that are known to be toxic have been shown to covalently bind to amino acids or DNA. It is this covalent binding that leads to toxic responses when the damaged DNA is neither repaired, nor excised [11].

However, not all PAH isomers have analogous toxicity. For example, Heidelberg demonstrated that dibenz[*a,h*]anthracene is a potent carcinogen, whereas the isomer dibenz[*a,c*]anthracene is not [14]. Since there is no a priori method for determining the toxicity of one isomer over another, experiments must be conducted for each isomer in order to determine the inherent toxicity.

From an analytical viewpoint, PAHs are important because of the large number of isomers and their associated toxicity. The separation of positional isomers presents a challenge that has direct benefits to the biological community. Qualitative analysis provides information that aids not only the identification of these toxicants, but also information about the degree of exposure in real-world samples. At the same time, an analysis of the molecular interactions of these solutes with chromatographic materials allows for a better understanding of retention and transport in chromatography. The investigation of substituted PAHs, such as azaarenes and amino-PAHs, allows quantitative differences to be determined and compared to the parent compounds. Substituted PAHs are

important because they are often more toxic than the parent PAHs. For example, 1-aminopyrene has been shown to be fifty times more toxic than benzo[*a*]pyrene [15]. By studying these compounds using chromatography, data that are applicable to several disciplines can be garnered.

1.2 Thermodynamic and Kinetic Theory

Given that the study of PAHs is of benefit to a multidisciplinary audience, a fundamental framework must be employed to demonstrate not only the utility of the studies found within this dissertation, but also the validity of the methods. Any description of retention in chromatography must begin with an understanding of the basics of thermodynamics and kinetics.

In order to characterize both the thermodynamic and kinetic aspects of retention, traditional thermodynamic and transition state theories must be synthesized. As illustrated in Figure 1.5, the retention event can be depicted by using an energy coordinate diagram as the molecule moves from mobile (X_m) to stationary phase (X_s). The thermodynamic changes in molar enthalpy (ΔH_{sm}) and molar volume (ΔV_{sm}) are simply the difference between the final and initial states. The kinetic aspects of the retention event are characterized by a fast equilibrium between the mobile phase and transition state ($X_{\ddagger}$) with equilibrium constant $K_{\ddagger m}$, followed by a rate-limiting step between the transition state and the stationary phase with rate constant k_{sm}. The corresponding changes in activation

Figure 1.8: Energy coordinate diagram

Figure 1.5: Energy coordinate diagram

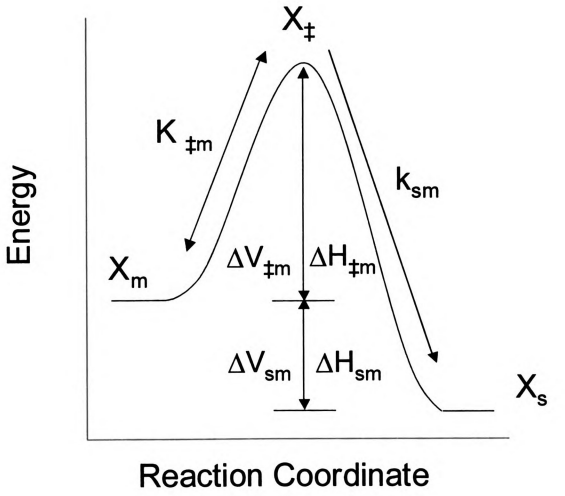

enthalpy (ΔH

a complete

constructed

the rate con

and activati

1.2.1 Therm

The

equilibrium

systems (i.

chromatog

molecules

equilibrium

$$K = \frac{a_s}{a_m} =$$

where a_m

respective

never atta

defined by

$$k = \frac{(t_r - t_0}{t_0}$$

where t_r a

respective

enthalpy ($\Delta H_{\ddagger m}$) and activation volume ($\Delta V_{\ddagger m}$) can also be calculated, allowing for a complete description of the retention event. A similar diagram can be constructed to illustrate the transition from stationary to mobile phase, from which the rate constant (k_{ms}) can be used to determine the activation enthalpy ($\Delta H_{\ddagger s}$) and activation volume ($\Delta V_{\ddagger s}$).

1.2.1 Thermodynamics

Thermodynamics is the study of systems, and their properties, in equilibrium. While the most common experiments involving equlibria are in static systems (i.e. materials are not entering or leaving), dynamic equilibria found in chromatographic systems can also be studied. Under the assumption that molecules have reached steady state by the time that they are detected, the equilibrium constant (K) for chromatographic separations can be expressed as

$$K = \frac{a_s}{a_m} = k\beta \qquad (1.1)$$

where a_m and a_s are the activity of the solute in the mobile and stationary phases, respectively. It should be noted that in liquid chromatography, true equilibrium is never attained because the system is under flow. The retention factor (k) is defined by

$$k = \frac{(t_r - t_0)}{t_0} \qquad (1.2)$$

where t_r and t_0 are the retention times of the solute and an unretained compound, respectively. The phase ratio (β) is defined as the volume of the stationary

phase

relate

ln K =

where

molar

molar

ΔG_{sr}

By su

lnk =

Thus,

logar

Unde

temp

the si

molar

ratio

canno

ΔH_{sr}

the re

change

phase divided by the volume of the mobile phase. The equilibrium constant is related to the change in the molar Gibbs free energy (ΔG_{sm})

$$\ln K = \frac{-\Delta G_{sm}}{RT} \tag{1.3}$$

where R is the universal gas constant and T is the absolute temperature. The molar Gibbs free energy can be further defined as a function of the changes in molar enthalpy (ΔH_{sm}) and molar entropy (ΔS_{sm})

$$\Delta G_{sm} = \Delta H_{sm} - T\,\Delta S_{sm} \tag{1.4}$$

By substitution,

$$\ln k = \frac{-\Delta H_{sm}}{RT} + \frac{\Delta S_{sm}}{R} - \ln\beta \tag{1.5}$$

Thus, the change in molar enthalpy can be determined by graphing the natural logarithm of the retention factor versus inverse temperature at constant pressure. Under the assumption that the changes in molar enthalpy and entropy are temperature independent, the change in molar enthalpy can be calculated from the slope of the line. The intercept contains information about the change in molar entropy as well as the phase ratio. Because it is not known how the phase ratio changes with temperature and pressure, the change in molar entropy cannot be reliably determined.

From the definition of the molar enthalpy,

$$\Delta H_{sm} = \Delta E_{sm} + P\,\Delta V_{sm} \tag{1.6}$$

the retention factor can be expressed as a function of the pressure (P), the change in molar internal energy (ΔE_{sm}), and the change in molar volume (ΔV_{sm})

$$\ln k = \frac{(-\Delta E_{sm} - P\,\Delta V_{sm} + T\,\Delta S_{sm})}{RT} - \ln\beta \qquad (1.7)$$

The change in molar volume can be determined by graphing the natural logarithm of the retention factor versus pressure at constant temperature. Under the assumption that the changes in molar volume, internal energy, and entropy are pressure independent, the change in molar volume is calculated from the slope of the line.

While the thermodynamic characterization of chromatography is important, thermodynamics only provides a partial description of the retention event. Since thermodynamic theory is focused exclusively upon the initial and final states of the system, the exact mechanism cannot be deduced without kinetic studies.

1.2.2 Kinetics

While the thermodynamics of retention have been well established, less work has been conducted to explain the kinetics of retention. Although the kinetics of retention have been studied (vide infra), the equations presented below represent the first kinetic derivations from Giddings theoretical treatment of retention.

As described above, transition state theory is used to evaluate the kinetics of retention. The measured kinetic event contains two contributions: the sorption event as well as the resistance to mass transfer in the mobile and stationary phases. The rate constants include both of these contributions because chromatography cannot decouple these events [16,17].

The rate constants can be calculated through an extrapolation of Giddings' work [18]. The mass transfer term (C_k) for slow kinetics in a system that exhibits a partition mechanism is given by

$$C_k = \frac{2R(1-R)}{k_{ms}} \tag{1.8}$$

where

$$R = \frac{1}{1+k} \tag{1.9}$$

and k_{ms} is the pseudo-first-order rate constant for the solute transfer from stationary to mobile phase. This mass transfer term can be related to the variance (σ_L^2) in the length domain via

$$\sigma_L^2 = C_k u L \tag{1.10}$$

where L is the column length and u is the linear velocity. By substitution, the variance in the length domain is related to the rate constant by

$$\sigma_L^2 = \frac{2 k L^2}{(1+k)^2 k_{ms} t_0} \tag{1.11}$$

The variance in the length domain can be related to the variance in the time domain (σ_t^2) by

$$\sigma_t^2 = \frac{(1+k)^2}{u^2} \sigma_L^2 = \frac{2 k L^2}{u^2 k_{ms} t_0} \tag{1.12}$$

From the definition of linear velocity,

$$u = \frac{L}{t_0} \tag{1.13}$$

the variance in the time domain is related to the rate constant by

$$\sigma_t^2 = \frac{2 k t_0}{k_{ms}} \tag{1.14}$$

When the time variance is measured in an experimental system, it intrinsically contains all sources of asymmetrical broadening (i.e. instrumental, nonlinear isotherms, and slow kinetics). If the contributions from the first two sources are eliminated, as discussed in Chapter 3, then the asymmetrical tailing of the zone contains only the contributions from slow kinetics (τ^2) such that

$$\tau^2 = \sigma_t^2 \tag{1.15}$$

The rate constants describing the transfer from stationary to mobile phase (k_{ms}) and from mobile to stationary phase (k_{sm}) are defined by

$$k_{ms} = \frac{2 k t_0}{\tau^2} \tag{1.16}$$

$$k_{sm} = k\, k_{ms} = \frac{2 k^2 t_0}{\tau^2} \tag{1.17}$$

In order to calculate the derived kinetic parameters ($\Delta H_{\ddagger m}$, $\Delta V_{\ddagger m}$), a thermodynamic approach toward transition state theory is applied [19,20]. The rate constant can be described by the Arrhenius equation

$$k_{sm} = A_{\ddagger m} \exp\left(\frac{-\Delta E_{\ddagger m}}{RT}\right) \tag{1.18}$$

where $A_{\ddagger m}$ is the pre-exponential factor and $\Delta E_{\ddagger m}$ is the activation energy. The activation energy, which is the sum of the internal energy and a kinetic energy term [19,20], can be expanded using thermodynamic relationships

$$\Delta E_{\ddagger m} = \Delta H_{\ddagger m} + RT - P\,\Delta V_{\ddagger m} \tag{1.19}$$

The natural logarithm of the resulting equation is useful for calculating the kinetic parameters of interest

$$\ln k_{sm} = \ln A_{\ddagger m} - \frac{\Delta H_{\ddagger m} + RT - P\,\Delta V_{\ddagger m}}{RT} \qquad (1.20)$$

From the equations above, the activation enthalpy ($\Delta H_{\ddagger m}$) can be determined from a graph of the natural logarithm of the rate constant versus inverse temperature at constant pressure. Under the assumption that the activation enthalpy and volume are temperature independent, the activation enthalpy can be calculated from the slope of the line. The activation volume can be determined by graphing the natural logarithm of the rate constant versus pressure at constant temperature. Under the assumption that the activation enthalpy and volume are pressure independent, the activation volume is calculated from the slope of the line. By using this method, the thermodynamic and kinetic parameters that characterize the partition and adsorption events in reversed-phase liquid chromatography can be determined (Chapters 4-6).

1.3 Previous Investigations

1.3.1 Thermodynamics

In order to better characterize the chromatographic retention event, a number of homologous series have been used to study the effect of repeating structural units. Such series have included fatty acids, alkyl benzenes, and PAHs. The benefit of using these series is that they offer a simple relationship between the retention factor (k) and the number of units, whether they be methylene (CH_2) or phenyl groups (C_6H_x, x = 2,3,4). Early studies determined

that an increase in methylene unit number results in a logarithmic increase in the retention factor. An early relationship between the number of methylene units (n) and the retention factor (k) was published by Grushka et al. [21]

$$\ln k_n = n \ln \alpha + \ln \beta \qquad (1.21)$$

where α is the chromatographic selectivity

$$\alpha = \frac{k_{n+1}}{k_n} \qquad (1.22)$$

and β is the retention factor for the parent functional group of the homologous series. Given that the solutes in a homologous series differ by a known number of functional units, the selectivity is used to characterize the difference in the Gibbs free energy ($\Delta\Delta G$) between solutes n and n+1. Using the thermodynamic relationships above, the differences in the molar enthalpy ($\Delta\Delta H$), molar entropy ($\Delta\Delta S$), and molar volume ($\Delta\Delta V$) as a function of methylene number can be examined.

One of the most pivotal studies using homologous series was published by Berendsen and de Galan [22]. In this work, the effect of stationary phase chain length was studied for a number of solutes with varying methylene unit number. The data from the study indicated that there is a critical chain length, beyond which retention does not change. According to the authors, the limiting chain length lies between 6 and 14 carbons for the alkyl-silica bonded phase material. This critical chain length is independent of mobile phase composition, but increases with increasing length of the solute alkyl chain, as well as increasing retention factor.

Further studies probed this idea of critical chain length in order to elucidate the retention mechanism. Colin and Guiochon studied a number of stationary phases for the separation of n-alkanes, n-alkyl benzenes, and n-methyl fatty acid esters [23]. Their work concluded that carbon adsorbents were more selective than chemically bonded phases (i.e. C_8 and C_{18}). In addition, the authors concluded that traditional hydrophobic predictors (i.e. water solubility, octanol-water partition coefficient) of retention failed to accurately estimate the selectivity of positional isomers on bonded phases. Similarly, Tchapla et al. investigated seven series of alkyl-substituted solutes (e.g. alkylbenzenes, alkylchlorides, carboxylic acids) on different stationary phases and concluded that the solute alkyl chains intercalate into the alkyl-silica stationary phase [24]. In addition to supporting the conclusions by Berendsen and de Galan, the authors demonstrated that the critical chain length is independent of the homologous series studied (i.e. it is dependent upon the number of methylene units in the solute).

In addition to studying the retention, the molar enthalpy and molar entropy have also been studied for homologous series. Issaq and Jaroniec calculated the molar enthalpy using Equation 1.5 for alkylbenzenes using binary mobile phases and four stationary phases (C_1, C_4, C_8, C_{18}) [25]. Using enthalpy-entropy compensation theory, they conclude that the molar enthalpy and molar entropy depend linearly on the number of carbon atoms (i.e. methylene units) in the alkyl chain of the homologous series, not the bonded phase. Sentell and Henderson further studied the effect of subambient temperatures on homologous series [26].

Their work concluded that at subambient temperatures, the structure of the stationary phase has a large effect on the retention, and is preferential for certain homologous series. McGuffin and Chen studied the retention of a series of even-numbered fatty acids (C_{10} through C_{22}) not only as function of temperature, but also pressure. From their experiments they quantitated the enthalpy changes ($\Delta\Delta H$) and volume changes ($\Delta\Delta V$) of –3.5 kcal/mol and –14.1 mL/mol, respectively [27], for ethylene units. Thus, these studies demonstrate that a significant amount of effort has been invested into understanding the chromatographic retention event.

In addition to the studies of retention as a function of methylene unit number, series containing phenyl units have also been investigated. Most notably PAHs have been used since they have repeating phenyl units in varied configurations. Whereas alkylated solutes can be characterized as a function of the number of methylene units and the degree of branching, PAHs have been studied as a function of ring number, annelation and planarity [28-31]. Studies have shown that an increase in the ring number leads to a logarithmic increase in the retention factor. Similarly, linear PAHs are retained longer than ortho-fused isomers, which are more retained than peri-fused isomers. Several reviews have been published in an attempt to collate the large amount of information that is known about PAH retention [32-35]. For example, an increase in the density of alkyl chains in the stationary phase leads to an increase in the retention of planar compounds, but a decrease in the retention of nonplanar compounds [28,29,32,36-38]. The current hypothesis is that an increase in density causes

nonplanar solutes to be excluded more efficiently. Increases in temperature result in a decrease in the retention for both planar and nonplanar solutes [28,39,40]. By contrast, the effect of pressure is much smaller [27,41]. As a result, little work has been conducted using this parameter.

From these experiments, many authors have attempted to explain the mechanism of retention (i.e. partition or adsorption) on the basis of the thermodynamically derived value of molar enthalpy and the general shape of the van't Hoff plot. A van't Hoff plot is simply a graph of the logarithm of the retention factor versus inverse temperature (Equation 1.5). However, such experiments have failed to stringently control pressure. As demonstrated in Chapters 4 through 6, failure to control pressure may result in erroneous values to be calculated for the change in molar enthalpy. In addition, the change in molar volume cannot be calculated without controlling pressure.

1.3.2 Kinetics

Although the thermodynamics of retention have been extensively probed, less work has been conducted into the kinetics of retention. Published work on kinetics has generally fallen into two classes based upon the techniques employed: non-chromatographic and chromatographic.

Non-chromatographic experiments have utilized pressure, temperature, and dipole jump methods [42-47], as well as fluorescence correlation spectroscopy [48,49] to investigate chromatographic materials. Jump experiments involve systems in which an abrupt perturbation is made to the system, after which the kinetic relaxation is measured. For example, pressure

jump methods involve two cells, which are connected to one another, but separated by a rupture disk. One cell contains the solute and the stationary phase, the other a compressible liquid. Once the sample cell has reached equilibrium, the second cell is pressurized until the disk ruptures, sending a pressure wave into the sample cell. The solutes are then studied as they kinetically relax from this perturbation wave. While this method provided information about the kinetics of interaction with alkyl bonded phases, the systems are not representative of a chromatographic column. The inherent limitation in jump methods is that the perturbation changes the thermodynamic and kinetic behavior of the system that is being measured. Thus, the kinetic measurements are representative only of the jump system.

In contrast, total-internal-reflection fluorescence correlation spectroscopy (TIRFCS) is more suited to measuring a flowing system [48,49]. Using TIRFCS Hansen and Harris modified a silica surface with octadecylsilica. Fluorescent molecules were flowed across the modified surface. As the molecules diffuse toward the surface, and into the region that is spectroscopically probed, they add to the low frequency noise of the system. This noise follows Poisson statistics and as such, allows for the number of molecules at the interface to be calculated. These data provide insight into the kinetics of the retention event. However, like the jump methods, this system provides only limited information about a dynamic system. The principle limitation of this method is that a highly fluorescent molecule must be used. For their work, Hansen and Harris chose rhodamine 6G, a dye commonly used for lasing. This molecule is very different from both the

methylene and phenyl homologues and provides limited information about their retention.

As noted, non-chromatographic techniques provide a method by which the kinetics of retention can be probed. However, the inherent differences between these systems and a packed chromatography bed provide limited information about the kinetics of an actual separation. In order to circumvent these difficulties, several chromatographic techniques have been used. These methods have included frontal analysis and pulse methods [50-52], with affinity chromatography being one of the more common applications [53,54]. Frontal analysis involves injecting a large concentration of the solute onto the chromatography column, and then analyzing the resultant curve. Also known as a breakthrough curve, this curve provides information about the kinetics of sorption. However, it does not represent the most common type of chromatography, which involves injecting smaller volumes of material onto the column.

Pulse methods better approximate a typical chromatographic separation since they involve the injection of smaller volumes/concentrations. However, the current method to elucidate the kinetics is also questionable. Most notably, Miyabe and Guiochon use a method in which plate height (H) can be related to axial dispersion, external mass transfer, intraparticle diffusivity and the adsorption rate constant. Since the plate height is a measurable quantity, and the first three parameters can be approximated, the adsorption rate constant can be quantitated [50,55-58]. However, this method is troublesome since there are

many processes that contribute to the broadening and asymmetry of the chromatographic zone profile that do not arise from kinetic sources. As discussed by Weiss [16] and Lenhoff [17], failure to accurately measure or estimate these sources can result in spurious kinetic data. Thus, the current chromatographic methods are not ideal for characterizing the kinetics of retention since these methods rely upon a number of assumptions and approximations.

1.4 Conclusions

Although significant efforts have been invested in understanding the molecular contributions to retention for homologous series, limitations in both theory and experimental design have hindered definitive quantitative analysis. Using novel theoretical and experimental designs, the thermodynamic and kinetic contributions to retention in liquid chromatography will be explored. By characterizing the thermodynamics and kinetics in tandem, and by measuring the zone profile on column versus post column, a more rigorous description of solute transfer is developed. Ultimately, such development will lead to a better understanding of retention in both synthetic and natural materials.

1.5 References

[1] M.L. Lee, M.V. Novotny, K.D. Bartle, Analytical Chemistry of Polycyclic Aromatic Hydrocarbons, Academic Press, New York, NY, USA, 1981.

[2] J. Malkin, Photophysical and Photochemical Properties of Aromatic Compounds, CRC Press, Ann Arbor, MI, USA, 1992.

[3] J.V. Goodpaster, J.F. Harrison, V.L. McGuffin, J. Phys. Chem. A 102 (1998) 3372-3381.

[4] A.D. McNaught, A. Wilkinson, IUPAC Compendium on Chemical Terminology, Royal Society of Chemistry, Cambridge, UK, 1997.

[5] E. Clar, Polycyclic Hydrocarbons, Academic Press, New York, NY, USA, 1964.

[6] E. Clar, The Aromatic Sextet, John Wiley & Sons, New York, NY, USA, 1972.

[7] M. Blumer, W.W. Youngblood, Science (Washington, D. C., 1883-) 188 (1975) 53-55.

[8] M. Blumer, Sci. Am. 234 (1976) 35-45.

[9] M. Cooke, A.J. Dennis, G.L. Fisher, Polynuclear Aromatic Hydrocarbons: Physical and Biological Chemistry, Battelle Press, Columbus, OH, 1982.

[10] T. Vo-Dinh, Chemical Analysis of Polycyclic Aromatic Hydrocarbons, John Wiley & Sons, New York, NY, 1988.

[11] R.F. Hertel, G. Rosner, J. Kielhorn, Selected Non-Heterocyclic Polycyclic Aromatic Hydrocarbons, World Health Organization, Geneva, 1998.

[12] K.M. Straub, T. Meehan, A.L. Burlingame, M. Calvin, Proc. Natl. Acad. Sci. U. S. A. 74 (1977) 5285-5289.

[13] M.F. Denissenko, M.-s. Tang, G.P. Pfeifer, Biomarkers Environ. Assoc. Dis. (2002) 139-157.

[14] C. Heidelberg, Cancer Res. 30 (1970) 1549-1569.

[15] C.H. Ho, B.R. Clark, M.R. Guerin, B.D. Barkenbus, T.K. Rao, J.L. Epler, Mutat. Res. 85 (1981) 335-345.

[16] G.H. Weiss, Sep. Sci. Technol. 16 (1981) 75-80.

[17] A.M. Lenhoff, J. Chromatogr. 384 (1987) 285-299.

[18] J.C. Giddings, J. Chem. Phys. 31 (1959) 1462-1467.

[19] K.J. Laidler, Chemical Kinetics, 3rd Ed., Harper & Row, New York, NY, USA, 1987.

[20] J.I. Steinfeld, J.S. Francisco, W.L. Hase, Chemical Kinetics and Dynamics, 2nd Ed., Prentice Hall, Upper Saddle River, NJ, USA, 1999.

[21] E. Grushka, H. Colin, G. Guiochon, J. Chromatogr. 248 (1982) 325-339.

[22] G.E. Berendsen, L. de Galan, J. Chromatogr. 196 (1980) 21-37.

[23] H. Colin, G. Guiochon, J. Chromatogr. Sci. 18 (1980) 54-63.

[24] A. Tchapla, S. Heron, H. Colin, G. Guiochon, Anal. Chem. 60 (1988) 1443-1448.

[25] H.J. Issaq, M. Jaroniec, J. Liq. Chromatogr. 12 (1989) 2067-2082.

[26] K.B. Sentell, N.I. Ryan, A.N. Henderson, Anal. Chim. Acta 307 (1995) 203-215.

[27] V.L. McGuffin, S.H. Chen, J. Chromatogr. A 762 (1997) 35-46.

[28] L.A. Cole, J.G. Dorsey, Anal. Chem. 64 (1992) 1317-1323.

[29] K.B. Sentell, J.G. Dorsey, J. Chromatogr. 461 (1989) 193-207.

[30] M. Olsson, L.C. Sander, S.A. Wise, J. Chromatogr. 477 (1989) 277-290.

[31] L.C. Sander, M. Pursch, S.A. Wise, Anal. Chem. 71 (1999) 4821-4830.

[32] L.C. Sander, S.A. Wise, Anal. Chem. 67 (1995) 3284-3292.

[33] J.F. Wheeler, T.L. Beck, S.J. Klatte, L.A. Cole, J.G. Dorsey, J. Chromatogr. A 656 (1993) 317-333.

[34] A. Tchapla, S. Heron, E. Lesellier, H. Colin, J. Chromatogr. A 656 (1993) 81-112.

[35] L.C. Sander, S.A. Wise, J. Chromatogr. A 656 (1993) 335-351.

[36] K.B. Sentell, J.G. Dorsey, Anal. Chem. 61 (1989) 930-934.

[37] S.R. Cole, J.G. Dorsey, J. Chromatogr. A 635 (1993) 177-186.

[38] J.H. Park, Y.K. Lee, Y.C. Weon, L.C. Tan, J. Li, L. Li, J.F. Evans, P.W. Carr, J. Chromatogr. A 767 (1997) 1-10.

[39] L.A. Cole, J.G. Dorsey, Anal. Chem. 64 (1992) 1324-1327.

[40] M.H. Chen, C. Horváth, J. Chromatogr. A 788 (1997) 51-61.

[41] V.L. McGuffin, C. Lee, J. Chromatogr. A 987 (2003) 3-15.

[42] D.B. Marshall, J.W. Burns, D.E. Connolly, J. Chromatogr. 360 (1986) 13-24.

[43] S.W. Waite, J.M. Harris, E.H. Ellusib, D.B. Marshall, Anal. Chem. 63 (1991) 2365-2370.

[44] S.W. Waite, D.B. Marshall, J.M. Harris, Anal. Chem. 66 (1994) 2052-2061.

[45] F.Y. Ren, J.M. Harris, Anal. Chem. 68 (1996) 1651-1657.

[46] J.M. Harris, D.B. Marshall, J. Microcolumn Sep. 9 (1997) 185-191.

[47] S.R. Shield, J.M. Harris, Anal. Chem. 74 (2002) 2248-2256.

[48] R.L. Hansen, J.M. Harris, Anal. Chem. 70 (1998) 2565-2575.

[49] R.L. Hansen, J.M. Harris, Anal. Chem. 70 (1998) 4247-4256.

[50] K. Miyabe, G. Guiochon, Anal. Chem. 72 (2000) 5162-5171.

[51] K. Miyabe, S. Sotoura, G. Guiochon, J. Chromatogr. A 919 (2001) 231-244.

[52] K. Miyabe, G. Guiochon, Anal. Chem. 74 (2002) 5754-5765.

[53] F.H. Arnold, H.W. Blanch, J. Chromatogr. 255 (1986) 13-27.

[54] P.D. Munro, D.J. Winzor, J.R. Cann, J. Chromatogr. A 659 (1994) 267-273.

[55] K. Miyabe, G. Guiochon, J. Chromatogr. A 857 (1999) 69-87.

[56] K. Miyabe, G. Guiochon, J. Chromatogr. A 830 (1999) 263-274.

[57] K. Miyabe, G. Guiochon, Anal. Chem. 72 (2000) 1475-1489.

[58] K. Miyabe, G. Guiochon, J. Chromatogr. A 961 (2002) 23-33.

Chapter 2: Experimental Methods

2.1 Introduction

In order to study the molecular level contributions to retention, a series of instruments was necessary. Although each experiment was customized for a specific measurement, a basic design was used and modified as needed. The manufacture of the chromatographic columns, the common components, as well as the specific modifications for each experiment are detailed below. In addition, the data treatment procedure is also described.

2.2 Experimental Systems

2.2.1 Column Preparation

In order for the thermodynamics and kinetics of retention to be accurately quantitated, the manufacture of a capillary column is necessary. This section details the choice of materials for the stationary phases as well as the methods employed to pack the columns.

In all instances, optically transparent, fused-silica capillary (Polymicro Technologies) is used for the column. The inner diameters of the columns were 200 μm for the synthetic stationary phases, and 320 μm for the natural material. These sizes are chosen such that the number of particles across the column is between 2 and 40. The number of particles across the column is important because a larger number of particles across the column results in a minimization of wall effects, which contribute to the asymmetrical tailing (vide infra). The

columns are terminated by quartz wool frits that prevent seepage of the stationary phases from the packed column.

2.2.1.1 Stationary Phases

2.2.1.1.1 Synthetic Materials

Two stationary phases, monomeric and polymeric octadecylsilica (ODS), were chosen to investigate the effects of bonding density on retention (Chapters 4-6). Both phases are prepared using an irregular silica material with 5.5 μm particle size, 190 Å pore size, and 240 m^2/g surface area (IMPAQ 200, PQ Corp.). Using mono- and trichlorosilanes, the silanization of these particles proceeds in the presence of trace water on the silica support. The presence of water causes a covalent bond to form between the silanol groups on the surface, and the silane functionality of the bonded phase. The reactions result in monomeric and polymeric stationary phases with bonding densities of 2.7 and 5.4 $\mu mol/m^2$, respectively.

2.2.1.1.2 Natural Material

In addition to the synthetic materials, a natural material is also used as a stationary phase. This material was chosen to represent natural soils in an attempt to better characterize retention in the environment (Chapter 7). The natural material used is a reference soil (CLN Soil-3 RTC Corp.). This soil contains 5.96% organic matter by mass and is 65% sand, 25% silt, and 10% clay. Physically this material has a large particle size distribution that ranges from the sub-micrometer to the millimeter scale. Since this range is too large to

pack efficiently, the material was sieved using a series of nylon meshes to yield a size range from 5 to 125 μm. This fraction was tested via batch isotherms to insure that the fractionation did not significantly alter the chemical behavior of the material (Chapter 7).

2.2.1.2 Packing Method

In order to pack the stationary phases, the slurry method is used [1]. This method involves suspension of the stationary phase in a solvent that prevents immediate precipitation. For the synthetic materials, acetone is chosen. For the natural material, methanol and ethylene glycol are used. Once suspended, the material is transferred to a stainless steel reservoir that is connected in series with a single piston reciprocating pump and a fused-silica capillary. The reservoir is pressurized rapidly, thus injecting the stationary phase into the open capillary. Depending upon the packing material, a different pressure limit is used. For the synthetic phases, the reservoir is pressurized to 5000 psi. This high pressure packs the column in a matter of minutes. By contrast, the natural phase is pressurized to 1000 psi, and slowly increased to 4000 psi over the course of several hours in order to create a well-packed bed of particles.

Once filled to the desired length, the column is then slowly depressurized to 1000 psi and maintained at that pressure for 24 hours. This lower pressure allows the packed bed to compress, thus removing any voids that could be left during the initial packing step.

2.2.2 Chromatographic System

Each experiment is carried out using one of three liquid chromatography systems. The common components of each include a single piston reciprocating pump (Model 114M, Beckman Instruments) operating in constant pressure mode (±15 psi) over the range of 500 to 4000 psi. The pump allows for the mobile phase to be supplied continuously without the need for depressurization during the refill cycle.

Samples are introduced via an injection valve (Model ECI4W1, Valco Instruments) with a 1 µL internal loop. Once the solutes are introduced, they are pumped to a 50 µm i.d. fused-silica capillary (Polymicro Technologies) that serves as the splitter. The length of the splitter is varied to change the amount of sample that is introduced into the column so as to prevent an overload of the stationary phase. Under normal operating conditions the volume introduced into the column is between 12 and 50 nL.

Once the sample is split, it is carried by the mobile phase to the column. At the end of the column, a 20 µm i.d. fused-silica capillary (Polymicro Technologies) is attached to serve as a restrictor. The length of the restrictor is reduced as the inlet pressure is decreased in order to maintain a constant pressure drop along the column of (~10 psi/cm).

The injector, splitter, column, and restrictor are all housed within a cryogenic oven (Model 3300, Varian Associates) that maintains a constant temperature (± 0.1 K) through the use of liquid nitrogen aspiration and resistive heating coils.

2.2.3 Spectroscopic System

Three different types of detectors were chosen for detection. Given that PAHs have absorption maxima in the ultraviolet portion of the electromagnetic spectrum, the systems chosen all used excitation sources in this range. The three systems are described in detail below.

2.2.3.1 Ultraviolet-Visible Absorbance

The default spectroscopic technique used for detection is ultraviolet-visible absorbance. As shown in Figure 2.1, a commercially available unit (Model 2050, Varian) is directly coupled to the capillary column such that the effluent is directed to a capillary flow cell. This flow cell is optically transparent, fused-silica capillary with a 50-μm i.d. A capillary flow cell is used to minimize zone broadening that arises from diffusional and mass transfer processes.

The wavelength for detection is chosen based upon the absorption maxima of the solutes. The time constant for the detector is 0.05 seconds. The output from the detector is directed to a chart recorder for further data analysis.

Figure 2.1: Generalized schematic diagram for the post-column detection of chromophores/fluorophores using both ultraviolet-visible absorbance and laser-induced fluorescence detection. I: injection valve, S: splitting tee, R: restrictor PMT: photomultiplier tube, AMP: current to voltage amplifier, UV-Vis: ultraviolet-visible absorbance spectrometer.

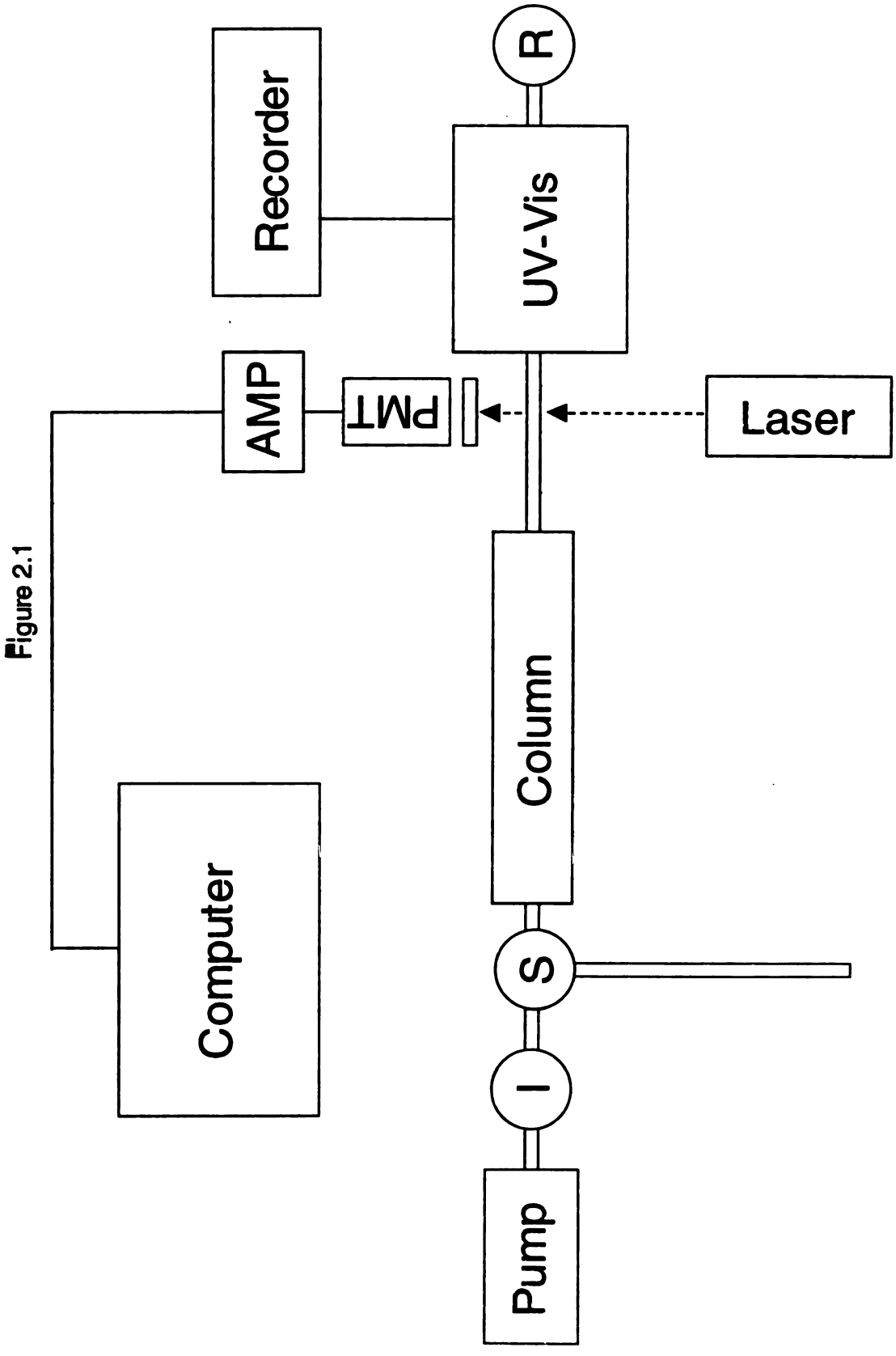

Figure 2.1

2.2.3.2 Laser-Induced Fluorescence

The second method employed for the detection of fluorophores is laser-induced fluorescence spectroscopy. As illustrated in Figure 2.2, this experimental system is used for the on column detection of PAHs (Chapters 4-6). The design and validation of this system were conducted by Dr. Chen [2]. A continuous-wave HeCd laser (Model 3074-20M, Melles Griot) is used as the excitation source. The laser beam is carried via UV-grade optical fibers (100 μm, Polymicro Technologies) to four locations along the column where the polyimide coating has been removed. The intensities at each location are balanced using fiber optic positioners and a fluorophore at the inception of each experiment. At each location, the fluorescence is collected orthogonal to the incident beam by optical fibers (500 μm, Polymicro Technologies) and is transmitted to a photomultiplier tube (Model R760, Hamamatsu), which has a 420 nm interference filter (S10-420-F, Corion). The resulting photocurrent is amplified using a gain of 100 nA/V and a time constant of 10 ms. The signal is then converted to the digital domain (PCI-MIO-16XE-50, National Instruments) and stored by a user-defined program (Labview v5.1, National Instruments). The acquisition rate of the program can be manually adjusted, and is typically set between 1 and 4 Hz.

Figure 2.2: Schematic diagram of the experimental system for capillary liquid chromatography with on-column laser-induced fluorescence detection. I: injection valve, S: splitting tee, R: restrictor, FOP: fiber-optic positioner, F: filter, PMT: photomultiplier tube, AMP: current to voltage amplifier.

Figure 2.2

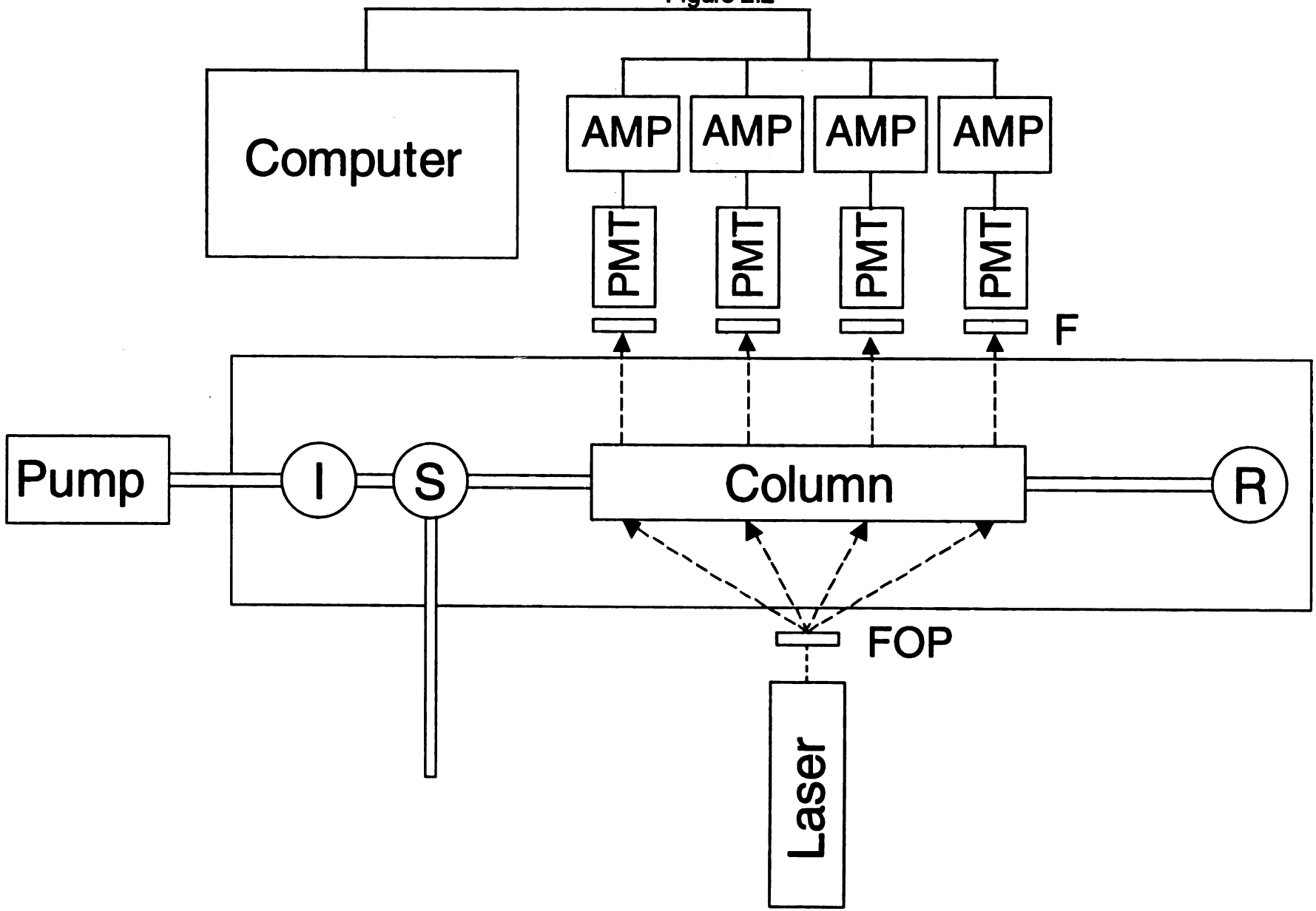
Computer
AMP
AMP
AMP
AMP
PMT
PMT
PMT
PMT
F
Pump
I
S
Column
R
FOP
Laser

2.2.3.3 Fl

Th

shown in

through a

from trivi

fluoresce

then filte

entrance

grating,

a charg

pixels).

0.15 nn

comme

and the

The ac

~100 r

is used

nitrom

used a

mocr

samp

2.2.3.3 Fluorescence Quenching

The third detection system employs selective florescence quenching. As shown in Figure 2.3, a HeCd laser is used to excite the solutes as they pass through a 75 μm i.d. flow cell. This capillary flow cell minimizes the interference from trivial processes such as primary or secondary absorption [3]. The fluorescence emission is collected orthogonal to the incident radiation, and is then filtered and collimated. The resulting emission is then refocused onto the entrance slit of a Czerny-Turner monochromator (Model 340E, 300 groove/mm grating, Instruments SA, 10 nm/mm reciprocal linear dispersion) and detected via a charge-coupled device (Model (A)TECCD-2000x800-7, Instruments SA, 15 μm pixels). This system provides a wavelength range of 300 nm and a resolution of 0.15 nm. Instrument control and data acquisition are achieved by using a commercially available electronic interface (Instruments SA, Model CCD 2000) and the associated software (Spectramax for Windows, v3.1, Instruments SA). The acquisition rate for this system was set to 2 s, with the integration time of ~100 ms. This system differs from the preceding designs in that a second pump is used to deliver a fluorescence quencher to the post column effluent. Using nitromethane, alternant PAHs are selectively quenched. Diisopropylamine is used as a post column addition to quench nonalternant PAHs. This slight modification allows for qualitative information to be collected about complex samples (Chapter 8).

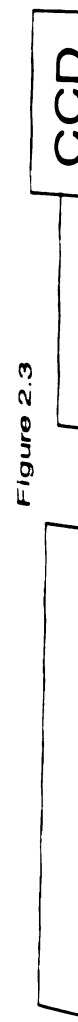

Figure 2.3: Schematic diagram of the experimental system for capillary liquid chromatography with laser-induced fluorescence quenching detection. I: injection valve, S: splitting tee, L: lens, F: filter; CCD: charge-coupled device, PMT: photomultiplier tube. (Note: Collection of fluorescence emission is orthogonal to the incident laser beam)

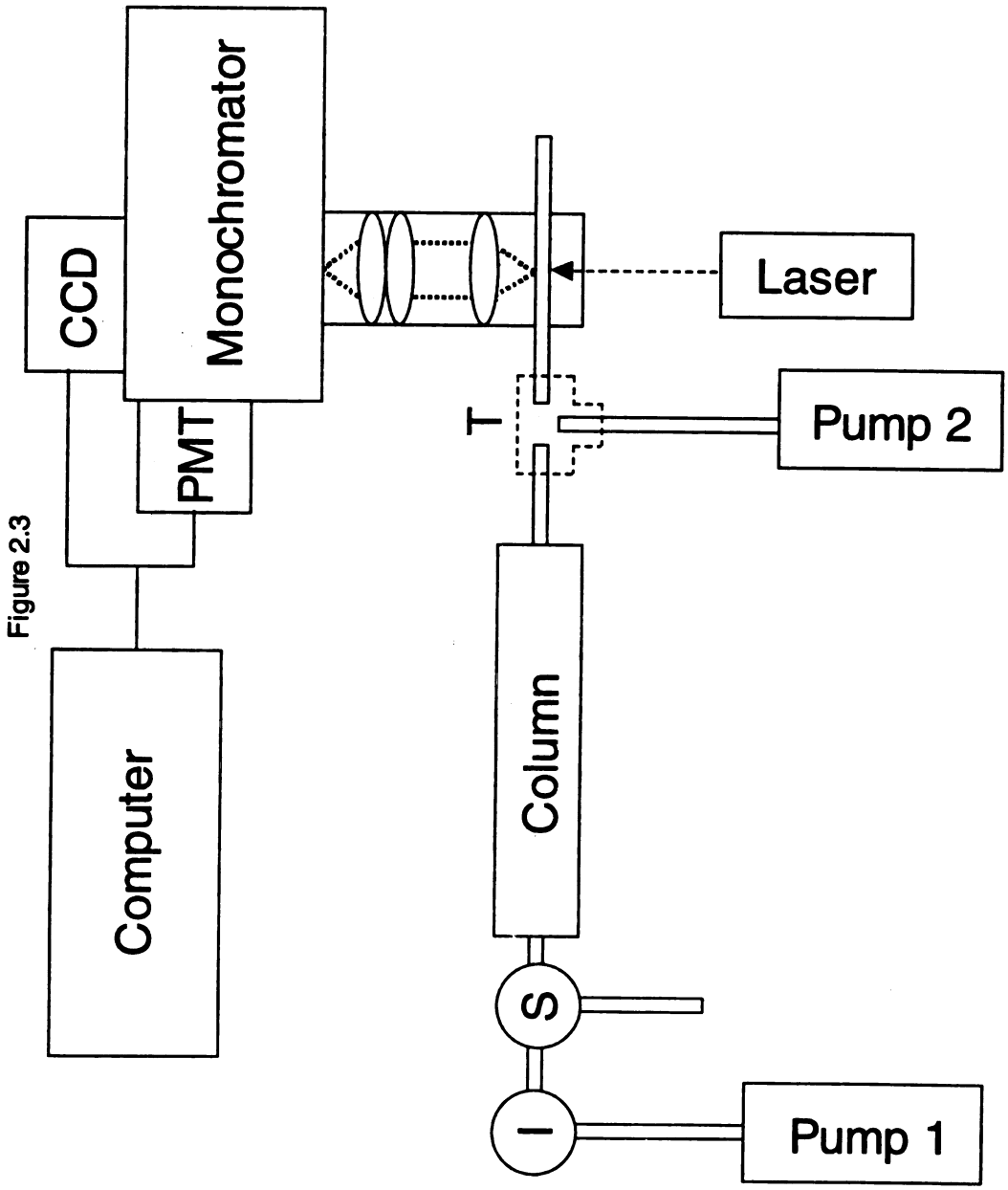

Figure 2.3

2.3 D

collect
desire
chroma
extract
remove
manua
using a
Since th
second
analysis
function
parame
thermod
Chapter

2.3.1 M

2.3.1.1

C
moment
describe
functiona

2.3 Data Treatment and Analysis

While the stringent control of each experimental system was critical for the collection of the data, the analysis also provides a series of obstacles. Since the desired data are individual peak profiles contained within a multicomponent chromatogram, the first challenge for the data analysis is the reproducible extraction of the individual profiles. Since the profiles must be manually removed, a series of experiments were carried out to explore the effects of this manual extraction (Chapter 3). Once removed, the peak profiles are iteratively fit using a commercially available program (Peakfit v3.18, SYSTAT Software). Since there are many functions available for the analysis of peak profiles, the second obstacle to the analysis is choice of an appropriate function for the analysis of the peak profiles. This section describes some of the mathematical functions that are used once the data have been extracted. Using the various parameters from the mathematical models described below, the thermodynamics and kinetics are quantitated using the equations found in Chapter 1.

2.3.1 Mathematical Functions

2.3.1.1 Statistical Moments

One of the most common methods to characterize peaks utilizes statistical moments [4-6]. Statistical moments are classical functions that are used to describe the distribution of any set of data with no assumptions about the functional form. For the purposes of this dissertation, the moments related to the

concer

by

$M_0 = \int$

the firs

$M_1 = \frac{\int}{}$

and the

$M_n = \frac{\int}{}$

The sec

represe

statistic

discrete

T

number

noise ca

alternati

nonlinea

function

EMG and

experime

study chr

concentration as a function of time C(t). The zeroth moment, or area, is defined by

$$M_0 = \int C(t)\,dt \approx \sum C(t)\,\Delta t \tag{2.1}$$

the first moment, or mean retention time, by

$$M_1 = \frac{\int t\,C(t)\,dt}{M_0} \approx \frac{\sum t\,C(t)\,\Delta t}{M_0} \tag{2.2}$$

and the higher central moments (M_n) by the general form

$$M_n = \frac{\int (t - M_1)^n C(t)\,dt}{M_0} \approx \frac{\sum (t - M_1)^n C(t)\,\Delta t}{M_0} \tag{2.3}$$

The second moment (M_2) represents the variance and the third moment (M_3) represents the asymmetry of the zone profile. In practical applications of the statistical moments, the integrals in Equations 2.1 – 2.3 are usually estimated by discrete summation.

The accurate description of asymmetrical peaks usually requires a large number of statistical moments and a large number of data points [7]. In addition, noise can affect the values for the moments [8]. As a result of these limitations, alternative equations such as the exponentially modified Gaussian (EMG) [9], the nonlinear chromatography (NLC) [10], and the Haarhoff–Van der Linde [11] function have been developed for evaluating non-Gaussian zone profiles. The EMG and NLC models provide variables that can be directly related to experimental parameters. As a result, these two functions were initially chosen to study chromatographic zones.

2.3.1.2

form o

C(t) =

where

standa

compo

use of

and Ya

semina

These

chroma

other e

conclud

the EM

comple

addition

physica

V

the then

2.3.1.2 Exponentially Modified Gaussian Equation

The EMG is a convolution of a Gaussian and an exponential function. The form of this equation is

$$C(t) = \frac{A}{2\tau} \exp\left[\frac{\sigma^2}{2\tau^2} + \frac{t_G - t}{\tau}\right]\left[\operatorname{erf}\left(\frac{t - t_G}{\sqrt{2}\sigma} - \frac{\sigma}{\sqrt{2}\tau}\right) + 1\right] \qquad (2.4)$$

where A is the area, t_G is the retention time of the Gaussian component, σ is the standard deviation of the Gaussian component and τ is the the exponential component.

Over the past thirty years, several authors have sought to characterize the use of the EMG function for chromatographic analysis. While Grushka [12,13] and Yau [14] presented some early work, Foley and Dorsey have published two seminal papers reviewing the EMG function in the intervening years [15,16]. These reviews have demonstrated the use of the EMG function for a variety of chromatographic applications. More recent studies have compared the EMG to other equations for the analysis of zone profiles [17,18]. These studies have concluded that high-order polynomials that exceed the four parameters used in the EMG function can describe asymmetrical peaks very well. However, the complex nature of such functions makes them impractical for common use. In addition, the parameters for these high-order polynomials may not have any physical significance as do those calculated using the EMG function.

Within this dissertation, the EMG is employed predominantly to calculate the thermodynamics and kinetics of retention. The thermodynamic and kinetic

param

into E

$t_r = t_G$

2.3.1.

chrom

curren

$C(t) =$

where

$T(u,v)$

and I_0

parame

(a_i), wi

from th

parame

$a_2 = \frac{}{k_m}$

Using th

constan

parameters can be calculated by substituting the measured values of t_G and τ into Equations 1.2, 1.16, and 1.17, where

$$t_r = t_G + \tau \tag{2.5}$$

2.3.1.3 Non-linear Chromatography

The second model employed to analyze the zone profiles is the nonlinear chromatography (NLC) model. Developed initially in 1944 [19], the NLC's most current form was developed by Wade et al. in 1987 [10]:

$$C(t) = \frac{a_0}{a_2 a_3}\left[1-\exp\left(-\frac{a_3}{a_2}\right)\right]\left[\frac{\sqrt{\frac{a_1}{x}}\, I_1\left(2\,\frac{\sqrt{a_1 x}}{a_2}\right)\exp\left(\frac{-x-a_1}{a_2}\right)}{1-T\left(\frac{a_1}{a_2},\frac{x}{a_2}\right)\left[1-\exp\left(-\frac{a_3}{a_2}\right)\right]}\right] \tag{2.6}$$

where

$$T(u,v) = e^{-v}\int_0^u e^{-t} I_0\left(\sqrt{2vt}\right)dt \tag{2.7}$$

and I_0 and I_1 are modified Bessel functions of the first kind. The fitting parameters that are incorporated in the NLC model are the area (a_0), position (a_1), width (a_2), and distortion (a_3). If the chromatographic data are transformed from the time domain to the retention factor domain via Equation 1.2, then these parameters can be used to calculate the lumped desorption rate constant

$$a_2 = \frac{1}{k_{ms} t_0} \tag{2.8}$$

Using the established relationship between the retention factor and the rate constants ($k = k_{sm}/k_{ms}$), the adsorption rate constant can also be calculated.

2.3.1.4

site ret

two dis

expone

Gauss

C(t) =

exp

where

standa

compo

orgina

equal

2.3.1.4 Bi-exponentially Modified Gaussian Equation

Neither the EMG nor NLC equations are capable of evaluating a multiple-site retention model. As a result, a new equation was developed to test whether two distinct sites were present at low temperatures (Chapter 6). The bi-exponentially modified Gaussian (E^2MG) equation is the convolution of a Gaussian and two exponential functions, with the resulting form

$$C(t) = \frac{h_G \sigma \sqrt{\frac{\pi}{2}} \exp\left(-\frac{(t-t_G)^2}{2\sigma^2}\right)}{\tau_1 - \tau_2} \times \left(\exp\left(\frac{\left(-t + t_G + \frac{\sigma^2}{\tau_1}\right)^2}{2\sigma^2} \right) \left(1 + \operatorname{erf}\left(\frac{t\tau_1 - \tau_1 t_G - \sigma^2}{\sqrt{2}\tau_1 \sigma}\right)\right) - \exp\left(\frac{\left(-t + t_G + \frac{\sigma^2}{\tau_2}\right)^2}{2\sigma^2} \right) \left(1 + \operatorname{erf}\left(\frac{t\tau_2 - \tau_2 t_G - \sigma^2}{\sqrt{2}\tau_2 \sigma}\right)\right) \right) \quad (2.9)$$

where h is the height, t_G is the retention time of the Gaussian component, σ is the standard deviation of the Gaussian component, and τ_1 and τ_2 are the exponential components for the first and second kinetic sites, respectively. This equation, originally developed by Delley [20] presumes that the two kinetic events are of equal probability.

2.4 Conclusions

The use of novel experimental design and theoretical treatment is necessary in order to study retention at the molecular level. This chapter details the experimental systems and mathematical functions that were necessary to collect and analyze the desired data.

2.5 References

[1] J.C. Gluckman, A. Hirose, V.L. McGuffin, M. Novotny, Chromatographia 17 (1983) 303-309.

[2] S.-H. Chen, in Chemistry, Michigan State University, East Lansing, 1993.

[3] S.-H. Chen, C.E. Evans, V.L. McGuffin, Anal. Chim. Acta 246 (1991) 65-74.

[4] E. Grushka, M.N. Myers, J.C. Giddings, Anal. Chem. 42 (1970) 21-26.

[5] J.C. Giddings, R.A. Keller, Advances in Chromatography, Marcel Dekker, New York, NY, USA, 1966.

[6] M.S. Jeansonne, J.P. Foley, J. Chromatogr. 461 (1989) 149-163.

[7] S.N. Chesler, S.P. Cram, Anal. Chem. 43 (1971) 1922-1929.

[8] J.V.H. Schudel, G. Guiochon, J. Chromatogr. 457 (1988) 1-12.

[9] W.E. Barber, P.W. Carr, Anal. Chem. 53 (1981) 1939-1942.

[10] J.L. Wade, A.F. Bergold, P.W. Carr, Anal. Chem. 59 (1987) 1286-1295.

[11] P.C. Haarhoff, H.J. Van der Linde, Anal. Chem. 38 (1966) 573-582.

[12] E. Grushka, Anal. Chem. 44 (1972) 1733-1738.

[13] E. Grushka, J. Phys. Chem. 76 (1972) 2586-2593.

[14] W.W. Yau, Anal. Chem. 49 (1977) 395-398.

[15] J.P. Foley, J.G. Dorsey, J. Chromatogr. Sci. 22 (1984) 40-46.

[16] M.S. Jeansonne, J.P. Foley, J. Chromatogr. Sci. 29 (1991) 258-266.

[17] M.L. Phillips, R.L. White, J. Chromatogr. Sci. (1997) 75-81.

[18] J.R. Torres-Lapasio, J.J. Baeza-Baeza, M.C. Garcia-Alvarez-Coque, Anal. Chem. 69 (1997) 3822-3831.

[19] H.C. Thomas, J. Am. Chem. Soc. 66 (1944) 1664-1665.

[20] R. Delley, Anal. Chem. 58 (1986) 2344-2346.

Chapter 3: Mathematical Analysis in Chromatographic Systems: A Comparison of the Exponentially Modified Gaussian Equation and Statistical Moments

3.1 Introduction

The reproducible extraction of individual zone profiles from multicomponent chromatograms is imperative if the thermodynamic and kinetic values are to have any meaning. This chapter describes the sources of both symmetrical and asymmetrical broadening that contribute to the peak shape of individual solutes. In addition, data from simulations and experiments are presented in order to validate the use of the exponentially modified Gaussian (EMG) equation as well as the experimental methods used to collect the data.

3.1.1 Sources of Broadening

In liquid chromatography, there are two main classes of broadening: symmetrical and asymmetrical. Symmetrical zone broadening arises from processes that are fast on the time-scale of the separation, such as diffusion and resistance to mass transfer in the mobile and stationary phases. These phenomena have been well characterized in the past [1]. Asymmetrical broadening arises from instrumental effects, nonlinear isotherms, and kinetics that are slow on the time-scale of the separation. These processes result in zone profiles that are skewed either to the front, or more commonly, to the rear.

Contributions to the asymmetrical broadening from instrumental effects have a variety of sources. The first source arises from volumetric contributions, such as exponential dilution chambers or regions of unswept fluid that occur in

the in

contri

proce

resul

isoth

capa

mole

a so

Slow

phas

to m

then

mec

3.1.

des

mor

Pre

faci

para

M_g

the injector, detector, or connectors. The second source arises from electronic contributions that occur during detection, amplification, or other signal processing.

The other two contributions to asymmetrical zone broadening are the result of interactions between the solute and stationary phase. Nonlinear isotherms typically occur when the concentration of the solute exceeds the capacity of the stationary phase, or when there are multiple sites where solute molecules can sorb. In a dynamic system, slow kinetics occur when the time for a sorption/desorption event is slow relative to the velocity of the mobile phase. Slow kinetics may also occur when the diffusion coefficient of the solute in one phase is much smaller than in the other, or when there is an interfacial resistance to mass transfer. Kinetic information is of interest because, together with thermodynamic information, it can be used to characterize the retention mechanism.

3.1.2 Mathematical Relationships

While the EMG function (Equation 2.4) has proven to be robust at describing asymmetrical peaks, many authors have chosen to use statistical moment analysis (Equations 2.1 – 2.3) since it requires fewer assumptions. Presented herein is a detailed comparison of these two methods. In order to facilitate this comparison, a relationship between the moments and the EMG parameters must be defined [2,3]:

$$M_0 = A \tag{3.1}$$

$$M_1 = t_G + \tau \quad (3.2)$$

$$M_2 = \sigma^2 + \tau^2 \quad (3.3)$$

$$M_3 = 2\tau^3 \quad (3.4)$$

It should be noted that the exponential component of the variance (τ^2) has been previously calculated by subtracting the Gaussian variance (σ^2) from the second moment via Equation 3.3 [2,3]. This approach implicitly assumes that σ and τ are independent of one another. However, the use of Equation 3.3 in this manner is problematic since there has been no proof to support the validity of this summation. This chapter directly tests this assumption of independence by using both simulated and experimental data. The simulation studies compare the results from both the statistical moment and EMG methods for a series of generated zone profiles. The experimental data characterize the differences between the two mathematical methods for a series of fatty acids separated by reversed-phase capillary liquid chromatography.

3.2 Simulation Methods

Using a conceptual framework by Chomin Lee, five different zone profiles were created by using commercially available software (Peakfit Version 3.18, SYSTAT Software) to be representative of the experimental data (*vide infra*). The profiles were generated by using the EMG equation with constant values for t_G and σ. The exponential contribution τ was varied, which results in a gradually increasing value for the τ/σ ratio from 0.5 to 10.0 (Table 3.1, Figure 3.1). The

Table 3.1: Input parameters for simulated chromatographic peaks according to the EMG model in Equation 2.4.

Table 3.1

Case	Area	t_G	σ	τ	σ/τ
1	137.41	5.0	0.5	0.25	0.5
2	159.83	5.0	0.5	0.5	1.0
3	210.42	5.0	0.5	1.0	2.0
4	366.39	5.0	0.5	2.5	5.0
5	623.41	5.0	0.5	5.0	10.0

Figure 3.1: Graphical representation of five simulated EMG peak profiles described in Table 3.1.

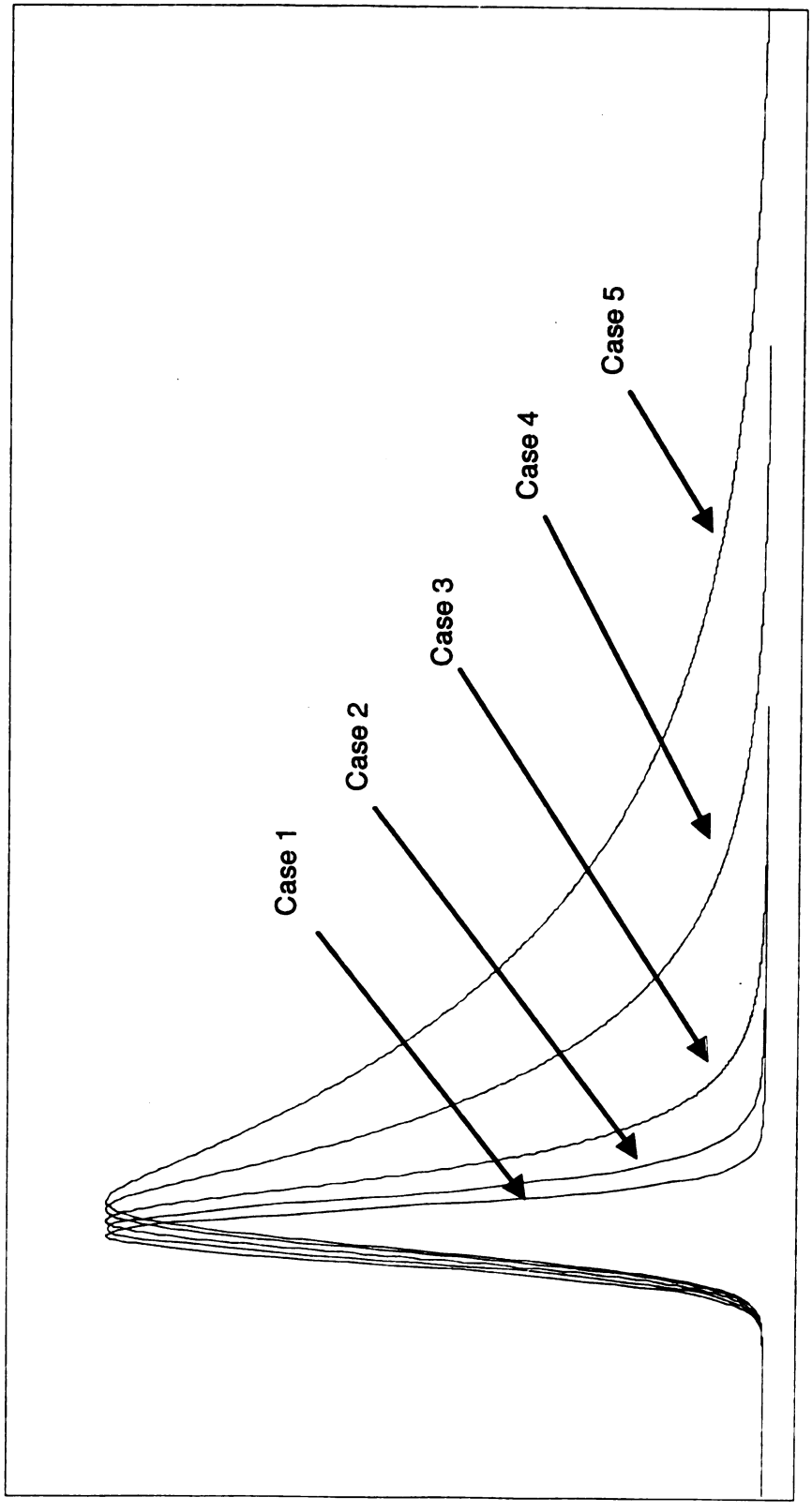

Figure 3.1

increa

symm

simula

integra

import

by nor

the EM

that is

3.2.1

nonlin

mathe

descrit

point o

the pro

The lim

(Figure

visual i

that the

infinity.

of 0.0%

limit ind

(e.g., a

increasing value of this ratio is indicative of profiles that vary from the symmetrical to the highly asymmetrical. The profiles were subjected to three simulation experiments, as described below, to examine the effect of the integration limits, number of points, and random noise. The profiles were then imported into Peakfit and evaluated by statistical moment calculation as well as by nonlinear regression using the EMG equation. The extracted parameters from the EMG equation (A_0, A_1, A_2, A_3) are the best fit for the true values (A, t_G, σ, τ), that is they yield the smallest standard error of the regression.

3.2.1 Integration Limits

The first simulation evaluated the effect of the integration limits on the nonlinear regression parameters and the resulting accuracy of the two mathematical methods. The process involved generating the profiles, as described above, and then truncating at different points along the baseline. The point of truncation corresponded to a fixed percentage of the maximum value for the profile and represented the boundaries of integration for Equations 2.1–2.3. The limits that were chosen varied from 0.0 to 1.0 % of the total peak height (Figure 3.2) and are representative of integration limits that might be selected by visual inspection of experimental data. For example, a limit of 0.0% indicates that the integrals in Equations 2.1–2.3 were evaluated from negative to positive infinity. Since the maximum peak height was equal to 100, an integration interval of 0.0% contained all points with a value greater than zero. A larger integration limit indicates that more of the zone profile was truncated before it was analyzed (e.g., a 1.0% truncation contains all points with a value greater than or equal to

Figure 3.2: Graphical representation of case 4 in which different integration limits were studied.

Figure 3.2

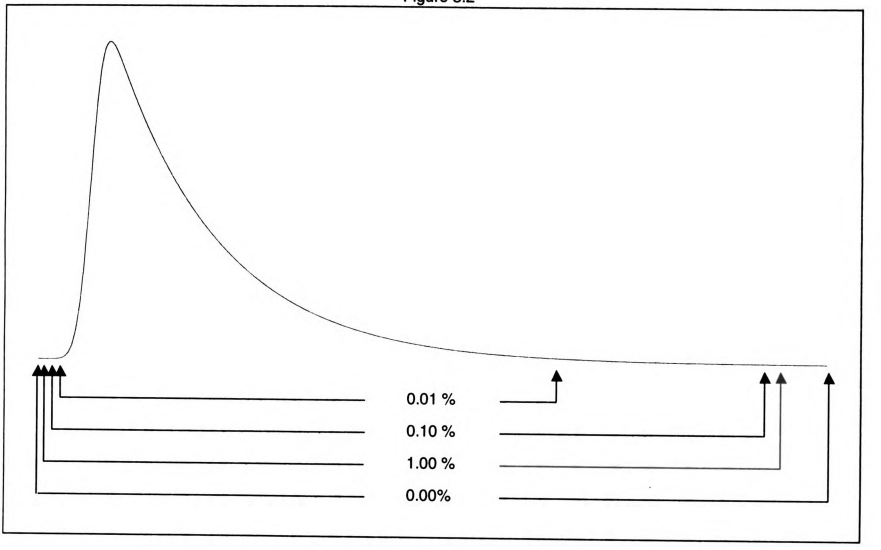

1). Th

above.

3.2.2 I

as mig

simula

asymr

profile

to extr

The t

profile

3.2.3

noise

maxi

to 1(

usin

nois

at e

sta

an

1). The resultant zone profiles were analyzed using the methodology described above.

3.2.2 Number of Points

The second simulation evaluated the effect of the number of data points, as might occur at different sampling rates. Case 4 was selected for this simulation, since it is representative of profiles with moderate levels of asymmetrical broadening. An integration limit of 0.10% was used to truncate the profile. In order to vary the number of points, a user-defined program was used to extract every n^{th} point, which were then exported to a separate file for analysis. The total number of points was varied from 10 to 398. The resultant zone profiles were analyzed using the methodology described above.

3.2.3 Noise

The final simulation evaluated the effect of random noise. Five different noise levels were chosen with standard deviations ranging from 0.1 to 10% of the maximum C(t) value. The corresponding signal-to-noise ratio varied from 1000 to 10. The random noise at each level was generated several different times using the random number generator in Microsoft Excel. Each of these generated noises was added separately to each profile, resulting in several different peaks at each τ/σ ratio. These replicate profiles were necessary to represent statistically the effect of random noise [4,5]. The resultant zone profiles were analyzed using the methodology described above.

3.3 Experimental Methods

A 10^{-3} M solution of saturated fatty acids ranging from C_{10} to C_{22} (Sigma) in anhydrous acetone was combined (1:1) with dry sodium sulfate, potassium bicarbonate, and dibenzo-18-crown-6 (Sigma). An excess of 4-bromomethyl-7-methoxycoumarin (Sigma) was added to the mixture and the solution was then allowed to react in the dark for 2 hours at 50 °C [6]. This reaction results in the addition of a fluorescent tag to the fatty acids and allows for detection via laser-induced fluorescence. The resultant solution was evaporated under a nitrogen stream and redissolved in high purity methanol (Baxter Healthcare, Burdick & Jackson Division) to yield a final concentration of 10^{-4} M. The unreacted 4-bromomethyl-7-methoxycoumarin serves as a void marker since it is unretained in this system. The fatty acids were then separated by capillary liquid chromatography [7] using the system (Figure 2.2) described in Chapter 2.2.3.2 by Dr. Chen. The zone profiles were extracted and analyzed by the statistical moment (Section 2.3.1.1) and EMG (Section 2.3.1.2) methods. The regression of the zone profiles to the EMG equation was excellent, with typical values for the square of the correlation coefficient (r^2) of 0.99 or greater. Other equations of kinetic origin, the Haarhoff–Van der Linde equation [8], and the non-linear chromatography equation [9] were also used. However, these functions were found to poorly fit the experimental data and evince nonrandom residuals.

3.4

3.4.1

from t

Table

of inte

of rec

statisti

statisti

conditi

3.4.1.1

interva

An inte

momer

larger i

emerge

regress

lack of

conseq

stati

3.4 Results and Discussion

3.4.1 Simulation Results

Zone profiles were generated with independent and varying contributions from the symmetrical (σ) and asymmetrical (τ) contributions, as summarized in Table 3.1. The purpose of the simulation experiments is to determine the effects of integration limits, number of points, and signal-to-noise ratio on the accuracy of recovery of the parameters of the EMG equation (A_0, A_1, A_2, A_3) and the statistical moments (M_0, M_1, M_2). In principle, both the EMG function and the statistical moments should accurately represent the simulated profiles if these conditions are properly chosen.

3.4.1.1 Integration Limits

The first simulation, detailed in Tables 3.2 and 3.3, varied the integration interval for the regression analysis from 0.0 to 1.0% of the maximum peak height. An integration interval of 0.00% results in no error between the EMG or statistical moments and the initial parameters, as would be expected. However, when the larger integration limits are evaluated, a deviation between the two methods emerges. The data in Table 3.2 demonstrate that there is no error in the regression parameters derived from the EMG equation for all five cases. This lack of error is attributed to the continuous nature of the EMG equation and its consequent ability to extrapolate beyond the provided integration limits. While the statistical moment method also returned no error at the 0.00% integration

Table 3.2: Regression parameters from the EMG model (A_0, A_1, A_2, A_3) recovered from simulated chromatographic peaks as a function of integration interval. (A) C(t) at limits of integration interval, expressed as % of maximum C(t) value, (B) Error A_0 (%) = $(A_0 - A) \times 100/A0$, (C) Error A_1 (%) = $(A_1 - t_G) \times 100/t_G$, (D) Error A_2 (%) = $(A_2 - \sigma) \times 100/\sigma$, (E) Error A_3 (%) = $(A3 - \tau) \times 100/\tau$

Table 3.2

Case	Integration Interval (%)[A]	EMG Parameters							
		A_0	Error A_0 (%) [B]	A_1 (s)	Error A_1 (%) [C]	A_2 (s)	Error A_2 (%) [D]	A_3 (s)	Error A_3 (%) [E]
1	0.0	137.41	0.00	5.000	0.00	0.500	0.00	0.250	0.00
	0.01	137.41	0.00	5.000	0.00	0.500	0.00	0.250	0.00
	0.1	137.41	0.00	5.000	0.00	0.500	0.00	0.250	0.00
	1.0	137.41	0.00	5.000	0.00	0.500	0.00	0.250	0.00
2	0.0	159.83	0.00	5.000	0.00	0.500	0.00	0.500	0.00
	0.01	159.83	0.00	5.000	0.00	0.500	0.00	0.500	0.00
	0.1	159.83	0.00	5.000	0.00	0.500	0.00	0.500	0.00
	1.00	159.83	0.00	5.000	0.00	0.500	0.00	0.500	0.00
3	0.0	210.42	0.00	5.000	0.00	0.500	0.00	1.000	0.00
	0.01	210.42	0.00	5.000	0.00	0.500	0.00	1.000	0.00
	0.1	210.42	0.00	5.000	0.00	0.500	0.00	1.000	0.00
	1.0	210.42	0.00	5.000	0.00	0.500	0.00	1.000	0.00
4	0.0	366.39	0.00	5.000	0.00	0.500	0.00	2.500	0.00
	0.01	366.39	0.00	5.000	0.00	0.500	0.00	2.500	0.00
	0.1	366.39	0.00	5.000	0.00	0.500	0.00	2.500	0.00
	1.0	366.39	0.00	5.000	0.00	0.500	0.00	2.500	0.00
5	0.0	623.41	0.00	5.000	0.00	0.500	0.00	5.000	0.00
	0.01	623.41	0.00	5.000	0.00	0.500	0.00	5.000	0.00
	0.1	623.41	0.00	5.000	0.00	0.500	0.00	5.000	0.00
	1.0	623.41	0.00	5.000	0.00	0.500	0.00	5.000	0.00

Table 3.3: Statistical moments (M_0, M_1, M_2) recovered from simulated chromatographic peaks as a function of integration interval. (A) C(t) at limits of integration interval, expressed as % of maximum C(t) value, (B) Error M_0 (%) = $(M_0 - A) \times 100/A_0$, (C) Error M_1 (%) = $(M_1 - (t_G + \tau)) \times 100/(t_G + \tau)$, (D) Error M_2 (%) = $(M_2 - (\sigma^2 + \tau^2)) \times 100/(\sigma^2 + \tau^2)$

Table 3.3

Case	Integration Interval (%)[A]	Moments					
		M_0	Error M_0 (%)[B]	M_1 (s)	Error M_1 (%)[C]	M_2 (s^2)	Error M_2 (%)[D]
1	0.0	137.40	0.00	5.250	0.00	0.312	0.00
	0.01	137.40	–0.01	5.250	0.00	0.312	–0.16
	0.1	137.36	–0.04	5.250	–0.01	0.311	–0.48
	1.0	136.85	–0.41	5.247	–0.06	0.299	–4.32
2	0.0	159.83	0.00	5.500	0.00	0.500	0.00
	0.01	159.82	–0.01	5.500	0.00	0.499	–0.20
	0.1	159.75	–0.05	5.499	–0.02	0.493	–1.40
	1.00	159.03	–0.50	5.490	–0.18	0.461	–7.80
3	0.0	210.42	0.00	6.000	0.00	1.250	0.00
	0.01	210.41	–0.01	5.999	-0.02	1.245	–0.40
	0.1	210.29	–0.06	5.996	–0.07	1.219	–2.48
	1.0	210.13	–0.14	5.974	–0.43	1.094	–12.5
4	0.0	366.39	0.00	7.500	0.00	6.500	0.00
	0.01	366.37	–0.01	7.498	–0.03	6.458	–0.65
	0.1	366.09	–0.08	7.487	–0.17	6.256	–3.75
	1.0	363.53	–0.78	7.411	–1.19	5.368	–17.4
5	0.0	623.41	0.00	10.000	0.00	25.250	0.00
	0.01	623.34	–0.01	9.995	–0.05	25.037	–0.84
	0.1	622.86	–0.09	9.971	–0.29	24.195	–4.18
	1.0	617.90	–0.88	9.801	–1.99	20.371	–19.3

limit, as v

errors be

in Table

cases.

the max

-0.88%

error is

momen

incapat

undere

the mo

differe

the eff

varian

chang

to -19

increa

limits.

mome

chose

mean

EMG

limit, as would be expected, the larger integration limits resulted in noticeable errors between the input parameters and the recovered parameters. As shown in Table 3.3, the error in the zeroth and first moments is relatively small for all five cases. While there is an increase in the error as the integration limits increase, the maximum error between M_0 and the true area (A) is only –0.88%, and between M_1 and the true retention time ($t_G + \tau$) is only –1.99%. This error is attributed to the discrete nature of the summation for the statistical moments in Equations 2.1 – 2.3. Consequently, the moment method is incapable of extrapolating beyond the provided data, which results in an underestimation of the true value. Note that the error generally increases with the moment number (n) for all cases. These larger errors arise because the difference ($t - M_1$) is raised to the n^{th} power in Equation 2.3, which exacerbates the effect of the integration limits. Accordingly, the error between M_2 and the true variance ($\sigma^2 + \tau^2$) becomes more pronounced as the integration limits are changed. The difference ranges from –0.16 to –4.32% for case 1 and from –0.84 to –19.3% for case 5. Thus, an increase in the asymmetry of the zone profile increases the error of the statistical moments that arises from the integration limits.

The conclusion that can be drawn from this simulation is that if statistical moments are to be used for experimental data, the integration limits must be chosen carefully (i.e. <0.10%) in order to insure that the retrieved values are meaningful. This observation has been noted previously [10]. In contrast, the EMG method can be used for larger integration limits without error.

3.4.1.2

numbe

Once a

the init

of the

Becau

error (

where

points

numb

for G

3.4.1.2 Number of Points

The second simulation, detailed in Tables 3.4 and 3.5, varied the point number used for the regression analyses from 10 to 398 points for case 4 only. Once again, there is no difference between the EMG regression parameters and the initial parameters (Table 3.4). This is another result of the continuous nature of the EMG function, which can interpolate between the provided data points. Because of its discrete nature, however, the statistical moment method results in error (Table 3.5). The overall error in the zeroth and first moments is small, whereas the error in the second moment becomes greater as the number of points is decreased. In general, the error is relatively minor as long as the number of points is greater than 50. This conclusion has been noted previously for Gaussian as well as more asymmetrical zone profiles [11].

Table 3.4: Regression parameters from the EMG model (A_0,A_1,A_2,A_3) recovered from simulated chromatographic peaks as a function of the number of points within the integration interval. (A) Number of points within the integration interval at 0.10% of maximum C(t) value, (B) Error A_0 (%) = $(A_0 - A) \times 100/A$, (C) Error A_1 (%) = $(A_1 - t_G) \times 100/t_G$, (D) Error A_2 (%) = $(A_2 - \sigma) \times 100/\sigma$, (E) Error A_3 (%) = $(A_3 - \tau) \times 100/\tau$

Table 3.4

Case	Point Number[A]	EMG Parameters							
		A_0	Error A_0 (%)[B]	A_1 (s)	Error A_1 (%)[C]	A_2 (s)	Error A_2 (%)[D]	A_3 (s)	Error A_3 (%)[E]
4	398	366.39	0.00	5.000	0.00	0.500	0.00	2.500	0.00
	284	366.39	0.00	5.000	0.00	0.500	0.00	2.500	0.00
	199	366.39	0.00	5.000	0.00	0.500	0.00	2.500	0.00
	153	366.39	0.00	5.000	0.00	0.500	0.00	2.500	0.00
	133	366.39	0.00	5.000	0.00	0.500	0.00	2.500	0.00
	111	366.39	0.00	5.000	0.00	0.500	0.00	2.500	0.00
	95	366.39	0.00	5.000	0.00	0.500	0.00	2.500	0.00
	83	366.39	0.00	5.000	0.00	0.500	0.00	2.500	0.00
	67	366.39	0.00	5.000	0.00	0.500	0.00	2.500	0.00
	57	366.39	0.00	5.000	0.00	0.500	0.00	2.500	0.00
	45	366.39	0.00	5.000	0.00	0.500	0.00	2.500	0.00
	20	366.39	0.00	5.000	0.00	0.500	0.00	2.500	0.00
	10	366.39	0.00	5.000	0.00	0.500	0.00	2.500	0.00

Table 3.5: Statistical moments (M_0,M_1,M_2) recovered from simulated chromatographic peaks as a function of the number of points within the integration interval. (A) Number of points within the integration interval at 0.10% of maximum C(t) value, (B) Error M_0 (%) = $(M_0 - A) \times 100/A$, (C) Error M_1 (%) = $(M_1 - (t_G + \tau)) \times 100/(t_G + \tau)$, (D) Error M_2 (%) = $(M_2 - (\sigma^2 + \tau^2)) \times 100/(\sigma^2 + \tau^2)$

Table 3.5

Case	Point Number[A]	Moments					
		M_0	Error M_0 (%)[B]	M_1 (s)	Error M_1 (%)[C]	M_2 (s^2)	Error M_2 (%)[D]
4	398	366.12	–0.07	7.487	–0.169	6.265	–3.608
	284	366.11	–0.08	7.487	–0.174	6.261	–3.682
	199	366.10	–0.08	7.487	–0.177	6.257	–3.741
	153	366.09	–0.08	7.486	–0.182	6.251	–3.834
	133	366.09	–0.08	7.486	–0.182	6.252	–3.823
	111	366.09	–0.08	7.486	–0.184	6.248	–3.873
	95	366.08	–0.09	7.486	–0.191	6.241	–3.992
	83	366.06	–0.09	7.485	–0.198	6.233	–4.115
	67	366.06	–0.09	7.485	–0.196	6.235	–4.080
	57	366.03	–0.10	7.484	–0.215	6.213	–4.414
	45	366.03	–0.10	7.484	–0.211	6.217	–4.352
	20	365.86	–0.14	7.473	–0.360	6.046	–6.987
	10	385.80	5.30	7.302	–2.641	5.905	–9.155

3.4.1.

noise

positi

repre

devia

the p

statis

a fini

zero.

More

than

discr

dem

stan

0.01

for t

leve

dev

This

valu

3.4.1.3 Noise

The final simulation, detailed in Table 3.6 and 3.7, varied the random noise from 0.1 to 10% of the total peak height. Since noise can take on both positive and negative values, a single profile would not be statistically representative of the effect on the regression parameters. Thus, the standard deviation for multiple profiles is reported in addition to the error as calculated in the previous studies.

As the number of profiles increases, the error in both the EMG and statistical moment methods is theoretically expected to approach zero. Because a finite number of profiles was used, typically five to ten, the error is small but not zero. In general, the error increases slightly as the noise level increases. Moreover, the error in the EMG regression parameters (Table 3.6) is slightly less than that in the statistical moments (Table 3.7) because of the continuous and discrete natures, respectively.

The standard deviations are more meaningful than the errors since they demonstrate the variability with increasing amounts of noise. The relative standard deviation for the EMG parameters is very small, typically ranging from 0.01 to 1.5% for A_0 to A_2. The greatest relative standard deviation is observed for the exponential component A_3, which is as high as 5.9% for the highest noise levels. An increase in asymmetry causes an increase in the relative standard deviation for A_0 to A_2, but a decrease in the relative standard deviation for A_3. This trend is observed because it is more difficult to accurately determine small values for the exponential component when noise is present.

Table 3.6: Regression parameters from the EMG model (A_0, A_1, A_2, A_3) recovered from simulated chromatographic peaks as a function of the noise level.

(A) Standard deviation of the random noise level, expressed as % of maximum C(t) value, (B) Error A_0 (%) = $(A_0 - A) \times 100/A$, (C) Error A_1 (%) = $(A_1 - t_G) \times 100/t_G$, (D) Error A_2 (%) = $(A_2 - \sigma) \times 100/\sigma$, (E) Error A_3 (%) = $(A_3 - \tau) \times 100/\tau$

Table 3.6

Case	Noise Level (%)[A]	EMG Parameters							
		A_0	Error A_0 (%)[B]	A_1 (s)	Error A_1 (%)[C]	A_2 (s)	Error A_2 (%)[D]	A_3 (s)	Error A_3 (%)[E]
1	0.1	137.41 ± 0.01	0.00	5.000 ± 0.000	0.001	0.500 ± 0.000	–0.002	0.250 ± 0.000	–0.008
	0.5	137.42 ± 0.03	0.01	5.000 ± 0.001	–0.004	0.500 ± 0.000	–0.013	0.250 ± 0.001	0.084
	1.0	137.42 ± 0.01	0.01	5.000 ± 0.001	0.004	0.500 ± 0.000	0.052	0.250 ± 0.001	–0.093
	5.0	137.54 ± 0.33	0.09	4.997 ± 0.005	–0.059	0.500 ± 0.002	0.028	0.254 ± 0.007	1.405
	10.0	137.22 ± 0.59	–0.14	5.009 ± 0.011	0.175	0.503 ± 0.003	0.572	0.239 ± 0.014	–4.211
2	0.1	159.83 ± 0.01	0.00	5.000 ± 0.000	0.000	0.500 ± 0.000	0.002	0.500 ± 0.000	–0.004
	0.5	159.82 ± 0.04	–0.01	5.000 ± 0.000	0.006	0.500 ± 0.000	0.037	0.500 ± 0.000	–0.087
	1.0	159.81 ± 0.08	–0.01	5.000 ± 0.000	0.002	0.500 ± 0.000	–0.030	0.500 ± 0.001	–0.053
	5.0	159.72 ± 0.26	–0.07	5.000 ± 0.004	–0.005	0.499 ± 0.003	–0.243	0.501 ± 0.008	0.176
	10.0	159.32 ± 1.22	–0.32	5.005 ± 0.006	0.091	0.505 ± 0.005	0.985	0.487 ± 0.010	–2.543
3	0.1	210.39 ± 0.01	–0.01	5.000 ± 0.000	0.001	0.500 ± 0.000	0.002	1.000 ± 0.000	–0.001
	0.5	210.37 ± 0.05	–0.03	5.000 ± 0.000	0.003	0.500 ± 0.000	0.007	0.999 ± 0.001	–0.053
	1.0	210.35 ± 0.12	–0.03	5.000 ± 0.000	–0.001	0.500 ± 0.000	–0.018	1.000 ± 0.001	–0.009
	5.0	210.74 ± 0.58	0.15	4.999 ± 0.004	–0.012	0.497 ± 0.003	–0.580	1.004 ± 0.011	0.352
	10.0	210.89 ± 0.85	0.22	5.003 ± 0.005	0.067	0.500 ± 0.006	0.012	1.000 ± 0.016	–0.026
4	0.1	366.51 ± 0.02	0.03	5.000 ± 0.000	0.001	0.500 ± 0.000	0.003	2.500 ± 0.000	0.000
	0.5	366.43 ± 0.07	0.01	5.000 ± 0.000	0.006	0.500 ± 0.000	–0.005	2.499 ± 0.001	–0.047
	1.0	366.52 ± 0.18	0.03	5.002 ± 0.005	0.045	0.500 ± 0.001	0.035	2.500 ± 0.004	0.012
	5.0	366.76 ± 0.72	0.10	5.000 ± 0.004	–0.003	0.501 ± 0.004	0.246	2.500 ± 0.007	0.010
	10.0	366.50 ± 1.83	0.03	5.001 ± 0.006	0.028	0.502 ± 0.007	0.492	2.485 ± 0.023	–0.592
5	0.1	623.40 ± 0.06	0.00	5.000 ± 0.000	0.001	0.500 ± 0.000	0.009	5.000 ± 0.001	0.003
	0.5	623.36 ± 0.14	–0.01	5.000 ± 0.000	0.000	0.500 ± 0.001	0.073	5.000 ± 0.001	0.000
	1.0	623.18 ± 0.26	–0.04	5.000 ± 0.001	–0.003	0.500 ± 0.001	0.008	4.999 ± 0.000	–0.025
	5.0	622.71 ± 1.20	–0.11	5.003 ± 0.006	0.057	0.500 ± 0.007	–0.068	5.010 ± 0.025	0.195
	10.0	626.12 ± 5.05	0.43	4.998 ± 0.011	–0.047	0.496 ± 0.012	–0.837	5.033 ± 0.070	0.668

Table 3.7: Statistical moments (M_0, M_1, M_2) recovered from simulated chromatographic peaks as a function of the noise level. (A) Standard deviation of the random noise level, expressed as % of maximum C(t) value, (B) Error M0 (%) = $(M_0 - A) \times 100/A$, (C) Error M_1 (%) = $(M_1 - (t_G + \tau)) \times 100/(t_G + \tau)$, (D) Error M_2 (%) = $(M_2 - (\sigma^2 + \tau^2)) \times 100/(\sigma^2 + \tau^2)$

Table 3.7

Case	Noise Level (%)[A]	Moments					
		M_0	Error M_0 (%)[B]	M_1 (s)	Error M_1 (%)[C]	M_2 (s^2)	Error M_2 (%)[D]
1	0.1	137.37 ± 0.01	–0.030	5.250 ± 0.000	–0.006	0.311 ± 0.000	–0.563
	0.5	137.38 ± 0.04	–0.018	5.250 ± 0.000	–0.006	0.311 ± 0.000	–0.504
	1.0	137.37 ± 0.02	–0.028	5.250 ± 0.001	–0.008	0.311 ± 0.000	–0.596
	5.0	137.47 ± 0.44	–0.041	5.249 ± 0.003	–0.016	0.311 ± 0.006	–0.421
	10.0	137.24 ± 0.68	–0.123	5.248 ± 0.006	–0.031	0.310 ± 0.006	–0.680
2	0.1	159.77 ± 0.01	–0.039	5.499 ± 0.000	–0.023	0.494 ± 0.001	–1.261
	0.5	159.75 ± 0.05	–0.048	5.499 ± 0.001	–0.025	0.493 ± 0.001	–1.324
	1.0	159.76 ± 0.05	–0.045	5.499 ± 0.001	–0.026	0.494 ± 0.002	–1.291
	5.0	159.49 ± 0.30	–0.210	5.500 ± 0.007	–0.003	0.489 ± 0.018	–2.130
	10.0	159.32 ± 1.47	–0.322	5.494 ± 0.009	–0.120	0.491 ± 0.026	–1.832
3	0.1	210.27 ± 0.01	–0.070	5.996 ± 0.000	–0.062	1.220 ± 0.001	–2.437
	0.5	210.24 ± 0.06	–0.086	5.996 ± 0.001	–0.071	1.218 ± 0.006	–2.555
	1.0	210.23 ± 0.16	–0.088	5.996 ± 0.002	–0.058	1.219 ± 0.012	–2.510
	5.0	210.59 ± 0.75	0.080	6.002 ± 0.008	–0.026	1.236 ± 0.050	–1.122
	10.0	210.74 ± 1.21	0.150	5.996 ± 0.009	–0.070	1.200 ± 0.042	–4.005
4	0.1	366.23 ± 0.03	–0.045	7.486 ± 0.002	–0.187	6.260 ± 0.004	–3.699
	0.5	366.15 ± 0.16	–0.064	7.486 ± 0.005	–0.192	6.265 ± 0.049	–3.620
	1.0	366.24 ± 0.30	–0.040	7.488 ± 0.015	–0.156	6.273 ± 0.224	–3.487
	5.0	366.61 ± 1.52	0.060	7.495 ± 0.028	–0.068	6.424 ± 0 .318	–1.172
	10.0	366.81 ± 2.13	0.113	7.489 ± 0.044	–0.148	6.455 ± 0.523	–0.689
5	0.1	622.88 ± 0.08	–0.084	9.971 ± 0.001	–0.283	24.228 ± 0.029	–4.049
	0.5	622.81 ± 0.20	–0.097	9.971 ± 0.005	–0.290	24.214 ± 0.096	–4.103
	1.0	622.51 ± 0.39	–0.143	9.966 ± 0.096	–0.338	24.158 ± 0.240	–4.326
	5.0	622.92 ± 1.74	–0.078	9.975 ± 0.042	–0.248	24.105 ± 0.877	–4.533
	10.0	625.52 ± 5.81	0.339	9.977 ± 0.156	–0.234	23.946 ± 3.177	–5.165

large

comp

M_2 a

for th

EMG

noise

most

unde

integ

analy

contr

relati

the a

3.4.2

math

resul

reliab

and p

can b

each

The standard deviation for the statistical moment method is somewhat larger than that for the EMG method. The relative standard deviation for M_0 is comparable to that for A_0. However, the relative standard deviations for M_1 and M_2 are significantly larger, typically ranging from 0.06 to 13.2%. The deviations for the moments increase with the asymmetry and the noise level, just as for the EMG parameters. The results summarized in Table 3.5 indicate that random noise does affect the statistical moments, with the second moment being the most susceptible to such fluctuations.

When all of the tables are analyzed, a single conclusion emerges: only under conditions in which the solute zone has a small amount of tailing, small integration limits, a large number of points, and low noise can statistical moment analysis be used without significant contributions from user defined errors. In contrast, for each of the simulations, the EMG function has been shown to be relatively insensitive to the variables and, as a result, should be better suited for the analysis of experimental data in which the amount of tailing is significant.

3.4.2 Experimental Results

The simulation studies provide insight into the differences between the two mathematical methods and the accuracy of the recovered parameters. The results of these studies are important because they can be used to determine the reliability of reported chromatographic figures of merit such as the plate number and plate height. In addition, the accuracy of thermodynamic and kinetic data can be established on the basis of the calculated errors and the limitations of each method.

Figure 3.3: Separation of saturated fatty acids ranging from C_{10} to C_{22} by capillary liquid chromatography with on-column laser-induced fluorescence detection at T = 303 K and P = 3000 psi. Experimental conditions as given in the text. (A) Detector 1, 23.2 cm from the head of the column, (B) Detector 2, 28.4 cm, (C) Detector 3, 51.4 cm,(D) Detector 4, 56.9 cm.

Figure 3.3

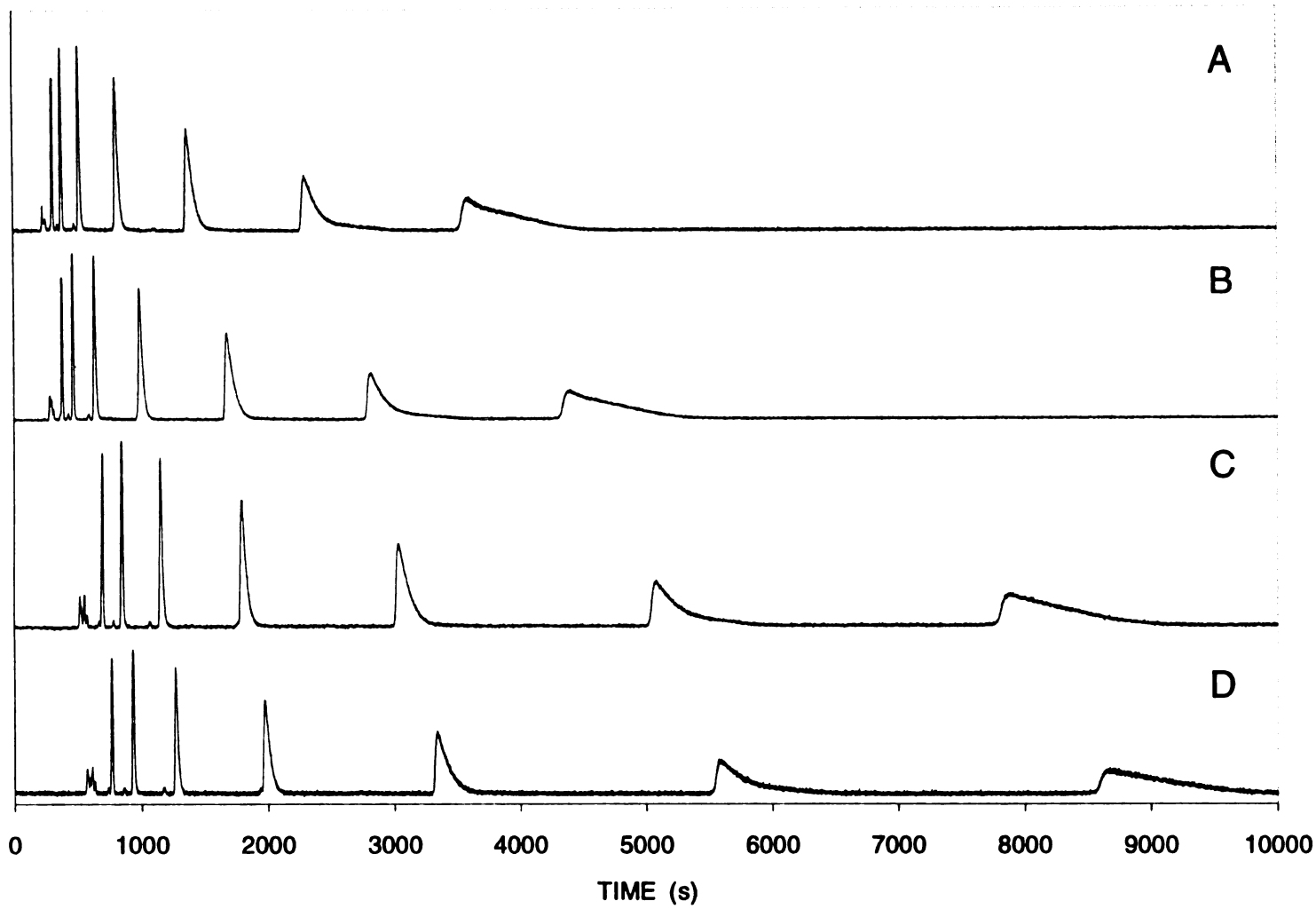
A
B
C
D
0
1000
2000
3000
4000
5000
6000
7000
8000
9000
10000
TIME (s)

Figure

distanc

column

volume

small a

contrib

to the s

that ar

be dire

the sol

the ret

distanc

therm

throug

3.5, σ^2

is equ

linearl

reache

σ^2 with

contri

A series of chromatograms of the saturated fatty acids is included in Figure 3.3. Each chromatogram is representative of the separation at specified distances of 23.2, 28.4, 51.4, and 56.9 cm along the column. The use of on-column detection minimizes extracolumn contributions to the zone profile. Any volumetric contributions that arise from the injector, detector, or connectors are small and constant at each of the detectors. In addition, the electronic contributions are also constant since each photomultiplier tube is directly coupled to the same amplifier and data acquisition system. The result of this design is that any changes in the solute zone profile that occur between the detectors can be directly attributed to mass transfer and retention events [12].

To ensure that the behavior of the solutes is consistent, the properties of the solute zones are graphed as a function of distance. As shown in Figure 3.4, the retention factor for all of the fatty acids remains constant with increasing distance. Having established that the retention factor and, hence, the thermodynamic behavior is constant, the kinetic behavior is then investigated through the symmetrical and asymmetrical contributions to broadening. In Figure 3.5, σ^2 is plotted versus distance on a logarithmic scale. The slope of these lines is equal to unity (1.000 ± 0.002), which indicates that variance is increasing linearly with distance and that the symmetrical broadening processes have reached steady state for all solutes. For C_{10} and C_{12}, there is little difference in σ^2 with increasing distance. Thus, the symmetrical broadening processes contribute only a minimal amount to the overall value of σ^2 for these solutes.

Figure 3.4: Logarithmic graph of the retention factor versus distance on the column for the saturated fatty acids C_{10} (○), C_{12} (□), C_{14} (△), C_{16} (◇), C_{18} (●), C_{20} (■), C_{22} (▲). Data derived from the chromatograms in Figure 3.3.

Figure 3.4

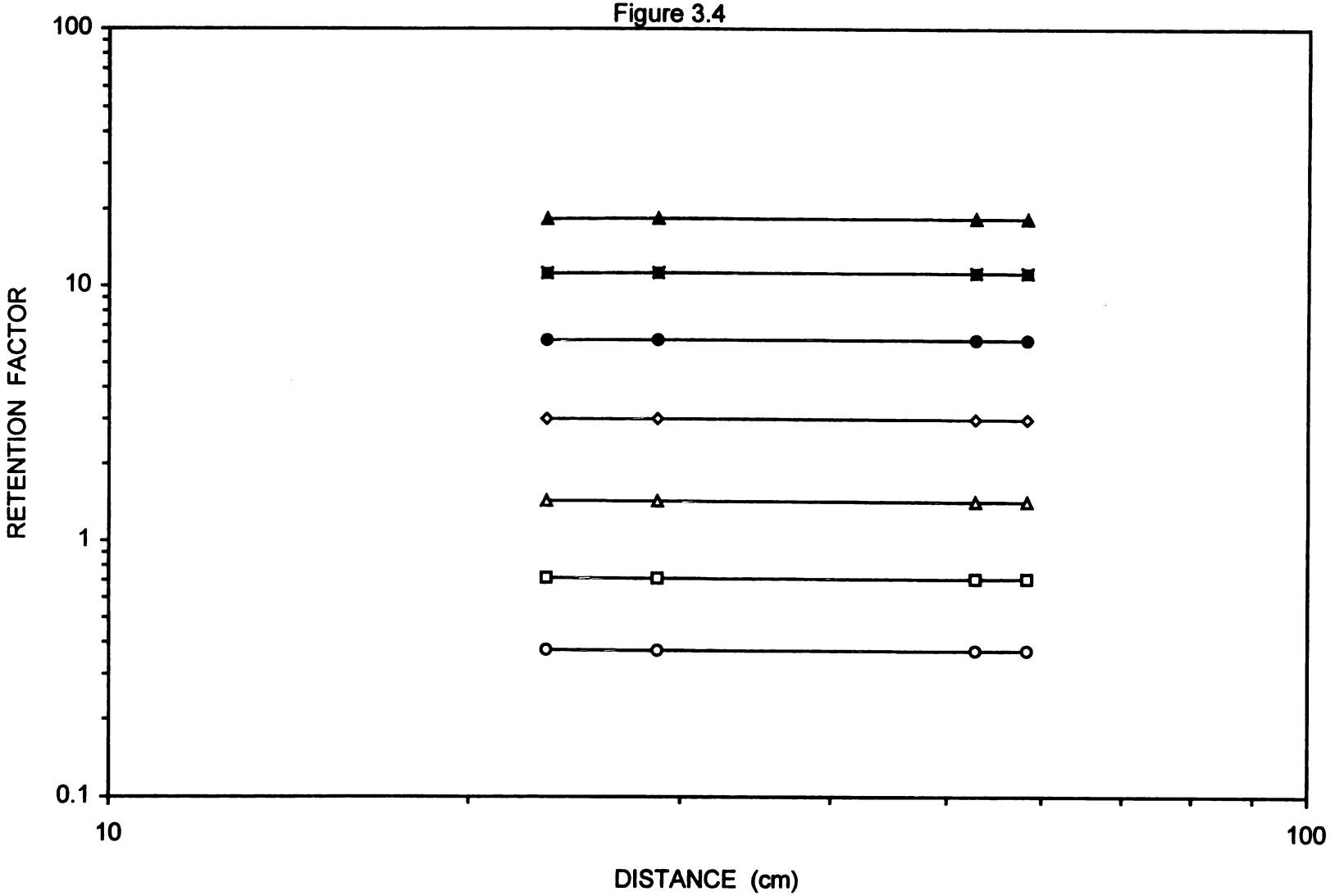

Figure 3.5: Logarithmic graph of σ^2 versus distance on the column for the saturated fatty acids. Data derived from the chromatograms in Figure 3.3, symbols defined in Figure 3.4.

Figure 3.5

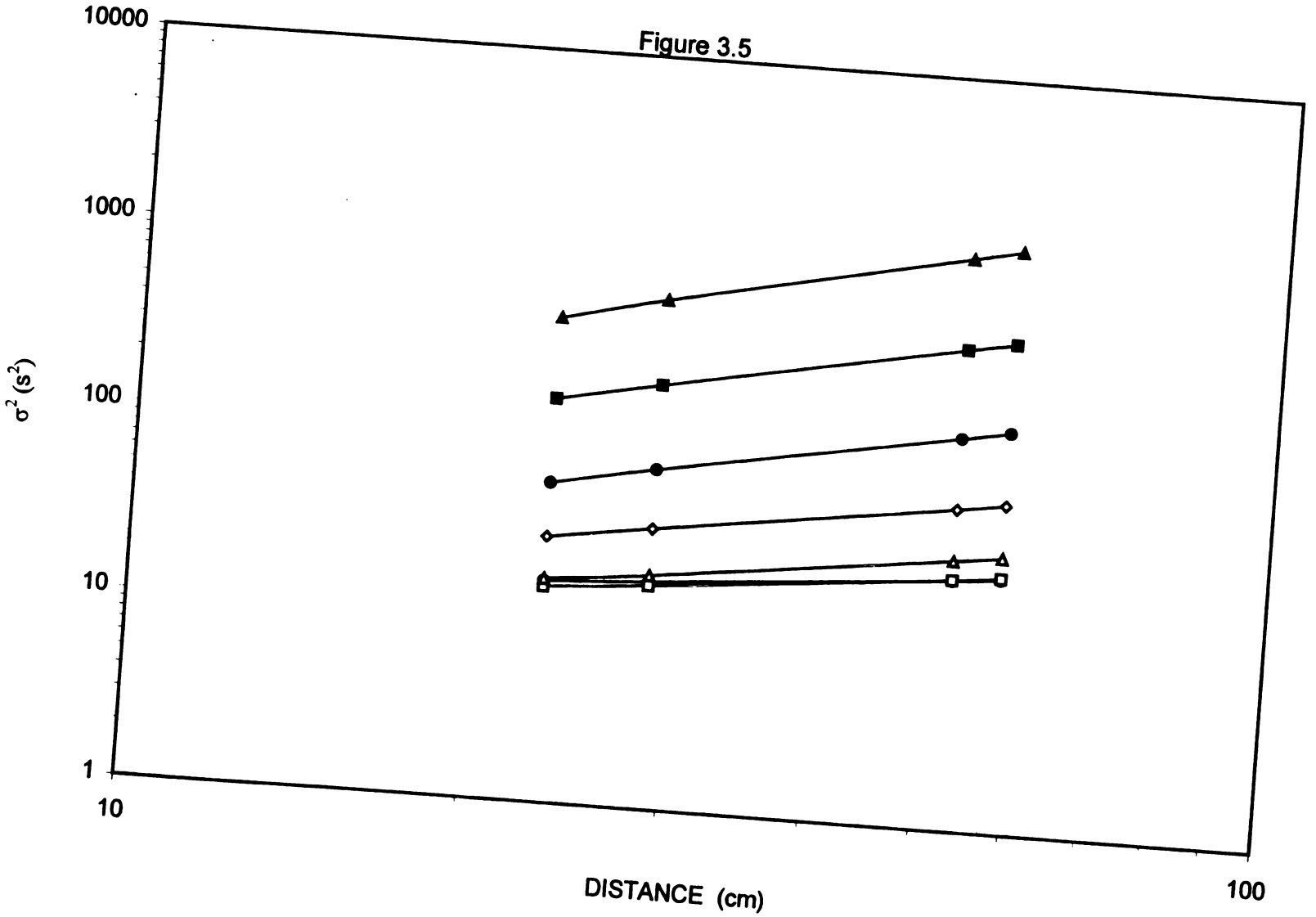

Howe

for C·

graph

(0.99

broac

in τ in

becor

possil

varyin

the lin

asymı

then t

contri

distan

τ is o

acids

and st

equati

mentic

The m

descri

However, a systematic increase in σ^2 is observed with increasing carbon number for C_{14} to C_{22}.

In Figure 3.6, τ^2 is plotted versus distance on a logarithmic scale. This graph also exhibits a linear increase with distance with a slope equal to unity (0.999 ± 0.002). This value of the slope indicates that the asymmetrical broadening processes have achieved steady state for all solutes. This increase in τ indicates that there is either a kinetic effect or nonlinear isotherm that becomes more pronounced with increased distance along the column. The possibility of a nonlinear isotherm can be rejected, since a series of solutions with varying concentration was injected to insure that the final concentration was on the linear portion of the isotherm. Similarly, instrumental contributions to the asymmetry can be discounted. Were τ to arise solely from instrumental effects, then the value would be constant with distance because the extracolumn contributions are the same at each detector. Thus, any increase in τ with distance must be the effect of slow kinetics. In addition, a systematic increase in τ^2 is observed with increasing carbon number for all solutes.

In order to demonstrate these trends more effectively, the data for the fatty acids are tabulated in Table 3.8 as a function of carbon number for both the EMG and statistical moment methods. The regression parameters from the EMG equation (A_0, A_1, A_2, A_3) show the expected increase with carbon number, as mentioned above. The statistical moments (M_0, M_1, M_2) show similar trends. The most interesting data, however, are contained in the final three columns that describe the differences between the moment and EMG methods. The first of

Figure 3.6: Logarithmic graph of τ^2 versus distance on the column for the saturated fatty acids. Data derived from the chromatograms in Figure 3.3, symbols defined in Figure 3.4.

Figure 3.6

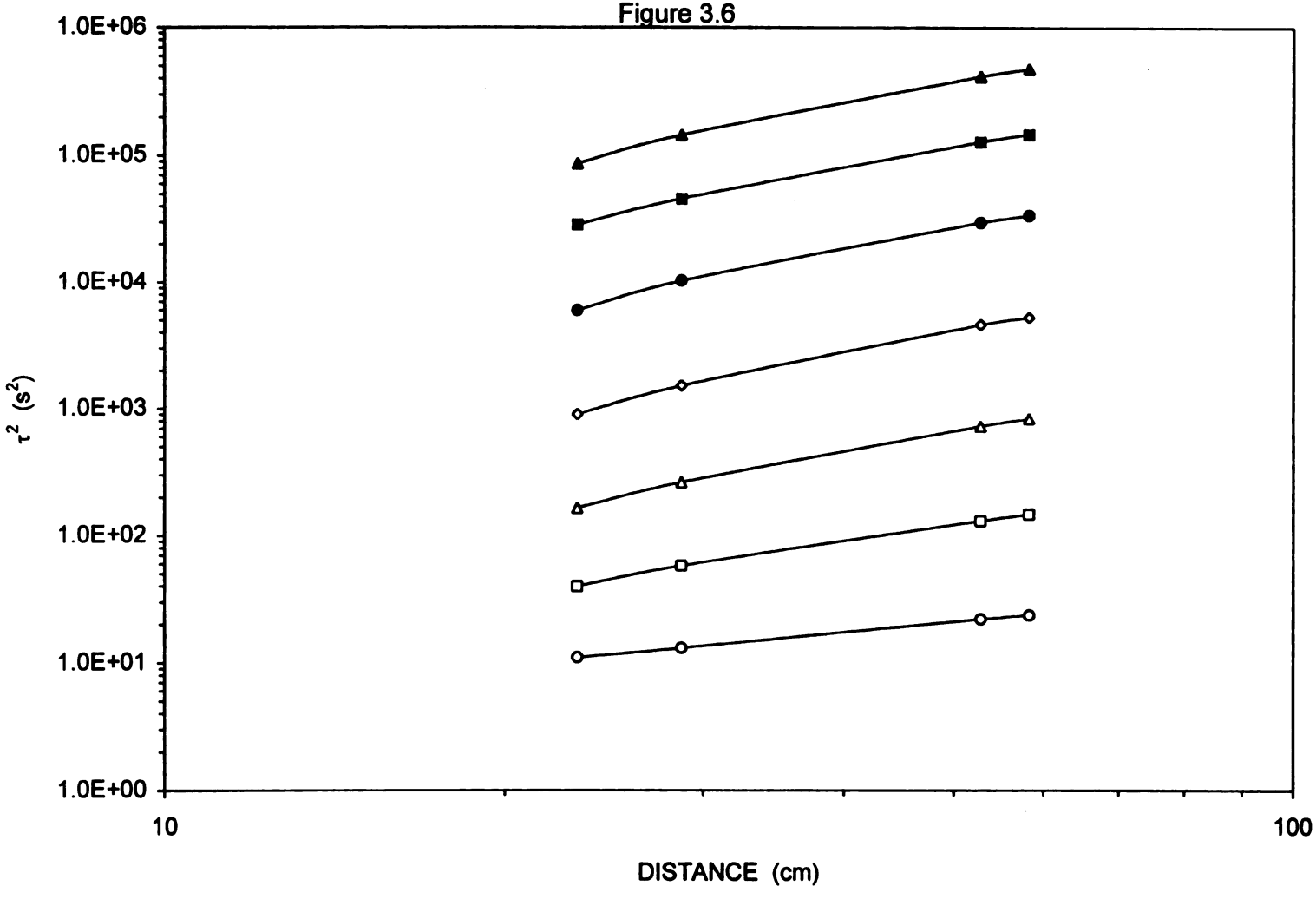
1.0E+06
1.0E+05
1.0E+04
1.0E+03
1.0E+02
1.0E+01
1.0E+00
τ² (s²)
10
100
DISTANCE (cm)

Table 3.8: Statistical indicators of fit and regression parameters from the EMG model (A_0, A_1, A_2, A_3) and statistical moments (M_0, M_1, M_2) recovered from experimental chromatographic peaks in Figure 3.1. (A) ΔM_0 (%) = $(M_0 - A_0) \times 100/A_0$, (B) ΔM_1 (%) = $(M_1 - (A_1 + A_3)) \times 100/(A_1 + A_3)$, (C) ΔM_2 (%) = $(M_2 - (A_2^2 + A_3^2)) \times 100/(A_2^2 + A_3^2)$

Table 3.8

Carbon Number	R^2 (F)	A_0	A_1 (s)	A_2 (s)	A_3 (s)	M_0	M_1 (s)	M_2 (s)	ΔM_0 (%)[A]	ΔM_1 (%)[B]	ΔM_2 (%)[C]
10	0.999 (50808)	106,500	799.2	4.74	4.88	104,100	803.7	36.80	–2.29	–0.04	–20.5
12	0.998 (33290)	175,700	995.5	4.79	12.18	164,900	1,006	90.11	–6.54	–0.20	–47.4
14	0.997 (33995)	282,700	1,409	5.43	28.97	239,100	1,428	231.4	–18.2	–0.67	–73.4
16	0.996 (71270)	464,400	2,318	7.50	72.63	401,100	2,369	1,545	–15.8	–0.90	–71.0
18	0.994 (60224)	754,600	4,130	11.73	183.3	653,400	4,257	9,588	–15.5	–1.29	–71.6
20	0.992 (47396)	1,086,000	7,093	20.21	382.0	962,500	7,372	47,540	–12.8	–1.38	–67.5
22	0.983 (20693)	1,263,000	11,200	35.69	687.3	1,103,000	11,680	140,400	–14.5	–1.70	–70.4

the

and

exh

bet

ran

time

less

larg

betv

the

is o

70%

disc

bee

that

Equ

cont

expe

lead

asyn

have

than

resid

these columns describes the error that is inherent in the area (M_0, A_0). For C_{10} and C_{12}, the errors are relatively small. However, for the larger molecules that exhibit greater symmetrical and asymmetrical broadening, the difference between the moment and the corresponding EMG parameter is much larger, ranging from –12.8 to –18.2%. The errors associated with the mean retention time (M_1, $A_1 + A_3$) are much smaller than those associated with the area, typically less than –1.7%. However, the error in the variance (M_2, $A_2^2 + A_3^2$) is much larger. Although the simulation results above suggest that the difference between the moment analysis and the EMG parameters may be as high as 20%, the experimental data demonstrate even larger errors. The error for C_{10} and C_{12} is on the order of 20 and 48%, respectively, whereas there is a consistent error of 70% for C_{14} to C_{22}. It should be noted that that any error arising from the sources discussed previously (integration limits, number of points, and noise) has already been minimized. Thus, the large difference between the two methods indicates that the second moment is not equal to the sum of σ^2 and τ^2, as given by Equation 3.3. As mentioned previously, this equation presumes that the contributions from σ^2 and τ^2 are independent, which may not be true for this experimental system. Rather, the data suggest that the retention processes leading to symmetrical broadening are coupled with those leading to asymmetrical broadening. This suggestion is reasonable, since each solute will have a wide range of possible residence times within the stationary phase rather than a fixed value [13]. An individual sojourn in the stationary phase with a short residence time will contribute to the symmetrical broadening, whereas those with

longer residence times will contribute to the asymmetrical broadening. As shown in Figure 3.7, the ratio of the asymmetrical and symmetrical contributions (τ^2/σ^2) increases systematically with carbon number for solutes up to C_{18}. In other words, the asymmetrical contribution from slow kinetics becomes more important with increasing carbon number. This observation is intuitively reasonable because the diffusion coefficient in the stationary phase will decrease with increasing carbon number, leading to longer residence times. It is noteworthy, however, that the τ^2/σ^2 ratio remains relatively constant for solutes larger than C_{18}. Since the C_{20} and C_{22} solutes cannot insert completely into the octadecylsilica stationary phase, their kinetic contribution is no greater than that for C_{18}. It is apparent from these results that the symmetrical (σ) and asymmetrical (τ) contributions are not independent in this system. Consequently, the method of calculating τ from Equation 3.3 [2,3,10] is incorrect and kinetic data derived in this manner should be considered suspect.

Figure 3.7: Logarithmic graph of τ^2/σ^2 versus carbon number for the saturated fatty acids. Data derived from the chromatograms in Figure 3.3.

Figure 3.7

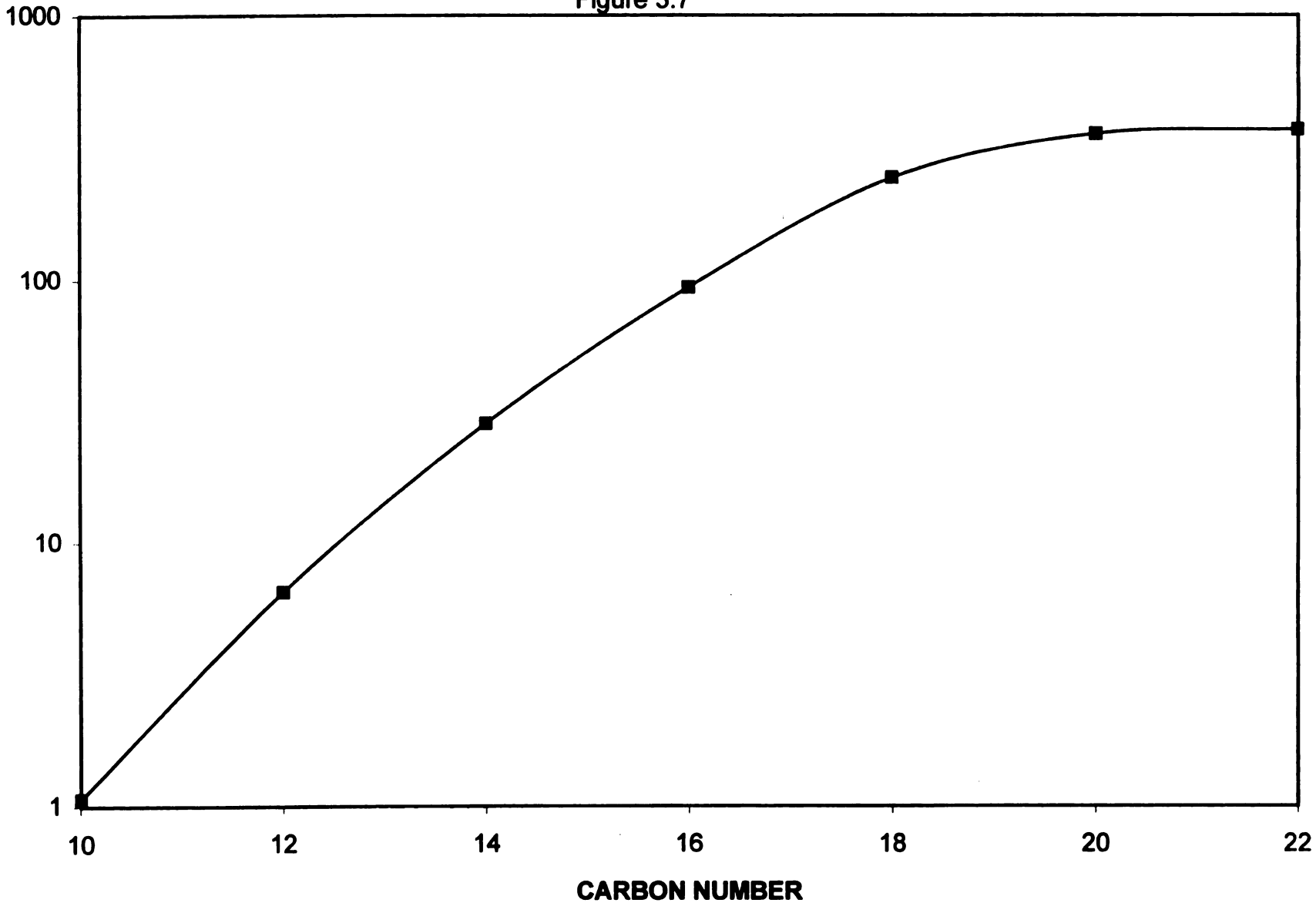

3.5 Conclusions

Although the use of statistical moments for the analysis of chromatographic data is commonplace, the use of moments in the derivation of secondary variables is problematic. As demonstrated by the simulation data, the use of moments to calculate parameters from the EMG model can lead to errors. As a result, the use of an appropriate model is critical for characterizing the molecular level processes that contribute to retention. In addition, the constant values for the retention factors as a function of distance, as well as the linear increases in σ and τ as a function of distance demonstrate that the experimental design and data collection do not lead to significant error. Thus, this chapter demonstrates that the method by which the data are collected and analyzed is valid for the analysis of the molecular contributions to retention.

3.6

[1]

[2]

[3]

[4]

[5]

[6]

[7]

[8]

[9]

[10]

[11]

[12]

[13]

3.6 References

[1] J.C. Giddings, Dynamics of Chromatography, Marcel Decker, New York, NY, USA, 1965.

[2] J.P. Foley, J.G. Dorsey, J. Chromatogr. Sci. 22 (1983) 40-46.

[3] M.S. Jeansonne, J.P. Foley, J. Chromatogr. 461 (1989) 149-163.

[4] J.V.H. Schudel, G. Guiochon, J. Chromatogr. 457 (1988) 1-12.

[5] V.B. Di Marco, C.G. Bombi, J. Chromatogr. A 931 (2001) 1-30.

[6] V.L. McGuffin, R.N. Zare, Appl. Spectrosc. 39 (1985) 847-853.

[7] V.L. McGuffin, S.-H. Chen, J. Chromatogr. A 762 (1997) 35-46.

[8] P.C. Haarhoff, H.J. Van der Linde, Anal. Chem. 38 (1966) 573-582.

[9] J.L. Wade, A.F. Bergold, P.W. Carr, Anal. Chem. 59 (1987) 1286-1295.

[10] D.J. Anderson, R.R. Walters, J. Chromatogr. Sci. 22 (1984) 353-359.

[11] S.N. Chesler, S.P. Cram, Anal. Chem. 43 (1971) 1922-1933.

[12] C.E. Evans, V.L. McGuffin, Anal. Chem. 60 (1988) 573-577.

[13] V.L. McGuffin, P.E. Krouskop, D.L. Hopkins, in J.F. Parcher, T.L. Chester (Editors), ACS Symp. Ser., Washington, DC, 1999, p. 37.

Chapter 4: Retention of Polycyclic Aromatic Hydrocarbons: Effect of Ring Number, Planarity and Stationary Phase Bonding Density

4.1 Introduction

One method traditionally used to investigate PAHs has been reversed-phase liquid chromatography (RPLC). By using RPLC, the retention of PAHs has been studied as a function of many parameters. Previous investigations have sought to explore the retention event as a function of solute structure [1-4], stationary phase chain length and bonding density [1,2,5-8], mobile phase composition [1,8], temperature [1,9,10], and pressure[11,12]. The investigations into solute structure demonstrated that ring number, annelation, and planarity have a large effect on the overall retention [2-5]. From these experiments, many authors have attempted to explain the mechanism of retention (i.e. partition or adsorption) on the basis of the thermodynamically derived value of molar enthalpy and the general shape of the van't Hoff plot. However, thermodynamic data alone fail to consider the kinetic aspects of retention. Without kinetic data, a thorough description of the retention mechanism cannot be developed.

Using the mathematical analyses in Chapter 1 and the chromatographic system described in Chapter 2, the retention behavior of a series of six polycyclic aromatic hydrocarbons (PAHs) was studied and characterized using thermodynamic and kinetic theory. These solutes were studied as a function of ring number and planarity. The thermodynamics and kinetics are measured simultaneously, permitting a correlation of these processes that has not

te

4

4

ch

th

(C

Te

(B

co

se

(S

be

c]p

to i

me

cor

eac

previously been possible. These studies were completed as a function of temperature, pressure, and stationary phase bonding density.

4.2 Experimental Methods

4.2.1 Solutes

As depicted in Figure 4.1, six polycyclic aromatic hydrocarbons have been chosen to investigate the effect of ring number and planarity on the thermodynamics and kinetics of retention. Phenanthrene (Ph) and chrysene (Chr) (Sigma-Aldrich), and picene (Pic) (National Institute of Standards and Technology) were obtained as solids and dissolved in high-purity methanol (Burdick and Jackson, Baxter Healthcare) to yield standard solutions at a concentration of 10^{-4} M. These three solutes were chosen as a homologous series to study the effects of ring addition on retention. In addition a sample (SRM 869, National Institute of Standards and Technology) containing benzo[*a*]pyrene (BaP), tetrabenzonaphthalene (TBN) and phenanthro[*3,4-c*]phenanthrene (PhPh) was used as received. These three solutes were chosen to investigate the effect of planarity on retention. A nonretained marker, 4-methylhydroxy-7-methoxycoumarin, was added to each solution at a concentration of 10^{-4} M. To ensure solubility, the solutions were equilibrated at each temperature prior to analysis.

Figure 4.1: Structure of polycyclic aromatic hydrocarbons used to study retention in monomeric and polymeric octadecylsilica.

Figure 4.1

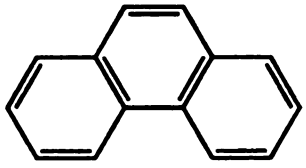

Phenanthrene

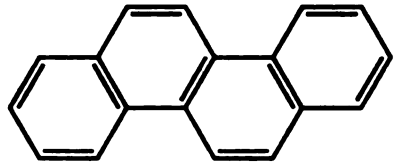

Chrysene

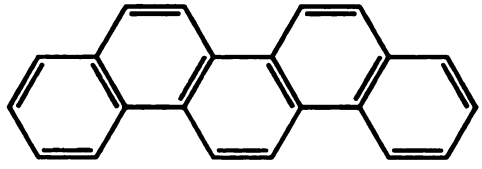

Picene

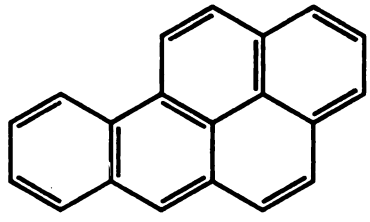

Benzo[*a*]pyrene

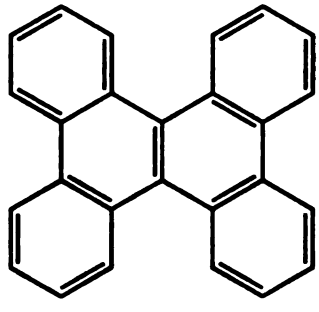

Tetrabenzonaphthalene

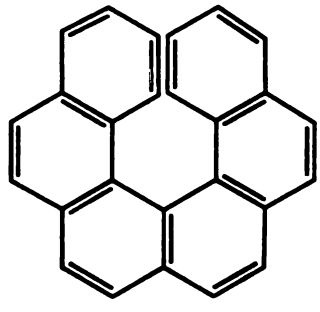

Phenanthro[*3,4-c*]phenanthrene

4.2.2 Experimental System

The system used to study the effect of ring number and planarity is depicted in Figure 2.2, and the data were collected by Dr. Chen. The mobile phase was pure methanol. Polymeric (5.4 μmol/m^2) and monomeric (2.7 μmol/m^2) octadecylsilica were used as the stationary phases to study the effect of bonding density. The temperatures for these experiments were 293, 298, 303, 308 and 313 K. The inlet pressures for these experiments were 830, 1000, 1930 and 3000 psi. These values correspond to average pressures of 400, 570, 1466, and 2566 psi, respectively, which were calculated assuming a linear pressure drop along the column. The inlet pressures were achieved by trimming the restrictor and splitter proportionally as described in Chapter 2. The data were analyzed using the exponentially modified Gaussian (EMG), which is described in section 2.3.1.

4.3 Results and Discussion

4.3.1 Thermodynamic Behavior

4.3.1.1 Retention Factor

The retention factor (k) is the simplest of the measurable parameters that allow for the comparison of the relative strength of interaction. A larger retention factor indicates that the PAH has greater affinity for the stationary phase. This comparison is useful to evaluate the effect of different PAH structural features as well as different stationary phase bonding densities.

Table 4.1: *Retention factors for PAHs*

Table 4.1: Retention factors for PAHs on monomeric and polymeric octadecylsilica (ODS).

Solute	Monomeric ODS[A]		Polymeric ODS[B]		Monomeric ODS[C]		Polymeric ODS[D]	
	293 K	313 K	293 K	313 K	395 psi	2605 psi	400 psi	2566 psi
Ph	0.28	0.25	0.65	0.44	0.27	0.28	0.65	0.65
Chr	0.49	0.41	2.66	1.15	0.49	0.49	2.51	2.65
Pic	0.99	0.71	N/A[d]	6.14	0.96	0.99	N/A	N/A
BaP	0.84	0.65	6.63	2.36	0.83	0.84	6.07	6.63
PhPh	0.58	0.51	1.12	0.70	0.58	0.58	1.15	1.12
TBN	1.31	1.10	1.75	1.29	1.32	1.31	1.87	1.75

[A] Retention factors calculated at P=2605 psi,

[B] Retention factors calculated at P=2566 psi,

[C] Retention factors calculated at T= 293 K

[D] N/A = not available

α
su
rel
rel
no
bel
phe
exp
has
elut
pres
pen
plan
pha
than
with
non
inte
incr
obs
the

Using Equation 1.2, the retention factor for each solute on the monomeric octadecylsilica was calculated. The results of theses calculations are summarized in Table 4.1. For the homologous series of planar PAHs, the retention factor increases with ring number (i.e. Pic > Chr > Ph). However, the retention factor decreases with increased ring condensation (i.e. Pic > BaP). As noted for the five-ring analogs, the retention factor for the more condensed benzo[*a*]pyrene is smaller than that for picene. The nonplanar PAH, phenanthro[*3,4,-c*]phenanthrene, has a smaller retention factor than would be expected based upon the number of rings. By contrast, tetrabenzonaphthalene has a retention factor that is consistent with an increased number of rings. The elution order follows the trend of PhPh < BaP < TBN at all temperatures and pressures. Of the three solutes, PhPh is the most nonplanar and cannot penetrate far into the bonded phase, resulting in small retention factors. The planar BaP, and the slightly nonplanar TBN, penetrate further into the stationary phase and thus have larger retention factors. The planar solute is less retained than TBN on the monomeric octadecylsilica due to the decreased interactions with the stationary phase that result from the decreased bonding density. The nonplanar TBN's larger retention factor likely results from a more optimal interaction distance with the stationary phase molecules, which leads to increased van der Waals interactions. Sander and Wise have previously observed this elution order and attributed it to the three-dimensional structure of the monomeric stationary phase [7,13].

By comparison, the retention factors for all solutes are larger on the polymeric phase than on the monomeric phase (Table 4.1). This increase can be attributed to two differences between the monomeric and polymeric phases. The first difference is simply a change in the phase ratio (Equation 1.1). As evidenced by the higher bonding density, 5.4 μmol/m^2 for the polymeric phase, a larger volume of stationary phase (V_s) allows for more interactions between the alkyl chains and the solutes. A second difference is the molecular structure arising from the trifunctional silane, which allows higher density and greater order of the alkyl chains than the monofunctional silane. This structural difference, coupled with the increased carbon load, allows solutes to interact more strongly with the polymeric phase. The increased interactions lead to higher retention factors, which are in agreement with previous work using high-density octadecylsilica [7,13-15].

The retention factor for phenanthrene on the polymeric phase is 76% larger than that on the monomeric phase. This increase in retention factor becomes systematically larger with ring number for chrysene (180%) and picene (~750%), whereas the more condensed benzo[*a*]pyrene changes by 260%. In contrast, the nonplanar phenanthro[*3,4-c*]phenanthrene and tetrabenzonaphthalene demonstrate smaller changes in the retention factors when compared to the planar solutes. In addition, the elution order on the polymeric phase has also changed from that on the monomeric phase, following the trend of PhPh<TBN<BaP at all temperatures and pressures. For the polymeric ODS, the nonplanar solutes are more excluded than the planar BaP.

thi

tes

bo

the

pic

ter

Ph

tet

co

ph

37

an

ret

on

pic

pre

Ph

tet

cor

This results in a decreased retention factor. Sander and Wise have observed this retention behavior previously and have used these solutes as an empirical test for the characterization of stationary phases [7,13].

The effect of temperature on the retention factor is very pronounced on both phases. For all solutes, an increase in temperature results in a decrease in the retention factor. For the homologous series, phenanthrene, chrysene and picene exhibit changes of –10.7%, –16.3%, and –28%, respectively, over the temperature range of 293 to 313 K at 2605 psi on the monomeric phase. Phenanthro[*3,4-c*]phenanthrene exhibits a change of –13%, whereas tetrabenzonaphthalene demonstrates a change of –19% under the same conditions. On the polymeric phase, the changes in retention factor are larger: phenanthrene –32.3 %, chrysene –56.7 %, phenanthro[*3,4-c*]phenanthrene –37.5 %, and tetrabenzonaphthalene –26.2%.

In contrast, the effect of pressure is relatively small on both the monomeric and polymeric phases. An increase in pressure results in an increase in retention factor for the planar solutes, but a decrease for the nonplanar solutes on both phases. For the homologous series, phenanthrene, chrysene, and picene exhibit changes of 3.7%, ~0.0%, and 3.1%, respectively, over the pressure range of 395 to 2605 psi at 293 K on the monomeric phase. Phenanthro[*3,4-c*]phenanthrene exhibits a change of ~0.0%, whereas tetrabenzonaphthalene demonstrates a change of –0.7% under the same conditions. On the polymeric phase, the changes in retention factor are slightly

larger for most solutes: phenanthrene ~0.0%, chrysene 5.6%, phenanthro[*3,4-c*]phenanthrene –2.6%, and tetrabenzonaphthalene –6.4%.

4.3.1.2 Molar Enthalpy

By applying the thermodynamic theory detailed above, the change in molar enthalpy can be calculated. Using Equation 1.5 and the methods described in Sections 1.3.1 and 2.3.1.2, the change in molar enthalpy was calculated. A representative graph used in the calculation of the change in molar enthalpy is shown in Figure 4.2. For all solutes at all pressures, the data are linear (R^2 = 0.994 – 0.999) and the slope of the line is positive. A linear graph indicates that the change in molar enthalpy is constant with temperature. A positive slope is demonstrative of a negative change in molar enthalpy, which indicates that the transition from the mobile to stationary phase is an energetically favorable exothermic process. Representative data for the PAHs are summarized in Table 4.2.

Overall, the change in molar enthalpy is relatively small on the monomeric phase, ranging from –0.8 to –2.9 kcal/mol. The homologous series illustrates a trend of decreasing molar enthalpy, where retention becomes more exothermic as ring number increases. A comparison of the five-ring analogs, picene and benzo[*a*]pyrene, indicates that the more condensed solute has a smaller change in molar enthalpy. This trend is conserved at all pressures in the range from 400 to 2600 psi. Previous work by Sentell and Henderson demonstrates the same trend for the four-ring analogs, pyrene and naphthacene [16].

Figure 4.2: Representative graph of the retention factor versus inverse temperature used to calculate the change in molar enthalpy according to Equation 1.5. Column: polymeric octadecylsilica. Mobile phase: methanol, 2566 psi, 0.08 cm/s. Solutes: phenanthrene (◇), chrysene (□), picene (○), benzo[*a*]pyrene (△), phenanthro[3,4-*c*]phenanthrene (●), tetrabenzonaphthalene (▲).

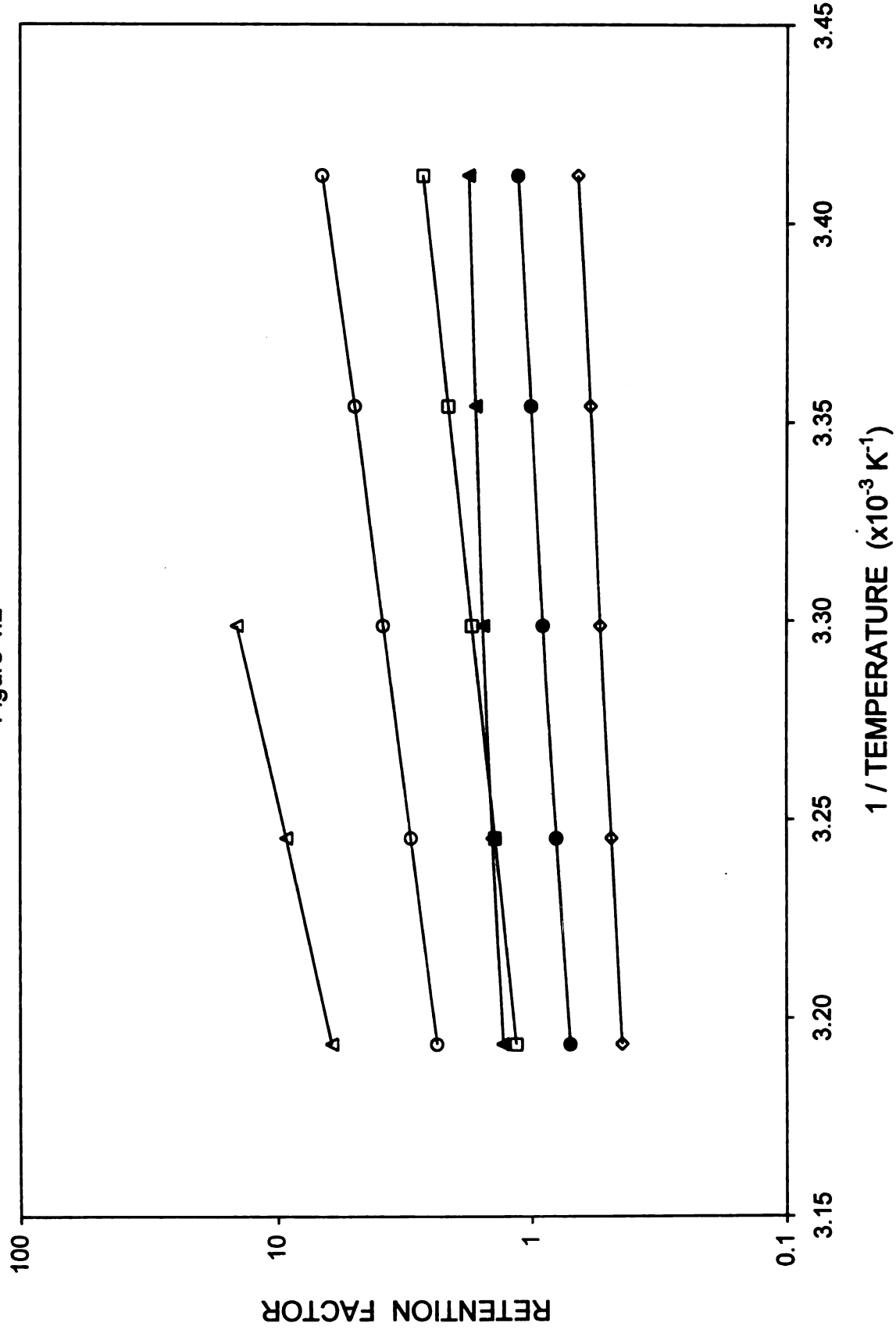
100
10
1
0.1
RETENTION FACTOR
3.15
3.20
3.25
3.30
3.35
3.40
3.45
1 / TEMPERATURE (x10-3 K-1)

Figure 4.2

Table 4.2: *Molar enthalpy and molar volume for PAHs on monomeric and polymeric octadecyl*

Table 4.2: Molar enthalpy and molar volume for PAHs on monomeric and polymeric octadecylsilica.

Solute	ΔH_{sm} (kcal/mol)		ΔV_{sm} (mL/mol)	
	Monomeric ODS [A]	Polymeric ODS [B]	Monomeric ODS[C]	Polymeric ODS[D]
Ph	–0.8 ± 0.1	–3.6 ± 0.1	–1.9 ± 1	–1.7 ± 2
Chr	–1.6 ± 0.1	–7.6 ± 0.1	–1.8 ± 1	–8.2 ± 1
Pic	–2.9 ± 0.1	–15.8 ± 0.2	–3.1 ± 1	–28.4 ± 1
BaP	–2.2 ± 0.1	–9.1 ± 0.1	–2.1 ± 1	–10.1± 1
PhPh	–1.0 ± 0.1	–4.5 ± 0.1	1.9 ± 1	1.7 ± 1
TBN	–1.5 ± 0.1	–3.2 ± 0.2	1.6 ± 1	6.8 ± 1

[A] Molar enthalpy (ΔH_{sm}) calculated at P=395 psi and T=288 to 303 K

[B] Molar enthalpy (ΔH_{sm}) calculated at P=400 psi and T=293 to 313 K

[C] Molar volume (ΔV_{sm}) calculated at T=303 K and P=395 to 2605 psi

[D] Molar volume (ΔV_{sm}) calculated at T=303 K and P=400 to 2566 psi

pha

is -

tetr

the

ph

fol

in

ch

ph

th

sy

bu

in

st

in

p

3

th

fa

re

th

The changes in molar enthalpy for the nonplanar PAHs on the monomeric phase are smaller than those for the planar PAHs. The change in molar enthalpy is –1.0 kcal/mol for phenanthro[*3,4-c*]phenanthrene and –1.5 kcal/mol for tetrabenzonaphthalene. These small values indicate that the nonplanar nature of these molecules inhibits their ability to interact optimally with the stationary phase. The changes in molar enthalpy for the PAHs on the polymeric phase follow the same trends as seen on the monomeric phase. However, as indicated in Table 4.2, the trends are more pronounced. For the planar solutes, the change in molar enthalpy ranges from –3.6 to –15.8 kcal/mol on the polymeric phase. The change in molar enthalpy for phenanthrene is 350% greater than that on the monomeric phase. This increase in molar enthalpy becomes systematically larger with ring number for chrysene (375%) and picene (444%), but becomes smaller for benzo[*a*]pyrene (314%). This is likely the result of increased interactions between the solute and the alkyl chains that comprise the stationary phase, as purported by Sander and Wise [17,18].

The data for the nonplanar solutes also demonstrate the large differences in molar enthalpy between the polymeric and monomeric phases. For phenanthro[*3,4-c*]phenanthrene and tetrabenzonaphthalene, the changes are 350% and 113%, respectively. On the polymeric phase, the absolute values of the molar enthalpy exhibit the trend of PhPh>TBN. However, the retention factors show the trend of TBN>PhPh. As demonstrated in Equation 1.5, retention is a function of both enthalpy and entropy. It is the entropic contribution that causes the retention factor to be larger for the TBN even though the

enthalpic term is smaller. Specifically, the difference in retention factors suggests that phenanthro[*3,4-c*]phenanthrene has greater entropic contributions that compensate for the enthalpic contributions, resulting in a shorter retention time.

4.3.1.3 Molar Volume

Similar to the molar enthalpy, the molar volume also provides insight into the effects that arise from structure. Using Equation 1.7 and the methods described in Sections 1.3.1 and 2.3.1.2, the change in molar volume was calculated. A representative graph used in the calculation of the change in molar volume is depicted in Figure 4.2. For the planar solutes at all temperatures, the data are linear (R^2=0.949 – 0.999) and the slope of the line is positive. A linear graph indicates that the molar volume is constant with pressure. A positive slope results in a negative molar volume, which indicates that the molecule occupies less space in the stationary phase than in the mobile phase. However, the nonplanar solutes exhibit linear behavior with a negative slope. A negative slope indicates that the transition from the mobile to stationary phase results in a larger volume for these nonplanar molecules. Representative data are contained in Table 4.2.

Overall, the change in molar volume is relatively small on the monomeric phase, ranging from –1.8 to –3.1 mL/mol for the planar solutes. The changes in molar volume for phenanthrene and chrysene are statistically indistinguishable. For chrysene and picene, however, an increase in ring number results in a more negative change in molar volume. This trend arises because the smaller PAHs

Figure 4.3: Representative graph of the retention factor versus pressure used to calculate the change in molar volume according to Equation 1.7. Column: polymeric octadecylsilica. Mobile phase: methanol, 308 K, 0.08 cm/s. Symbols defined in Figure 4.1.

Figure 4.3

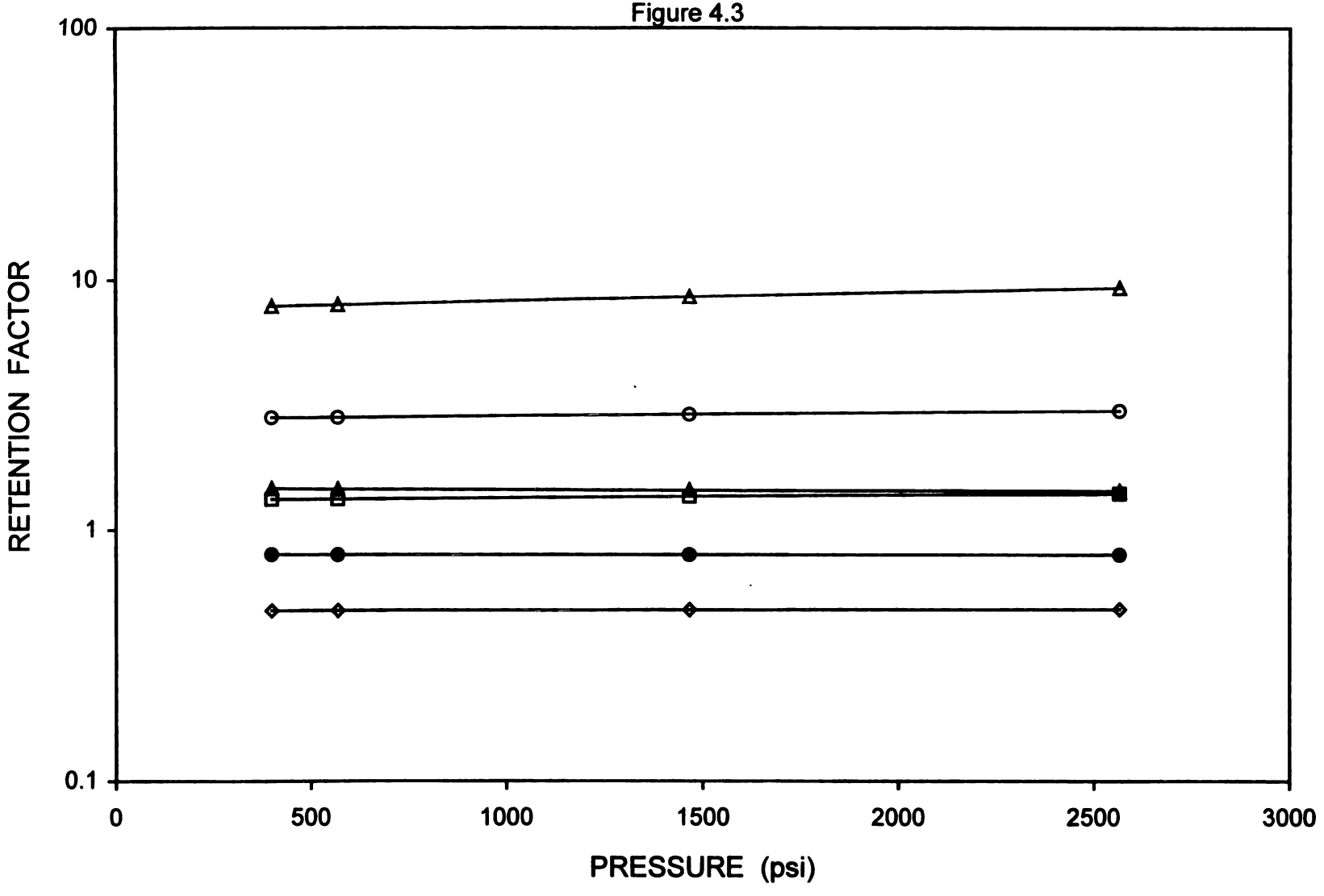
100
10
1
0.1
RETENTION FACTOR
0
500
1000
1500
2000
2500
3000
PRESSURE (psi)

penetrate only a short distance into the stationary phase [19], where the alkyl chains exhibit a high degree of disorder [15,20,21]. Since the larger PAHs can penetrate more deeply, they are able to probe regions that are more ordered and more dense. This closer arrangement of the PAHs and alkyl chains leads to a smaller molar volume than in the disordered regions of the stationary phase and in the randomly oriented mobile phase. A similar rationale can be used to explain the effect of annelation structure. The more condensed solute, benzo[*a*]pyrene, penetrates to a smaller depth than does picene. As a result, the overall change in molar volume is less negative for benzo[*a*]pyrene than for picene. In contrast, the change in molar volume is positive and statistically indistinguishable for the nonplanar PAHs, tetrabenzonaphthalene and phenanthro[*3,4-c*]phenanthrene. The positive molar volume implies that these molecules do not penetrate deeply and are not effectively solvated by the alkyl chains. The increase in molar volume for TBN results from the inability of the polymeric phase to encapsulate the solute as efficiently as the monomeric phase. These trends are conserved at all temperatures in the range from 293 to 313 K.

The changes in molar volume on the polymeric phase are, in general, more pronounced than those on the monomeric phase. For the planar solutes, the change in molar volume ranges from -1.7 ± 1 to -28.4 ± 1 mL/mol on the polymeric phase. The change in molar volume for phenanthrene is statistically indistinguishable on the monomeric and polymeric phases. Chrysene and picene exhibit changes of 355% and 816%, respectively, whereas the more condensed

Figure 4.4: Representative graph of the change in molar enthalpy versus the change in molar volume. Planar solutes (◆), nonplanar solutes (■).

Figure 4.4

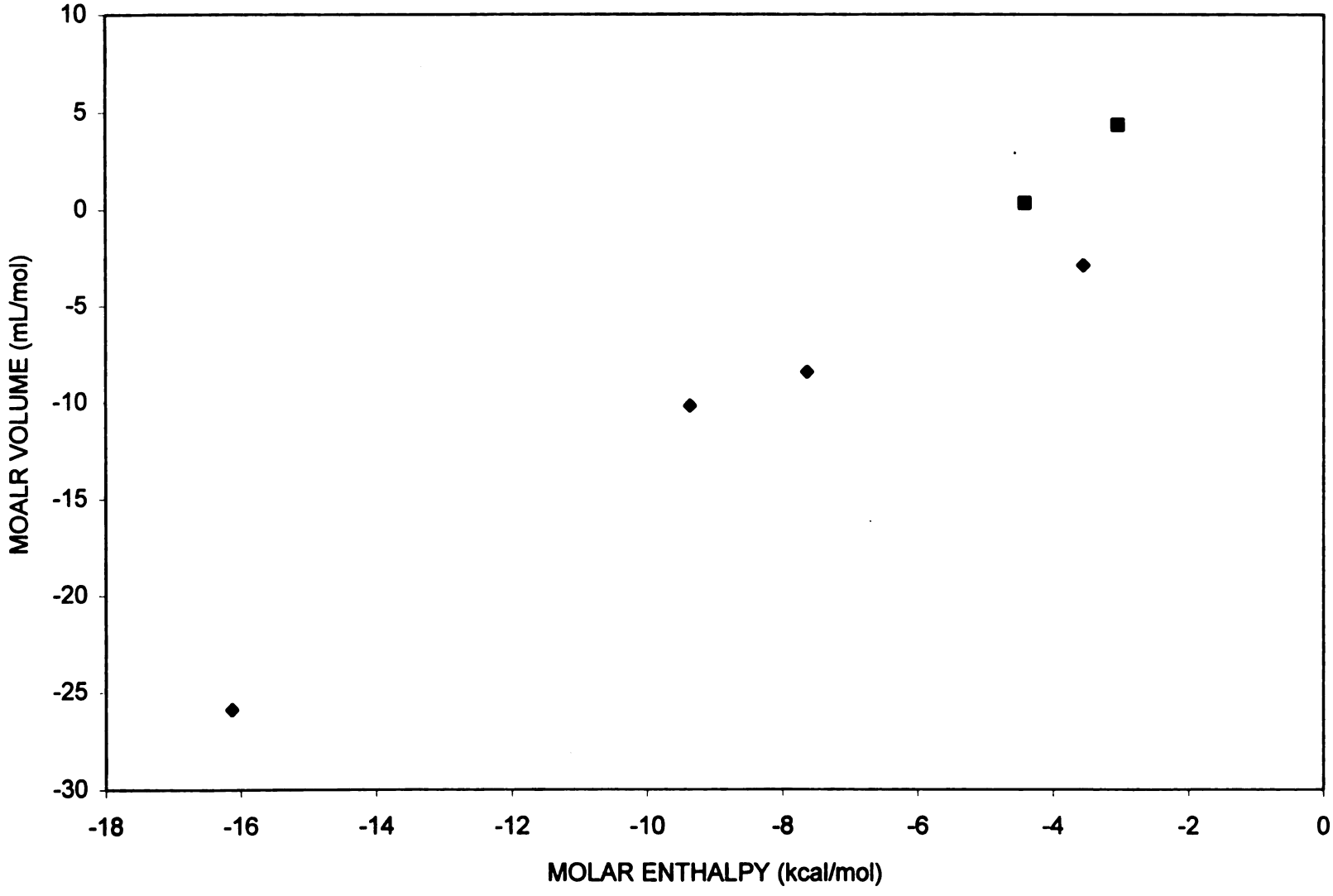
10
5
0
-5
-10
-15
-20
-25
-30
MOALR VOLUME (mL/mol)
-18
-16
-14
-12
-10
-8
-6
-4
-2
0
MOLAR ENTHALPY (kcal/mol)

benzo[*a*]pyrene changes by 380%. As with the monomeric phase, all of the planar PAHs exhibit negative changes in molar volume, whereas the nonplanar molecules exhibit positive changes. Phenanthro[*3,4-c*]phenanthrene undergoes changes that are statistically indistinguishable, whereas tetrabenzonaphthalene undergoes a much larger change of 325% on the monomeric and polymeric phases.

Finally, it is interesting to note the correlation between the changes in molar enthalpy and molar volume. As illustrated in Figure 4.4, for the planar PAHs, a linear correlation ($R^2 = 0.98$) is observed between these thermodynamic parameters on the polymeric phase. The nonplanar PAHs lie nearly along the same line, such that the overall correlation is still quite high ($R^2 = 0.96$). This trend occurs because the molar enthalpy and molar volume can be compensated through the internal energy (Equation 1.6), similar to the compensation of molar enthalpy and molar entropy through the free energy (Equation 1.4) [22,23]. The physical reason for this correlation can be attributed to the varying extents of solute penetration and the varying extents of disorder in the stationary phase. At the proximal end that is bound to the silica, the alkyl chains are highly ordered in the all-trans configuration. As distance increases, some flexibility is possible and gauche configurations may be formed. At the distal end, these gauche bonds are most prevalent and result in a highly disordered region [20,21]. As the PAH penetrates into the more ordered regions, there arises simultaneously an increase in the interaction with the alkyl chains and a decrease in the available

space. Accordingly, the changes in molar enthalpy (ΔH_{sm}) and molar volume (ΔV_{sm}) are observed to be correlated.

4.3.2 Kinetic Behavior

4.3.2.1 Rate Constant

Although the thermodynamic data demonstrate the steady-state aspects, they do not fully explain the mechanism of retention. Using Equations 1.16, 1.17 and 1.20 and the methods described in Sections 1.3.2 and 2.3.1.2, the pseudo-first-order rate constants, activation enthalpies, and activation volumes were calculated. These values help to quantify the kinetic aspects of solute transfer between the mobile and stationary phases.

Representative values of the rate constants are summarized in Table 4.3. Several solutes, notably phenanthrene, chrysene, phenanthro[*3,4-c*]phenanthrene, and tetrabenzonaphthalene, have rate constants that exceed the resolution capabilities of this method. The upper limit of reliability was determined through a series of simulations and experiments. For the data contained herein, the τ/σ ratio must be greater than 0.4 to yield reliable rate constants. For smaller τ/σ ratios, the zones are nearly Gaussian in shape and the exponential component cannot be accurately determined. The τ/σ ratio of 0.4 corresponds to a rate constant of 400 s^{-1}.

For the monomeric phase, the transfer of phenanthrene and chrysene is sufficiently fast that no reliable conclusions can be drawn. However, the rate constants decrease with increasing ring number, such that picene and

benzo[*a*]pyrene can be evaluated. The more condensed structure of benzo[*a*]pyrene results in larger rate constants for the mobile to stationary phase (k_{sm}), and the stationary to mobile phase (k_{ms}), when compared to picene. Both molecules exhibit a retention mechanism in which the rate-limiting step is the transfer from mobile to stationary phase (i.e., $k_{ms} > k_{sm}$). In addition, an increase in temperature yields an increase in the rate constants for all molecules. For example, the rate constant (k_{sm}) for picene ranges from 26 to 78 s^{-1} for temperatures from 288 to 313 K. In contrast, an increase in pressure yields only slight changes. The rate constant (k_{sm}) for picene ranges from 38 to 34 s^{-1} for pressures from 605 to 2605 psi at 303 K.

As the rate constants for all planar compounds with ring numbers equal to five can be determined, those for the six-ring compounds were also anticipated to be sufficiently small. However, phenanthro[*3,4-c*]phenanthrene and tetrabenzonaphthalene are fast and cannot be quantitated on either the monomeric or polymeric phases. This suggests that the kinetic behavior, similar to the thermodynamic behavior, is heavily influenced by the nonplanar structure of these solutes.

On the polymeric phase, the rate constant for phenanthrene is very large but those for chrysene, picene, and benzo[*a*]pyrene are small enough to be quantified. As shown in Table 4.3, the rate constants for the transfer from stationary to mobile phase are smaller than those observed on the monomeric phase. In contrast, the rate constants for the transfer from mobile to stationary phase are generally larger than those observed on the monomeric phase. Thus,

Table 4.3: Kinetic rate constants for PAHs on monomeric and polymeric octadecylsilica.

Solute	Monomeric ODS[A]		Polymeric ODS[B]	
	k_{ms} (s^{-1})	k_{sm} (s^{-1})	k_{ms} (s^{-1})	k_{sm}(s^{-1})
Ph	≥400	≥400	≥400	≥400
Chr	≥400	≥400	132	221
Pic	43	36	9	118
BaP	79	57	57	207
PhPh	≥400	≥400	≥400	≥400
TBN	≥400	≥400	≥400	≥400

[A] Rate constants for the stationary to mobile (k_{ms}), and mobile to stationary phases transition (k_{sm}) calculated at T=303 K and P=1005 psi,

[B] Rate constants calculated at T=303 K and P=1066 psi.

the data indicate barrier for entry into the higher density phase requires more time and more energy (vide infra), and that the barrier for exit is noticeably lower. For chrysene and picene, the rate constants decrease sharply as the ring number increases. For picene and benzo[*a*]pyrene, the more condensed structure allows faster transitions.

Overall, the data indicate that the rate constants (k_{ms} and k_{sm}) decrease as the retention factor increases. These results imply that the solutes become more retained as ring number and bonding density increase, with each retention event becoming longer in duration.

4.3.2.2 Activation Enthalpy

Given that many of the molecules exhibit very fast transitions, the additional kinetic parameters cannot be determined on the monomeric phase. Although the rate constants for picene and benzo[*a*]pyrene are quantifiable at low temperature, they too become unreliable at higher temperatures. As a result, the activation enthalpies and activation volumes can only be calculated on the polymeric phase with any statistical certainty.

Using Equation 1.20 and the methods described in Sections 1.3.2 and 2.3.1.2, the activation enthalpies were calculated. Figure 4.5 illustrates a typical graph of the natural logarithm of the rate constant versus inverse temperature used in the calculation of the activation enthalpy. Table 4.4 contains those activation enthalpies that could be reliably calculated from the kinetic rate constants. As demonstrated for chrysene and picene, an increase in ring number results in an increase in the activation enthalpy. Similarly, a comparison

Figure 4.5: Representative graph of the rate constants versus inverse temperature used to calculate the activation enthalpy according to Equation 1.20. Column: polymeric octadecylsilica. Mobile phase: methanol, 2566 psi, 0.08 cm/s. Solutes: chrysene k_{ms} (◇), k_{sm} (◆); benzo[*a*]pyrene k_{ms} (○), k_{sm} (●).

Figure 4.5

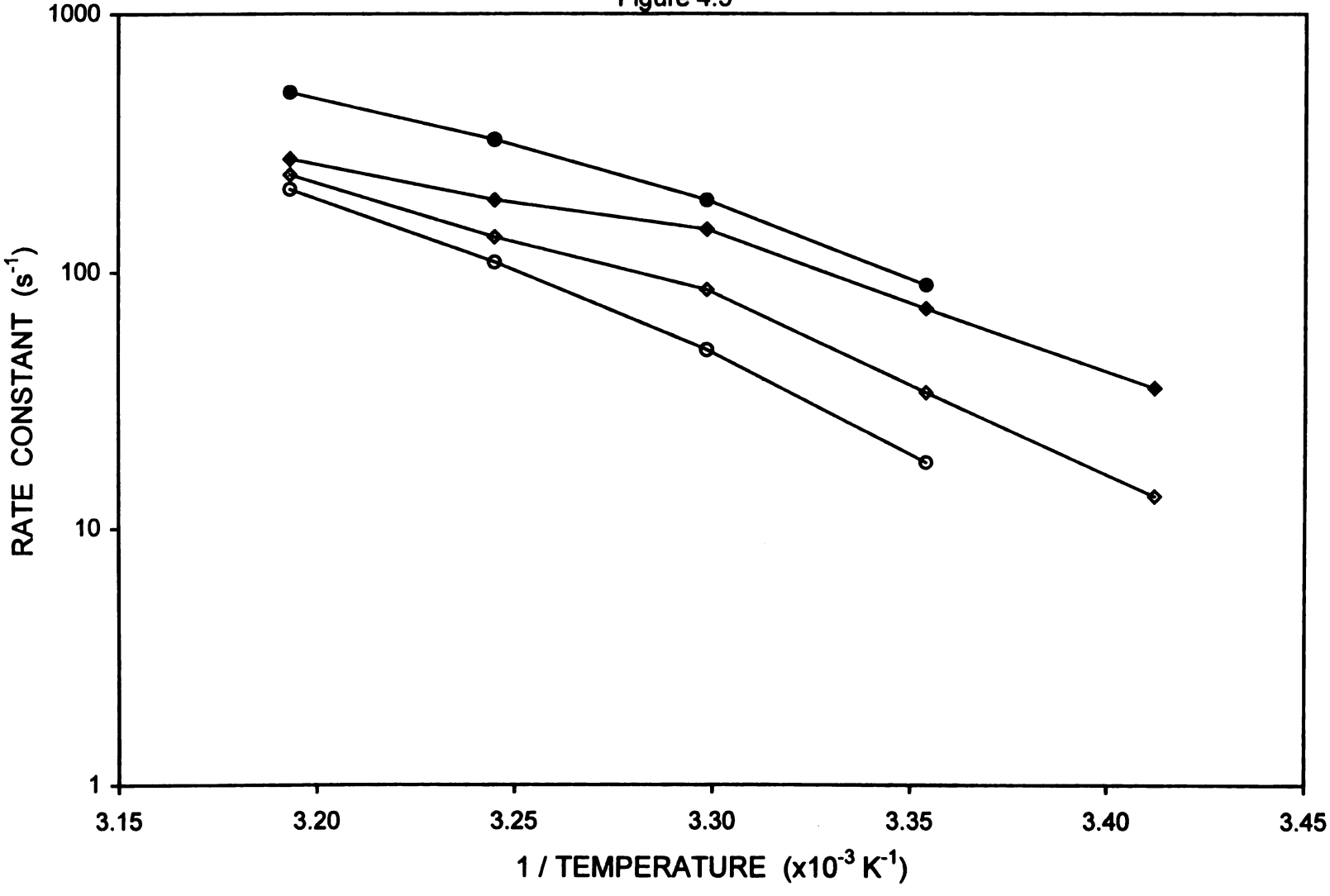
1000
100
10
1
RATE CONSTANT (s^{-1})
3.15
3.20
3.25
3.30
3.35
3.40
3.45
1 / TEMPERATURE ($x10^{-3}$ K^{-1})

Table 4.4: Activation enthalpy and activation volume for selected PAHs on polymeric octadecylsilica calculated at T=308 K and P=1466 psi.

Solute	$\Delta H_{\ddagger s}$ (kcal/mol)[A]	$\Delta H_{\ddagger m}$ (kcal/mol)	$\Delta V_{\ddagger s}$ (mL/mol)[B]	$\Delta V_{\ddagger m}$ (mL/mol)
Chr	27 ± 1	19 ± 1	78 ± 18	72 ± 17
Pic	71 ± 23	54 ± 23	139 ± 19	107 ± 18
BaP	26 ± 3	17 ± 3	26 ± 28	15 ± 27

[A] Activation enthalpies for the stationary phase to transition state ($\Delta H_{\ddagger s}$), and mobile phase to transition state ($\Delta H_{\ddagger m}$) were calculated at T=308 K and P=1466 psi

[B] Activation volumes for the stationary phase to transition state ($\Delta V_{\ddagger s}$), and mobile phase to transition state ($\Delta V_{\ddagger m}$) were calculated at T=308 K and P = 400 to 2566 psi

of benzo[*a*]pyrene and picene indicates that the more condensed solute has a smaller activation enthalpy. Thus, the structure of the molecule affects the energy needed to transfer between mobile and stationary phases. This general conclusion is consistent with the results of Miyabe, Sotoura, and Guiochon [24] who have estimated the activation energy for surface diffusion of the alkylbenzenes on octadecylsilica to be in the range of 3.5 to 5.2 kcal/mol. These values are significantly smaller than those reported herein because of the smaller molecular size, the lower bonding density of the octadecylsilica, as well as the different computational method used by Miyabe and coworkers. Nevertheless, they confirm the importance of molecular structure in the kinetic processes. As the activation enthalpies for the stationary to transition state ($\Delta H_{\ddagger s}$), and the mobile phase to transition state ($\Delta H_{\ddagger m}$) in Table 4.4 are compared to one another and to the change in molar enthalpy (ΔH_{sm}) in Table 4.2, a trend emerges: $\Delta H_{\ddagger s} > \Delta H_{\ddagger m} >> \Delta H_{sm}$. Thus, this trend reveals the inherent danger of drawing conclusions about mechanism and the relative energies of transition from the thermodynamic parameter alone. It should be noted that the difference between the activation enthalpies is equivalent to the change in molar enthalpy, indicating an internal consistency in the method of calculation.

In addition to the slope of the line, the intercept of the line contains information about collisional frequency of the system. For a bimolecular system, the pre-exponential factor (A), also known as the frequency factor, has values on the order of 10^{13} [25]. For the data contained in this chapter, as well as the following chapters, the pre-exponential factor ranges from 10^{16} to 10^{24}, implying a

larger number of collisions per unit time. The large differences between the typical values and those shown here could result from the large concentrations of the solutes, or a large contribution from the activation entropy ($\Delta S_{\ddagger s}$, $\Delta S_{\ddagger m}$), which is a component of the pre-exponential factor. However, it should be noted that the kinetic theory is derived for gas phase systems. Thus, the assumptions inherent not only to the kinetic theory of gases, but also the differences between the liquid and gas states should be recognized as likely contributions to the differences in the values for the pre-exponential factor.

4.3.2.3 Activation Volume

Using Equation 1.20 and the methods described in Sections 1.3.2 and 2.3.1.2, the activation volumes were calculated. A representative graph of the natural logarithm of the rate constant versus pressure is depicted in Figure 4.6 and the resulting values for the activation volume are presented in Table 4.4. For chrysene and picene, an increase in ring number correlates with an increase in the activation volume. The activation volume for benzo[*a*]pyrene is smaller than that for picene, indicating once again that annelation structure has a significant effect on the kinetics. Similar to the activation enthalpy, when the activation volumes for the stationary to transition state ($\Delta V_{\ddagger s}$), and the mobile phase to transition state ($\Delta V_{\ddagger m}$) in Table 4.4 are compared to one another and to the change in molar volume (ΔV_{sm}) in Table 4.2, another trend emerges: $\Delta V_{\ddagger s} > \Delta V_{\ddagger m} >> \Delta V_{sm}$. This trend indicates that the barrier for the transition event is very large, although the overall change in molar volume may be small. Akin to the activation enthalpies and the molar enthalpy, the difference between the.

Figure 4.6: Representative graph of the rate constants versus pressure used to calculate the change in activation volume according to Equation 1.20. Column: polymeric octadecylsilica. Mobile phase: methanol, 303 K, 0.08 cm/s. Symbols defined in Figure 4.5.

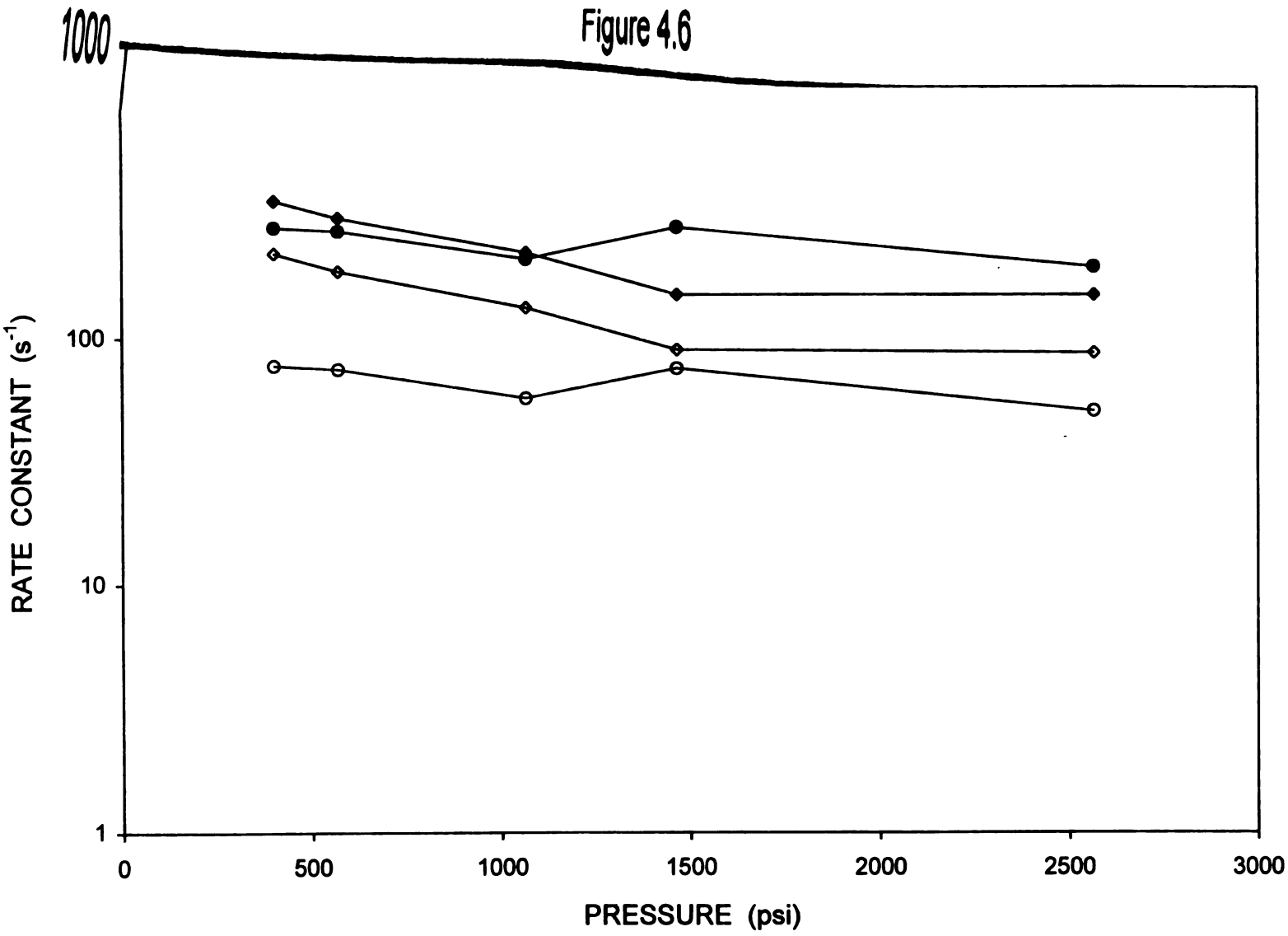
1000
100
10
1
RATE CONSTANT (s^{-1})
0
500
1000
1500
2000
2500
3000
PRESSURE (psi)

Figure 4.6

activation volumes and the molar volume are similar, demonstrating and internal consistency in the method of calculation.

Similar to the thermodynamic parameters, the activation enthalpy and activation volume are positively correlated for the planar PAHs. However, there are insufficient data to determine whether or not this correlation is linear

4.4 Conclusions

To illustrate the full implications of the data presented above, it is helpful to describe the entire retention event for a single solute. For example, as picene transfers from the mobile to stationary phase, it passes through a high-energy transition state. This transition state may be envisioned as a cavity created within the stationary phase that incorporates the solute as well as some associated solvent molecules. The creation of this transition state requires an enthalpy change of 54 kcal/mol and a volume change of 107 mL/mol. Given these large changes, it is likely that this transfer does not occur in a single step, but in a series of discrete and sequential steps. As the system approaches equilibrium, the solvent molecules are released and the alkyl chains rearrange to optimally solvate the solute. As a result of this rearrangement, the net energy of the system decreases by –15.8 kcal/mol and the volume decreases by –28.4 mL/mol. This transfer occurs with a rate constant of 118 s^{-1}. As picene transfers from the stationary to mobile phase, it passes through another high-energy transition state. This transition requires an enthalpy change of 71 kcal/mol and a volume change of 139 mL/mol. This large change suggests, once again, that the transfer is characterized by a series of discrete steps. This transfer occurs with a

rate constant of 9 s^{-1}, which is 13-fold slower than the transfer from mobile to stationary phase.

This holistic view of the transition event illustrates that both the thermodynamics and kinetics are necessary to fully describe the retention event. Thus, previous investigations that have used the change in molar enthalpy to describe the mechanism of retention are inherently flawed and highly suspect. By using the necessary theoretical foundation and instrumental design, this chapter demonstrates the first comprehensive study of retention for a series of known toxicants/pollutants.

Throughout this chapter, and those that follow, the main driving force for retention is described as the solvation of the nonpolar solute into the nonpolar stationary phase. As noted by Ranatunga and Carr[23] the enthalpy of retention (i.e. transfer from the mobile phase to stationary phase) is favorable and large. The authors demonstrate that the contribution from the mobile phase is enthalpically unfavorable, but is overcome by the large enthalpy imparted by the solvation of the solute into the lipophilic stationary phase. In addition, the entropy is shown to contribute very little to the retention event. Thus, the contributions from the mobile phase are not incorporated into the description of the retention event.

4.5 References

[1] L.A. Cole, J.G. Dorsey, Anal. Chem. 64 (1992) 1317-1323.

[2] K.B. Sentell, J.G. Dorsey, J. Chromatogr. 461 (1989) 193-207.

[3] M. Olsson, L.C. Sander, S.A. Wise, J. Chromatogr. 477 (1989) 277-290.

[4] L.C. Sander, M. Pursch, S.A. Wise, Anal. Chem. 71 (1999) 4821-4830.

[5] K.B. Sentell, J.G. Dorsey, Anal. Chem. 61 (1989) 930-934.

[6] L.A. Cole, J.G. Dorsey, J. Chromatogr. 635 (1993) 177-186.

[7] L.C. Sander, S.A. Wise, Anal. Chem. 67 (1995) 3284-3292.

[8] J.H. Park, Y.K. Lee, Y.C. Weon, L.C. Tan, J. Li, L. Li, J.F. Evans, P.W. Carr, J. Chromatogr. A 767 (1997) 1-10.

[9] L.A. Cole, J.G. Dorsey, Anal. Chem. 64 (1992) 1324-1327.

[10] M.H. Chen, C. Horváth, J. Chromatogr. A 788 (1997) 51-61.

[11] V.L. McGuffin, S.-H. Chen, J. Chromatogr. A 762 (1997) 35-46.

[12] V.L. McGuffin, C. Lee, J. Chromatogr. A 987 (2003) 3-15.

[13] L.C. Sander, S.A. Wise, J. Chromatogr. A 656 (1993) 335-351.

[14] A. Tchapla, S. Heron, E. Lesellier, H. Colin, J. Chromatogr. A 656 (1993) 81-112.

[15] J.F. Wheeler, T.L. Beck, S.J. Klatte, L.A. Cole, J.G. Dorsey, J. Chromatogr. A 656 (1993) 317-333.

[16] K.B. Sentell, A.N. Henderson, Anal. Chim. Acta 246 (1991) 139-149.

[17] L.C. Sander, S.A. Wise, CRC Crit. Rev. Anal. Chem. 18 (1987) 299-415.

[18] L.C. Sander, S.A. Wise, Anal. Chem. 61 (1989) 1749-1754.

[19] G.E. Berendsen, L. de Galan, J. Chromatogr. 196 (1980) 21-37.

[20] M.W. Ducey, Jr., C.J. Orendorff, J.E. Pemberton, L.C. Sander, Anal. Chem. 74 (2002) 5576-5584.

[21] M.W. Ducey, Jr., C.J. Orendorff, J.E. Pemberton, L.C. Sander, Anal. Chem. 74 (2002) 5585-5592.

[22] W. Melander, D.E. Campbell, C. Horváth, J. Chromatogr. 158 (1978) 215-225.

[23] R.P.J. Ranatunga, P.W. Carr, Anal. Chem. 72 (2000) 5679-5692.

[24] K. Miyabe, S. Sotoura, G. Guiochon, J. Chromatogr. A 919 (2001) 231-244.

[25] S.W. Benson, The Foundations of Chemical Kinetics, Robert E. Krieger Publishing, Malabar, FL, USA, 1982.

Chapter 5: Retention of Polycyclic Aromatic Hydrocarbons: Effect of Annelation

5.1 Introduction

As demonstrated in Chapter 4, the effect of ring number and planarity are very important to the thermodynamics and kinetics of retention in liquid chromatography. While a large number of studies have been carried out to study the aforementioned parameters, fewer investigations have sought to characterize the effect of annelation [1-5]. The effect of annelation is important since it can affect the biological impact of one isomer over another.

Four-ring polycyclic aromatic hydrocarbon (PAH) isomers have been used to study the effect of annelation structure with regard to stationary-phase bonding density [3,4], mobile-phase composition [2], and temperature [4,5] in reversed-phase systems. Sentell and Dorsey reported that selectivity increases with increasing bonding density [3]. Chmielowiec and Sawatzky reported thermodynamic values for three- and four-ring homologues, which indicate that an increase in length-to-breadth ratio results in more negative changes in molar enthalpy and molar entropy [2]. The more recent investigations by Sentell and Henderson [4] and Sentell *et al.* [5] have used a homologous series of four-ring PAHs to study the effect of sub-ambient temperature on retention and selectivity. Their data indicate that the selectivity between these solutes increases at lower temperature. This increased selectivity is attributed to the larger surface area for interaction that results from the higher order of the alkyl chains near the proximal terminus, as purported by Stalcup *et al.* [6]. In addition to four-ring PAHs, six-ring

PAHs have also been used as probes of reversed-phase systems. Most notably, phenanthro[*3,4-c*]phenanthrene and tetrabenzonaphthalene have been used to examine the effect of planarity on retention [1,6-10]. However, without the comparison to other six-ring compounds, these nonplanar PAHs provide little direct information about the effect of annelation structure.

To date, there have been no systematic studies that consider both the thermodynamic and kinetic behavior as a function of annelation structure. In the present study, a series of four-ring PAHs with planar and nonplanar structures are separated on a polymeric octadecylsilica stationary phase with a methanol mobile phase. Using a temperature range from 273 to 303 K and an average pressure range from 585 to 3585 psi, the thermodynamic and kinetic behavior are characterized by previously established methodology [11-13] detailed in Chapters 1,2 and 4. The retention factors are calculated, together with the concomitant changes in molar enthalpy and molar volume, to characterize the thermodynamic behavior. The rate constants are calculated, together with the concomitant changes in activation enthalpy and activation volume, to characterize the kinetic behavior. These data provide a holistic view of the effect of annelation structure on the retention mechanism in reversed-phase liquid chromatography.

5.2 Experimental Methods

5.2.1 Solutes

As depicted in Figure 5.1, four polycyclic aromatic hydrocarbons have been chosen to investigate the effect of annelation on the thermodynamics and kinetics of retention. Pyrene, benz[*a*]anthracene, chrysene, and benzo[*c*]phenanthrene (Sigma-Aldrich) were obtained as solids and dissolved in high-purity methanol (Burdick and Jackson, Baxter Healthcare) to yield standard solutions at a concentration of 10^{-4} M. A nonretained marker, 4-methylhydroxy-7-methoxycoumarin, was added to each solution at a concentration of 10^{-4} M. To ensure solubility, the solutions were equilibrated at each temperature prior to analysis.

5.2.2 Experimental System

The system used to study the effect of annelation is depicted in Figure 2.2. The mobile phase was pure methanol, and the stationary phase polymeric octadcecylsilica (5.4 μmol/m^2). The temperatures for these experiments were 273, 283, 288, 293 and 303 K. The inlet pressures for these experiments were 1000, 1750, 2500, 3250 and 4000 psi. These values correspond to average pressures of 585, 1335, 2085, 2835, and 3585 psi, respectively, which were calculated assuming a linear pressure drop along the column. The data were analyzed using the exponentially modified Gaussian (EMG), non-linear chromatography (NLC) and bi-exponentially modified Gaussian (E^{2}MG) functions, which are described in section 2.3.1.

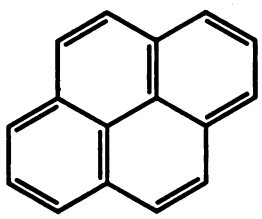

Pyrene

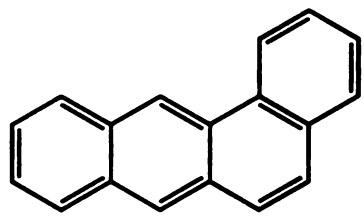

Benz[*a*]anthracene

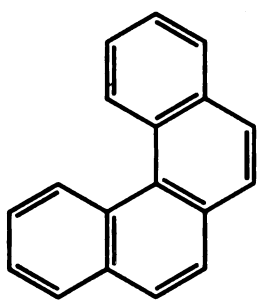

Benzo[*c*]phenanthrene

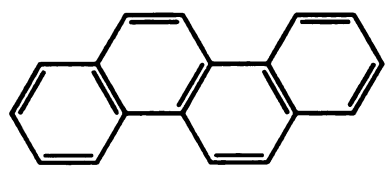

Chrysene

Figure 5.1: Structure of polycyclic aromatic hydrocarbons used to study the effect of annelation in polymeric octadecylsilica.

5.3 Results and Discussion

5.3.1 Thermodynamic Behavior

5.3.1.1 Retention Factor

Using Equations 1.2 and 2.5, the retention factor was calculated for each solute at each temperature and pressure. Representative values of the retention factor are summarized in Table 5.1. It is apparent that the retention factor for all PAHs decreases with increasing temperature and increases with increasing pressure. Retention also decreases as a function of the length-to-breadth ratio (i.e., pyrene < benz[*a*]anthracene < chrysene), with the exception of benzo[*c*]phenanthrene. As noted previously, benzo[*c*]phenanthrene is slightly nonplanar due to steric hindrance of the hydrogen atoms in the bay region. When compared to data reported in Chapter 4 for nonplanar six-ring PAHs [12], the retention factor for benzo[*c*]phenanthrene is larger than those for phenanthro[*3,4-c*]phenanthrene and tetrabenzonaphthalene. This suggests that the smaller degree of nonplanarity of benzo[*c*]phenanthrene allows for greater interaction with the stationary phase. Moreover, an increase in pressure causes a slight increase in retention for benzo[*c*]phenanthrene, but causes a decrease in retention for phenanthro[*3,4-c*]phenanthrene and tetrabenzonaphthalene. Hence, compression of the stationary phase causes greater interaction of the alkyl chains with benzo[*c*]phenanthrene, similar to the planar solutes, but causes expulsion the other nonplanar solutes.

Table 5.1: Retention factors for PAH isomers.

Solute[A]	k [B]		k [C]	
	273 K	303 K	585 psi	3585 psi
Pyr	1.89	0.84	1.31	1.36
BaA	5.33	1.45	2.99	3.26
Chr	8.12	1.83	4.20	4.64
BcP	1.59	0.80	1.19	1.21

[A] Pyr = pyrene, BaA= benz[*a*]anthracene, Chr = chrysene,

BcP = benzo[*c*]phenanthrene

[B] Retention factor (k) calculated at 3585 psi

[C] Retention factor (k) calculated at 283 K

5.3.1.2 Molar Enthalpy

A representative graph of the logarithm of the retention factor versus the inverse temperature is shown in Figure 5.1. The change in molar enthalpy is calculated from the slope of this graph, according to Equation 1.5. The graph for each PAH is linear (R^2 = 0.991 – 0.999) and the slope is positive. A positive slope is indicative of a negative change in molar enthalpy and suggests that the transfer from mobile to stationary phase is enthalpically favorable. As shown in Table 5.2, the most condensed of the planar solutes, pyrene, has the smallest change whereas the least condensed, chrysene, has the greatest change in molar enthalpy. These differences in molar enthalpy can be attributed to the depth that each PAH penetrates into the stationary phase. The proximal regions, where the alkyl group is bound to the silica surface, are highly ordered with all trans carbon-carbon bonds. As the distance from the surface increases, there are more gauche bonds and greater disorder [14,15]. The more condensed PAHs, such as pyrene, probe only the distal regions, whereas less condensed PAHs, such as chrysene, penetrate more deeply into the ordered regions of the stationary phase. The change in molar enthalpy becomes more negative the farther the PAH penetrates into the stationary phase. It is noteworthy that benzo[*c*]phenanthrene exhibits changes in molar enthalpy that are smaller than the other PAHs, even though it is not the most condensed. It is hypothesized that the nonplanar character of benzo[*c*]phenanthrene does not allow it to penetrate as deeply into the high-density polymeric stationary phase. This effect has been noted previously with other nonplanar PAHs [4,5,7-9]. The molar

Figure 5.2: Representative graph of the retention factor versus inverse temperature used to calculate the change in molar enthalpy according to Equation 1.5. Column: polymeric octadecylsilica. Mobile phase: methanol, 3585 psi, 0.08 cm/s. Solutes: pyrene (◆), benz[*a*]anthracene (■), chrysene (▲), benzo[*c*]phenanthrene (O).

Figure 5.2

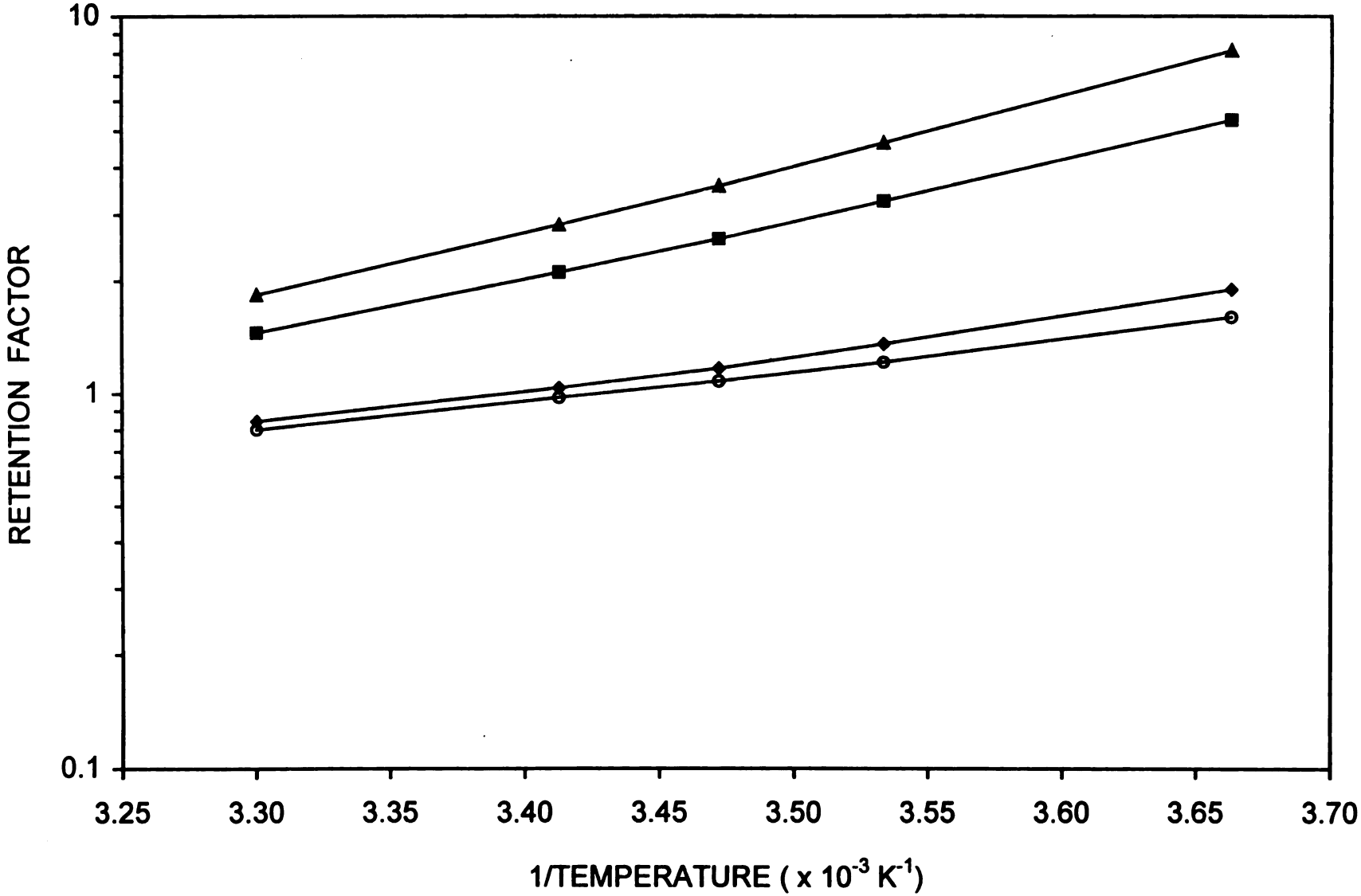
10
1
0.1
RETENTION FACTOR
3.25
3.30
3.35
3.40
3.45
3.50
3.55
3.60
3.65
3.70
1/TEMPERATURE (x 10-3 K-1)

Table 5.2: Molar enthalpy and molar volume for PAH isomers

Solute	ΔH_{sm} (kcal/mol)[A]	ΔV_{sm} (mL/mol)[B]
Pyr	–4.4 ± 0.2	–1.9 ± 1
BaA	–7.1 ± 0.2	–9.6 ± 1
Chr	–8.2 ± 0.2	–11.7 ± 1
BcP	–3.8 ± 0.2	–1.3 ± 1

[A] Molar enthalpy (ΔH_{sm}) calculated at 3585 psi

[B] Molar volume (ΔV_{sm}) calculated at 283 K

enthalpies reported herein are consistent with those for other PAHs in Chapter 4 [12].

5.3.1.3 Molar Volume

A representative graph of the logarithm of the retention factor versus pressure is shown in Figure 5.2. The change in molar volume is calculated from the slope of this graph, according to Equation 1.7. Again, the graph for each PAH is linear (R^2 = 0.984 – 0.998) and the slope is positive. A positive slope is indicative of a negative change in molar volume and suggests that the PAH occupies less volume in the stationary phase than in the mobile phase. As shown in Table 5.2, the most condensed of the planar solutes, pyrene, has the smallest change whereas the least condensed, chrysene, has the greatest change in molar volume. These differences in molar volume, like the changes in molar enthalpy, can be attributed to the depth that each PAH penetrates into the stationary phase. The more condensed PAHs, such as pyrene, probe only the distal regions, whereas less condensed PAHs, such as chrysene, penetrate more deeply into the ordered regions of the stationary phase. The change in molar volume becomes more negative the farther the PAH penetrates into the stationary phase. Again, it is noteworthy that the nonplanar solute, benzo[*c*]phenanthrene, has a smaller change in molar volume than the planar solutes. This is consistent with a smaller depth of penetration, as discussed above. However, it is not as extreme as for the six-ring nonplanar PAHs, phenanthro[*3,4-c*]phenanthrene and tetrabenzonaphthalene, which exhibit

Figure 5.3: Representative graph of the retention factor versus pressure used to calculate the change in molar volume according to Equation 1.7. Column: polymeric octadecylsilica. Mobile phase: methanol, 283 K, 0.08 cm/s. Symbols defined in Figure 5.1.

Figure 5.3

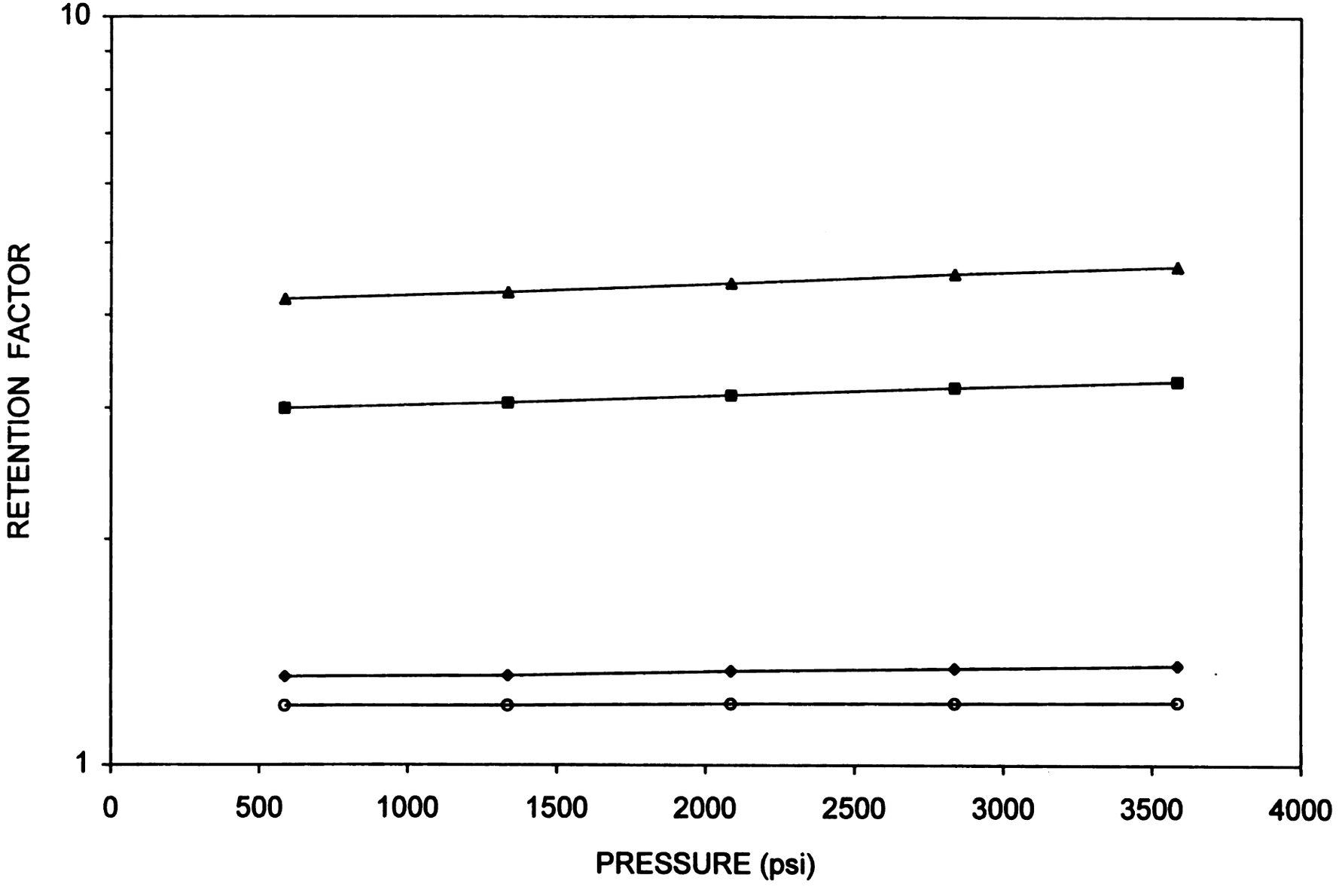
10
1
RETENTION FACTOR
0
500
1000
1500
2000
2500
3000
3500
4000
PRESSURE (psi)

positive changes in molar volume [12,16]. The molar volumes reported herein are consistent with those in Chapter 4 [12].

5.3.2 Kinetic Behavior

5.3.2.1 Rate Constant

Although the thermodynamic data demonstrate the steady-state aspects of chromatographic behavior, they do not fully explain the retention mechanism. Using the equations and methods developed in Chapters 1 and 2, the pseudo-first-order rate constants, activation enthalpies, and activation volumes were calculated. These values help to quantify the kinetic aspects of PAH transfer between the mobile and stationary phases as a function of the annelation structure.

Representative values of the rate constants, calculated using Equations 1.16 and 1.17, are summarized in Tables 5.3 and 5.4. The most condensed of the planar solutes, pyrene, has the largest rate constants, whereas the least condensed, chrysene, has the smallest rate constants for transport from mobile to stationary phase (k_{sm}) and from stationary to mobile phase (k_{ms}). However, the nonplanar solute, benzo[*c*]phenanthrene, has larger rate constants than the planar solutes. As for the solutes in Chapter 4, the transition from the stationary to mobile phase is the rate-limiting step for all of the four-ring PAHs. As shown in Table 5.3, the rate constants for all PAHs increase with increasing temperature. This behavior is a consequence of the increased diffusion coefficients and the enhanced fluidity of the stationary phase. As more kinetic energy is imparted,

Table 5.3: Rate constants for PAH isomers calculated by using the exponentially modified Gaussian (EMG) model as a function of temperature

Solute	k_{ms} (s^{-1}) [A]		k_{sm} (s^{-1}) [A]	
	283 K	293 K	283 K	293 K
Pyr	198	1137	269	1179
BaA	74	521	241	1099
Chr	7	58	34	163
BcP	216	1360	262	1330

[A] Rate constants from stationary to mobile phase (k_{ms}) and from mobile to stationary phase (k_{sm}) calculated at 3585 psi

Table 5.4: Rate constants for PAH isomers calculated by using the exponentially modified Gaussian (EMG) model as a function of pressure

Solute	k_{ms} (s^{-1}) [A]		k_{sm} (s^{-1}) [A]	
	585 psi	3585 psi	585 psi	3585 psi
Pyr	313	198	411	269
BaA	73	62	224	202
Chr	14	7	61	34
BcP	330	216	395	262

[A] Rate constants from stationary to mobile phase (k_{ms}) and from mobile to stationary phase (k_{sm}) calculated at 283 K

the alkyl chains become more labile and can more readily undergo rotation of the carbon-carbon bonds from the trans to gauche conformation. In fact, this polymeric octadecylsilica stationary phase is known to undergo a phase transition in the vicinity of 318 K [13,16]. This increased lability enables the PAHs to diffuse in and out of the stationary phase more freely. As shown in Table 5.4, the rate constants for all PAHs decrease with increasing pressure. This behavior is a consequence of the compression of the alkyl chains, which impedes the PAH diffusion in and out of the stationary phase.

5.3.2.2 Activation Enthalpy

A representative graph of the logarithm of the rate constant versus the inverse temperature is shown in Figure 5.3. The activation enthalpy is calculated from the slope of this graph, according to Equation 1.20. As shown in Table 5.5, there are slight differences that indicate the most condensed solute, pyrene, has the smallest activation enthalpies whereas the least condensed solute, chrysene, has the greatest activation enthalpy. However, given the uncertainties in these values, the differences are not statistically significant. The similarity in values implies that the activation enthalpy is largely independent of annelation structure, and suggests that the PAHs encounter a similar barrier at the interface between the mobile and stationary phases. As the activation enthalpies for the stationary to transition state ($\Delta H_{\ddagger s}$), as the mobile phase to transition state ($\Delta H_{\ddagger m}$) are compared to one another and to the change in molar enthalpy in(ΔH_{sm}) Table 5.2, a trend emerges: $\Delta H_{\ddagger s} > \Delta H_{\ddagger m} >> \Delta H_{sm}$. Thus, the enthalpic barrier for the

Figure 5.4: Representative graph of the logarithm of the rate constant (k_{ms}) versus inverse temperature used to calculate the activation enthalpy according to Equation 1.20. Column: polymeric octadecylsilica. Mobile phase: methanol, 3585 psi, 0.08 cm/s. Symbols defined in Figure 5.1.

Figure 5.4

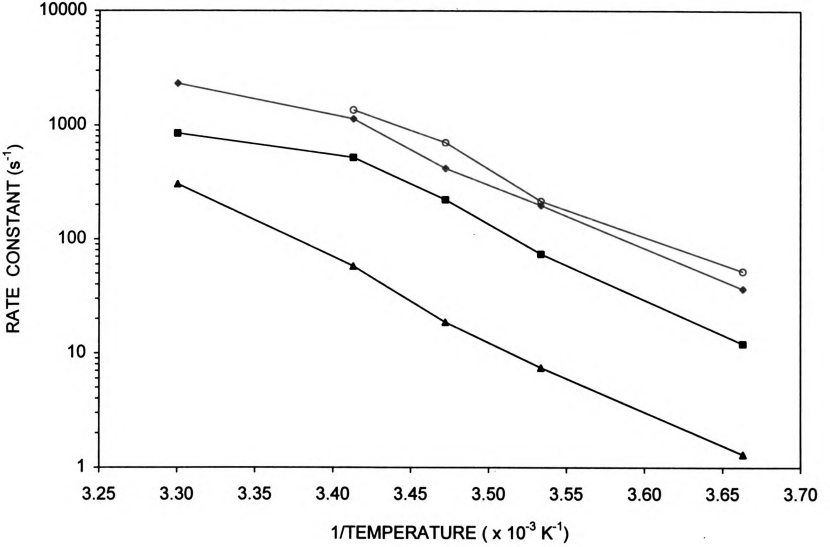
10000
1000
100
10
1
RATE CONSTANT (s-1)
3.25
3.30
3.35
3.40
3.45
3.50
3.55
3.60
3.65
3.70
1/TEMPERATURE (x 10-3 K-1)

Table 5.5: Activation enthalpies for PAH isomers

Solute	$\Delta H_{\ddagger s}$ (kcal/mol) [A]	$\Delta H_{\ddagger m}$ (kcal/mol) [A]
Pyr	24 ± 3	19 ± 3
BaA	25 ± 4	17 ± 3
Chr	31 ± 2	23 ± 2
BcP	27 ± 3	23 ± 3

[A] Activation enthalpies from stationary phase to transition state ($\Delta H_{\ddagger s}$) and from mobile phase to transition state ($\Delta H_{\ddagger m}$) calculated at 283 K and 3585 psi

transition is significantly greater than the thermodynamic change in molar enthalpy. This result is consistent with the data in Chapter 4.

5.3.2.3 Activation Volume

A representative graph of the logarithm of the rate constant versus pressure is shown in Figure 5.4. The activation volume is calculated from the slope of this graph, according to Equation 1.20. In contrast to the activation enthalpies, the activation volumes are a statistically significant function of the annelation structure. As shown in Table 5.6, the most condensed solute, pyrene, has the smallest activation volume whereas the least condensed solute, chrysene, has the greatest activation volume. The nonplanar solute, benzo[*c*]phenanthrene has a smaller activation volume than the planar chrysene, but can not be statistically differentiated from pyrene. Similar to the enthalpic trends, the activation volumes for the stationary to transition state ($\Delta V_{\ddagger s}$) and the mobile phase to transition state ($\Delta V_{\ddagger m}$), when compared to the change in molar volume (ΔV_{sm}) demonstrate the trend of $\Delta V_{\ddagger s} > \Delta V_{\ddagger m} >> \Delta V_{sm}$. Hence, the volumetric barrier for the transition is large, even though the overall change in molar volume is relatively small. This conclusion conforms to the data discussed in Chapter 4.

Figure 5.5: Representative graph of the rate constant (k_{ms}) versus pressure used to calculate the activation volume according to Equation 1.20. Column: polymeric octadecylsilica. Mobile phase: methanol, 283 K, 0.08 cm/s. Symbols defined in Figure 5.1.

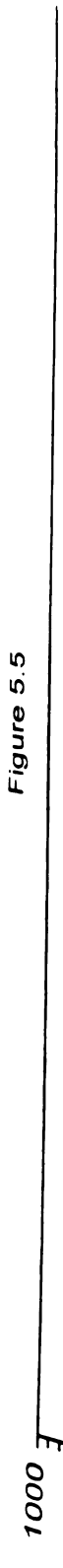

Figure 5.5

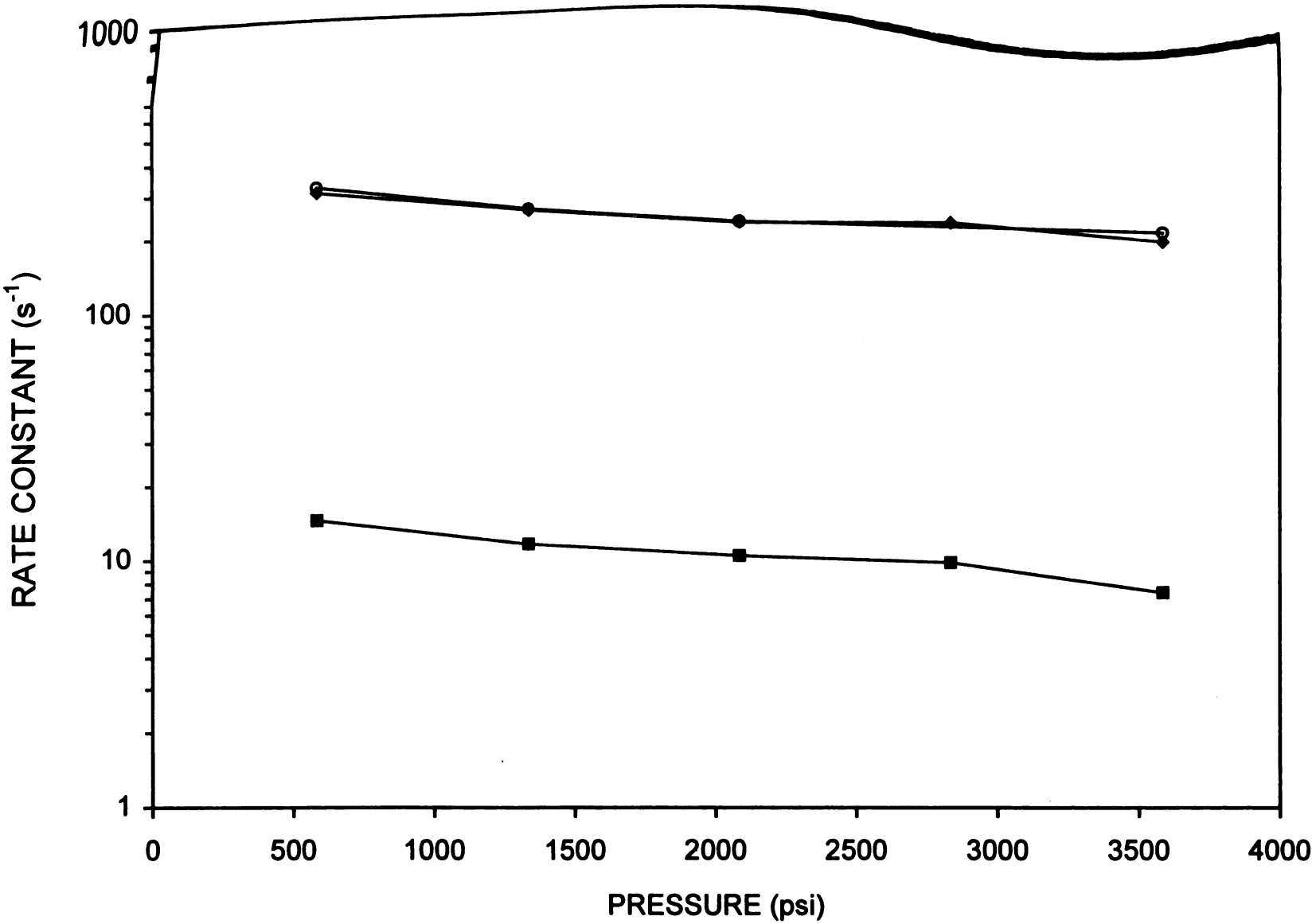
1000
100
10
1
RATE CONSTANT (s^{-1})
0
500
1000
1500
2000
2500
3000
3500
4000
PRESSURE (psi)

Table 5.6: Activation volumes for PAH isomers[A]

Solute	$\Delta V_{\ddagger s}$ (mL/mol)	$\Delta V_{\ddagger m}$ (mL/mol)
Pyr	47 ± 7	43 ± 7
BaA	NR [B]	NR
Chr	69 ± 9	57 ± 9
BcP	38 ± 13	37 ± 13

[A] Activation volumes from stationary phase to transition state ($\Delta V_{\ddagger s}$) and from mobile phase to transition state ($\Delta V_{\ddagger m}$) calculated at 283 K

[B] Values for benz[*a*]anthracene are not statistically reliable (NR) owing to large relative standard deviation (>100 % RSD).

5

th

no

te

re

tha

de

ret

to e

wer

diff

EM

mec

nonl

with

the s

linea

used

This r

resid

exhib

5.3.2.4 Kinetic Deviations

In the studies presented above, the PAH zone profiles were fit very well by the EMG equation, with typical R^2 values of 0.99 or greater. However, it was noted that the quality of fit was degraded slightly for some PAHs at the lowest temperature (273 K), with R^2 values of 0.98 – 0.99 and small nonrandom residuals along the tailing edge of the zone profile. Figure 5.5 illustrates a profile that exhibits this high R^2, but poor fit using the EMG equation. As these deviations from the EMG model may potentially arise from a change in the retention mechanism, more detailed investigation was warranted. First, in order to ensure that this effect did not arise from limited solubility, the PAH solutions were equilibrated at 273 K prior to injection. No statistically significant differences were observed in the PAH zone profiles or the quality of fit to the EMG equation.

To examine whether the low temperature causes a change in the retention mechanism, two alternative models were examined. The first alternative was the nonlinear chromatography model. The retention factors for the PAHs increase with decreasing temperature (Table 5.1), thereby increasing the concentration in the stationary phase. Hence, the isotherm might be expected to deviate from linearity at low temperature. Accordingly, the NLC model (Equation 2.6) was used to iteratively fit each of the PAH zone profiles that showed deviant behavior. This model, too, gave R^2 values of 0.98 – 0.99 and exhibited small nonrandom residuals from the observed zone profiles. Figure 5.6 illustrates a profile that exhibits this high R^2, but poor fit using the NLC equation. As shown in Table 5.7,

Figure 5.6: Representative graph from the nonlinear regression of experimental data using the exponentially modified Gaussian equation (EMG). The points represent collected data, while the line results from the predicted values from the EMG equation. Solute: chrysene, 273 K, 585 psi

Figure 5.6

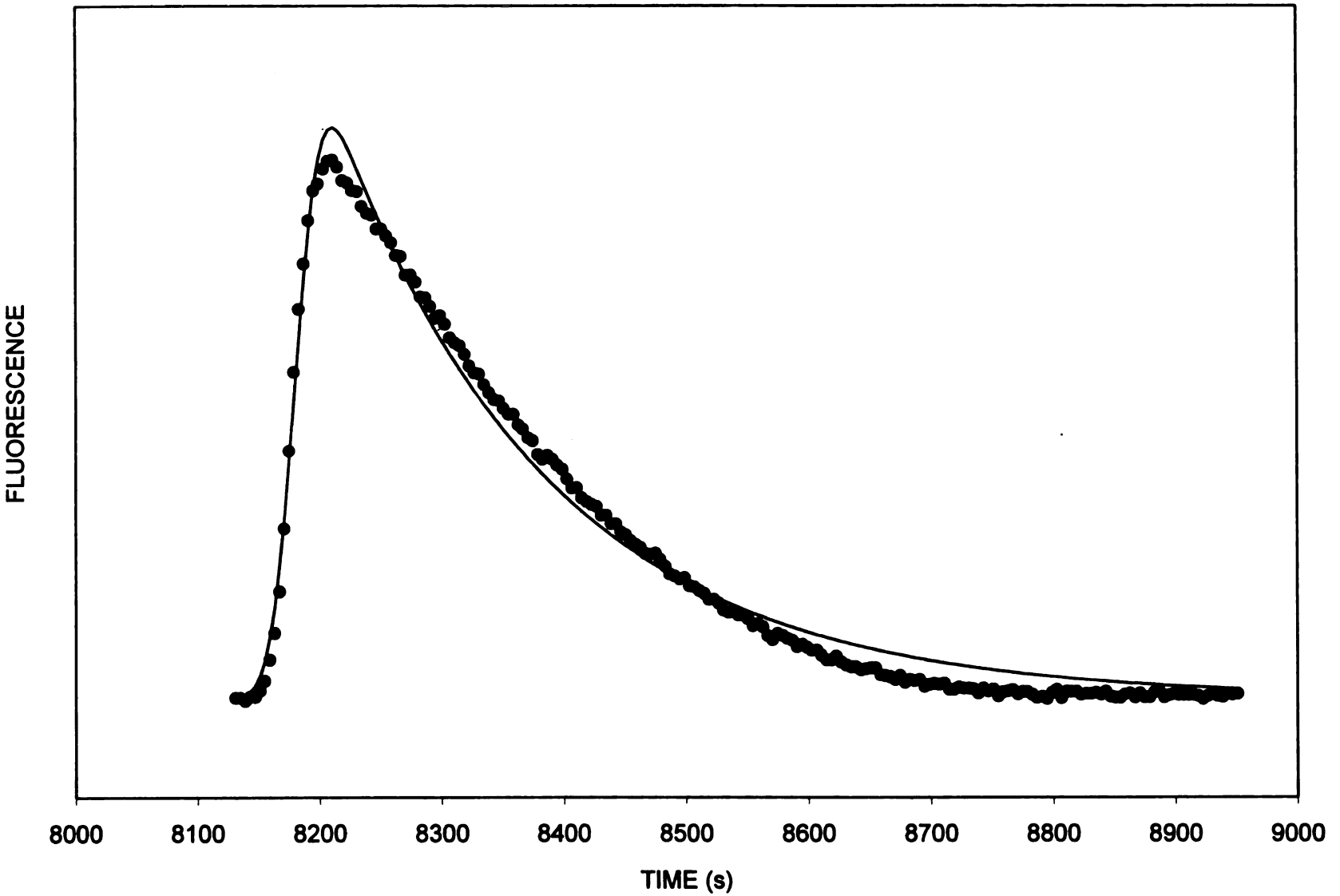
FLUORESCENCE
8000
8100
8200
8300
8400
8500
8600
8700
8800
8900
9000
TIME (s)

Figure 5.7: Representative graph from the nonlinear regression of experimental data using the non-linear chromatography equation (NLC). The points represent collected data, while the line results from the predicted values from the NLC equation. Solute: chrysene, 273 K, 585 psi

Figure 5.7

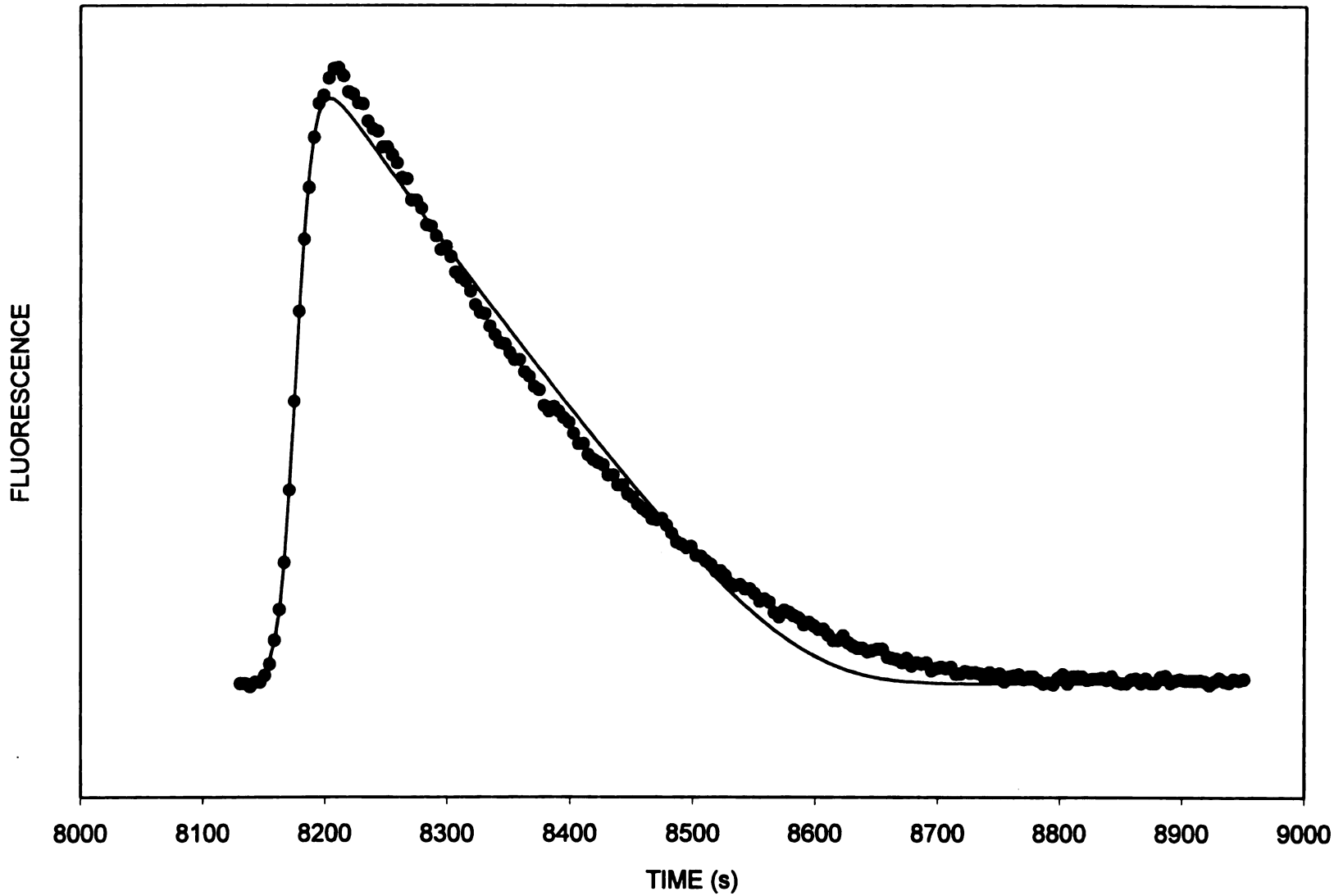
FLUORESCENCE
8000
8100
8200
8300
8400
8500
8600
8700
8800
8900
9000
TIME (s)

Table 5.7: Rate constants for PAH isomers calculated by using the EMG and NLC models

Solute	EMG [A]			NLC [A]		
	k_{ms} (s^{-1})	k_{sm} (s^{-1})	$R^{2,B}$	k_{ms} (s^{-1})	k_{sm} (s^{-1})	$R^{2,B}$
Pyr	38	69	0.996	12	23	0.999
BaA	12	64	0.994	7	37	0.999
Chr	1	11	0.987	6	44	0.993
BcP	52	84	0.997	12	20	0.999

[A] Rate constants from stationary to mobile phase (k_{ms}) and from mobile to stationary phase (k_{sm}) calculated at 273 K and 3585 psi

[B] Square of correlation coefficient for nonlinear regression (R^2)

the quality of fit for the NLC and EMG models was similar. The rate constants are of the same order of magnitude, but those determined by the NLC model are somewhat smaller than those determined by the EMG model for pyrene, benz[*a*]anthracene, and benzo[*c*]phenanthrene but somewhat larger for chrysene. This difference is a result of the peak shape of chrysene, which demonstrates more asymmetry than the other solutes.

As neither the EMG nor NLC model described the data well, a third model, the bi-exponentially modified Gaussian equation, was examined. This model is appropriate if there are two sites in the stationary phase with significantly different kinetic behavior. This behavior may arise from two partition sites or partition and adsorption sites. Accordingly, the E^2MG model (Equation 2.9) was used to iteratively fit each of the PAH zone profiles that showed deviant behavior. As shown in Table 5.8, this equation also had difficulty in fitting the zone profiles. For chrysene, the regression failed owing to overflow and underflow errors. Figure 5.7 demonstrates the visual aspects of this failure that result in a truncation of the regressed line. For the other PAHs, the E^2MG equation forces τ_1 and τ_2 to assume values very close to one another. The rate constants are the same for both sites, but are larger than those calculated using either the EMG or NLC models. These values imply that the kinetic sites are equally distributed and the same in their energetic natures. Thus, Tables 5.7 and 5.8 indicate that neither the NLC nor the E^2MG model provides a more accurate description of the solute zone profiles than the EMG model.

Table 5.8: Rate constants for PAH isomers calculated by using the bi-exponentially modified Gaussian (E^2MG) model for two sites

Solute	Site 1 [A]		Site 2		$R^{2,B}$
	k_{ms} (s^{-1})	k_{sm} (s^{-1})	k_{ms} (s^{-1})	k_{sm} (s^{-1})	
Pyr	79	148	79	148	0.999
BaA	32	171	32	171	0.998
Chr	NR [C]	NR	NR	NR	–
BcP	24	37	24	37	0.998

[A] Rate constants from stationary to mobile phase (k_{ms}) and from mobile to stationary phase (k_{sm}) calculated at 273 K and 3585 psi

[B] Square of correlation coefficient for nonlinear regression (R^2)

[C] Values for chrysene are not statistically reliable (NR) owing to overflow and underflow errors in nonlinear regression.

Figure 5.8: Representative graph from the nonlinear regression of experimental data using the biexponentially modified Gaussian equation (E2MG). The points represent collected data, while the line results from the predicted values from the E^2MG equation. Solute: chrysene, 273 K, 585 psi

Figure 5.8

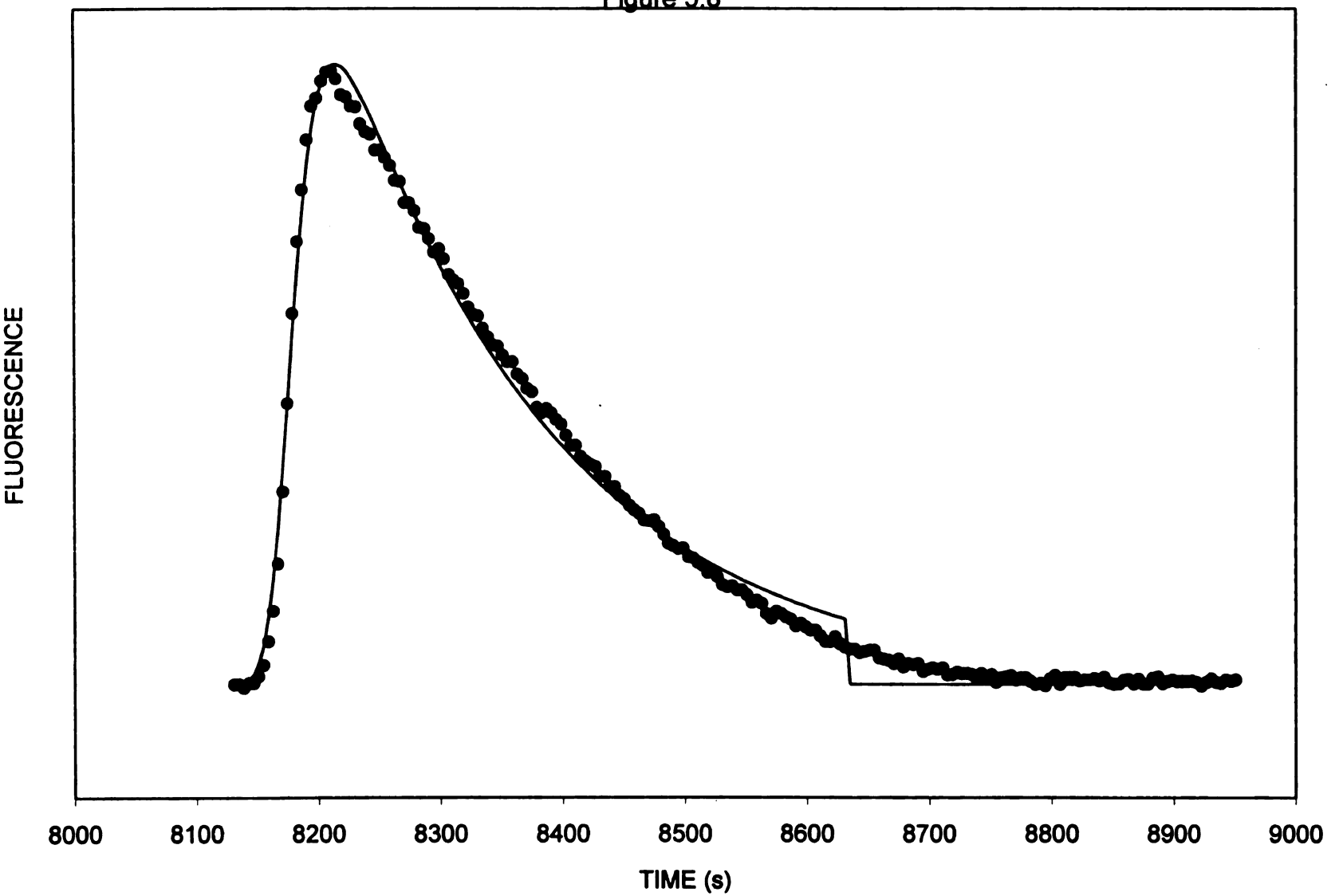
FLUORESCENCE
8000
8100
8200
8300
8400
8500
8600
8700
8800
8900
9000
TIME (s)

5.4 Conclusions

In this study, the thermodynamic and kinetic behavior of four-ring PAHs was examined in reversed-phase liquid chromatography. Even though the changes in molar enthalpy and molar volume are relatively small, the kinetic data suggest that the barrier for transition between mobile and stationary phases is large. For a solute like chrysene, the activation enthalpy is 23 kcal/mol for entry into the stationary phase, and 31 kcal/mol for exit from the stationary phase. There is a similarly large activation volume for each transition of 69 and 57 mL/mol, respectively. These relatively large values for activation enthalpy and activation volume suggest that the transition is more likely to occur in a series of discrete steps rather than in a single step. When the values for chrysene are compared to those for pyrene, it is apparent that the annelation structure influences the energy and volume contributions to the retention mechanism.

In addition, the anomalous behavior at 273 K suggests that the retention mechanism may change from a partition to an adsorption or mixed-mode mechanism. It is important to emphasize that this behavior is not apparent from the thermodynamic (steady state) measurements. The kinetic measurements are essential to make inferences about the mechanism. It is also important that these measurements be derived concurrently from the same data, so that the thermodynamic and kinetic measurements are internally consistent. From the examined models, there is no conclusive evidence for a nonlinear isotherm or for multiple sites with different kinetic behavior. The lack of data for a multiple site

model does not imply that such a mechanism is not present; simply that it is immeasurable using the current mathematical model.

5.5 References

[1] S.R. Cole, J.G. Dorsey, J. Chromatogr. 635 (1993) 177-186.

[2] J. Chmielowiec, H. Sawatzky, J. Chromatogr. Sci. 17 (1979) 245-252.

[3] K.B. Sentell, J.G. Dorsey, J. Chromatogr. 461 (1989) 193-207.

[4] K.B. Sentell, A.N. Henderson, Anal. Chim. Acta 246 (1991) 139-149.

[5] K.B. Sentell, N.I. Ryan, A.N. Henderson, Anal. Chim. Acta 307 (1995) 203-213.

[6] A.M. Stalcup, D.E. Martire, S.A. Wise, J. Chromatogr. 442 (1988) 1-13.

[7] L.C. Sander, S.A. Wise, J. Chromatogr. A 656 (1993) 335-351.

[8] L.C. Sander, S.A. Wise, Anal. Chem. 67 (1995) 3284-3292.

[9] L.C. Sander, M. Pursch, S.A. Wise, Anal. Chem. 71 (1999) 4821-4830.

[10] J. Wegmann, K. Albert, M. Pursch, L.C. Sander, Anal. Chem. 73 (2001) 1814-1820.

[11] S.B. Howerton, C. Lee, V.L. McGuffin, Anal. Chim. Acta 478 (2003) 99-110.

[12] S.B. Howerton, V.L. McGuffin, Anal. Chem. 75 (2003) 3539-3548.

[13] V.L. McGuffin, C. Lee, J. Chromatogr. A 987 (2003) 3-15.

[14] C.J. Orendorff, M.W. Ducey, Jr., J.E. Pemberton, J. Phys. Chem. A 106 (2002) 6991-6998.

[15] M.W. Ducey, Jr., C.J. Orendorff, J.E. Pemberton, L.C. Sander, Anal. Chem. 74 (2002) 5576-5584.

[16] V.L. McGuffin, S.-H. Chen, J. Chromatogr. A 762 (1997) 35-46.

Chapter 6: Thermodynamic and Kinetic Characterization of Nitrogen-Containing Polycyclic Aromatic Hydrocarbons in Protic and Aprotic Mobile Phases

6.1 Introduction

As demonstrated in Chapters 4 and 5, the effect of ring number and annelation are very important to the thermodynamics and kinetics of retention in liquid chromatography for polycyclic aromatic hydrocarbons (PAHs). This chapter presents similar measurements for a series of nitrogen containing polycyclic aromatic hydrocarbons.

At elevated temperatures, PAHs are capable of reacting to form compounds that contain substituent moieties that alter their toxicity. Two substitutions that lead to highly toxic analogues involve the exchange of a carbon with nitrogen to form an azaarene, and the replacement of hydrogen with an amino or nitro group. These solutes are collectively known as nitrogen-containing polycyclic aromatic hydrocarbons (NPAHs). NPAHs are commonly found in fossil fuels and their derivatives, though some form during combustion related events.

Relative to their parent PAH, NPAHs are more soluble in aqueous environments. Increased water solubility results in an increased potential for harm. For example, 1-aminopyrene has been reported to demonstrate a fifty-fold increase in mutagenic activity when compared to the parent PAH [1]. Similarly, azaarenes demonstrate increased carcinogenicity when compared to their parent compounds [2,3].

Studies have been carried out to determine the presence of NPAHs in fossil fuels [4-8], coal substitutes [9], lake sediment [10], urban aerosols [11], and polymer degradation products [12]. In order to identify and differentiate nitrogenous-PAHs, many investigators have used chromatographic techniques due to the high resolving power. These techniques have included gas [8,13,14], thin layer [15], supercritical fluid [16], and liquid chromatography [4-7,12,13,17-22]. However, in nearly all instances the chromatographic applications have focused only upon the optimization of the separation, and not a detailed probe of the molecular contributions to retention. Colin and co-workers noted the large amount of asymmetry in reversed-phase systems, and postulated that this tailing results from the presence of unreacted silanols or the slow equilibrium between the protonated and nonprotonated forms of the NPAHs [17]. Although the retention of these solutes has been studied extensively, no quantitative explorations of these solutes in reversed-phase liquid chromatography have been published. To overcome this dearth of information, the thermodynamics and kinetics of retention in RPLC for a series of NPAHs are presented.

Using the previously established methodology for the analysis of PAHs [23,24] described in Chapters 1,2, and 4, the thermodynamics and kinetics of retention are studied as a function of temperature, pressure, and mobile phase. By using protic (methanol) and aprotic (acetonitrile) solvents, the effect of mobile phase can be quantitated. This analysis provides insight into the mechanism of retention for these highly toxic compounds.

6.2 Experimental Methods

6.2.1 Solutes

As depicted in Figure 6.1, five NPAHs were chosen to study the effect of position, annelation, and ring number on the thermodynamics and kinetics of retention. 1-Aminopyrene (Sigma-Aldrich), 1-azapyrene, 4-azapyrene, benz[*a*]acridine, and dibenz[*a,j*]acridine (Institüt für PAH Forschung) were obtained as solids and dissolved in high-purity methanol and acetonitrile (Burdick and Jackson, Baxter Healthcare) to yield standard solutions at a concentration of 10^{-4} M. A nonretained marker, 4-methylhydroxy-7-methoxycoumarin,[25] was added to each solution at a concentration of 10^{-4} M.

6.2.2 Experimental System

The system used to study the NPAHs is depicted in Figure 2.2. The mobile phases were methanol and acetonitrile, and the stationary phase polymeric octadcecylsilica (5.4 μmol/m^2). The temperatures for these experiments were 283, 288, 293, 298 and 303 K for methanol, and 298, 303, 308, 313, and 323 K for acetonitrile. The inlet pressure for the methanol experiments were 1000, 1750, 2500, 3250 and 4000 psi. These values correspond to average pressures of 585, 1335, 2085, 2835, and 3585 psi, respectively, which were calculated assuming a linear pressure drop along the column. The inlet pressure for the acetonitrile experiments was 2500 psi, which

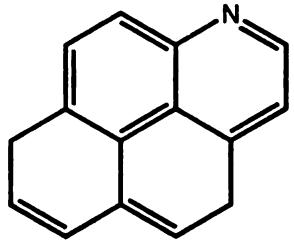

1-azapyrene

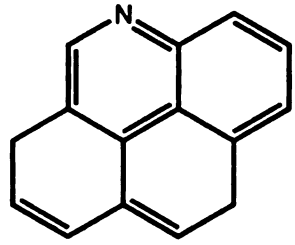

4-azapyrene

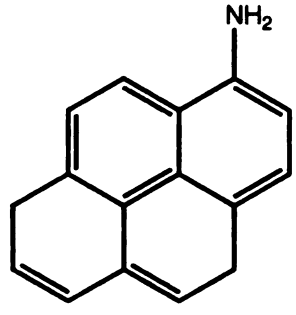

1-aminopyrene

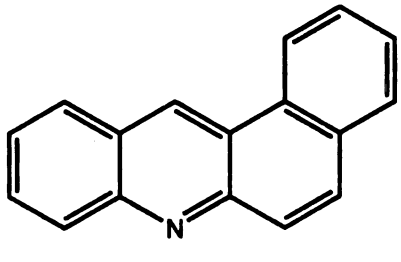

Benz[*a*]acridine

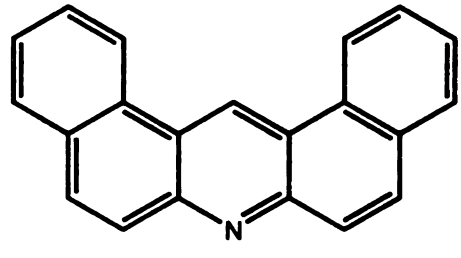

Dibenz[*a,j*]acridine

Figure 6.1: Structure of several nitrogen containing polycyclic aromatic hydrocarbons

corresponds to an average pressure of 2175 psi, which was calculated assuming a linear pressure drop along the column. The data were analyzed using the exponentially modified Gaussian (EMG) and the non-linear chromatography (NLC) equations, which are described in section 2.3.1.

6.3 Results and Discussion

6.3.1 Peak Profiles

For all of the analyses described below, the EMG function was used. The overall quality of fit for the data collected using a methanol mobile phase was high with random residuals, large correlation coefficients ($R^2 > 0.98$), and large F-statistics ($F > 1000$). The zone profiles (Figure 6.2A) are similar to those observed in previous studies [23,24]. However, the zone profiles for the data collected using acetonitrile are different, demonstrating a much larger degree of asymmetry (Figure 6.2B). This asymmetry likely results from a change in mechanism from partition to either an adsorptive or mixed mode (i.e. partition/adsorption). As a result, several zone profiles in acetonitrile were analyzed by using the NLC model. However, the NLC model failed to produce any improvement in the quality of fit ($R^2 > 0.95$, $F > 1000$) and was not used for comprehensive analysis of the data.

Figure 6.3 illustrates the difference between a peak fit with the EMG (6.3A) and the NLC (6.3B) functions for 4-azapyrene in acetonitrile. As illustrated, neither function demonstrates a high degree of visual correlation

Figure 6.2: Representative chromatograms of 4-azapyrene in A) methanol, 303 K 2085 psi, 0.08 cm/s and B) acetonitrile, 303 K, 2175 psi, 0.08 cm/s. Column: polymeric octadecylsilica. The inset is an expansion of the methanol chromatogram.

Figure 6.2

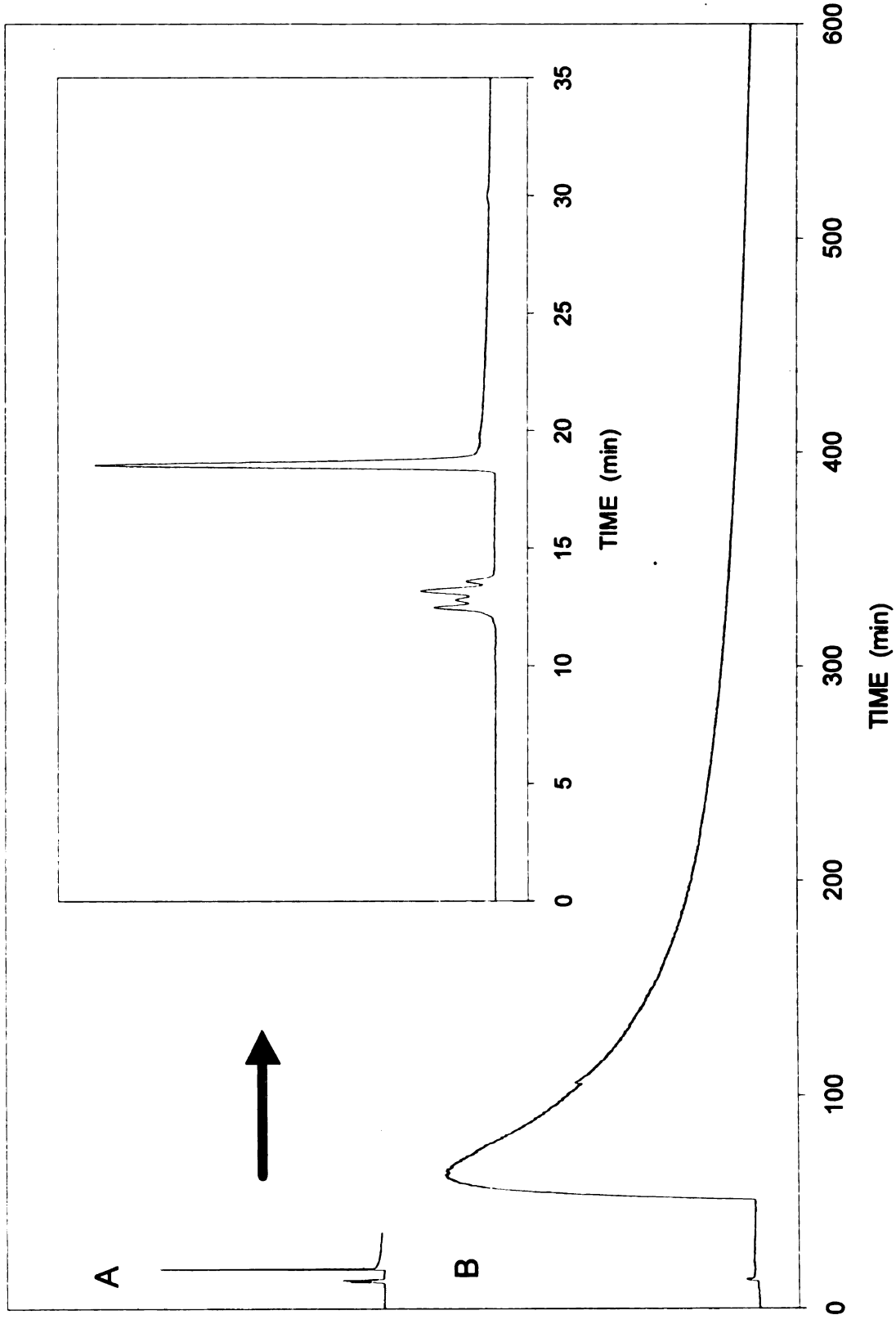

Figure 6.3: Representative chromatogram of 4-azapyrene in acetonitrile fit with the A) exponentially modified Gaussian equation and the B) non-linear chromatography equation.

Figure 6.3

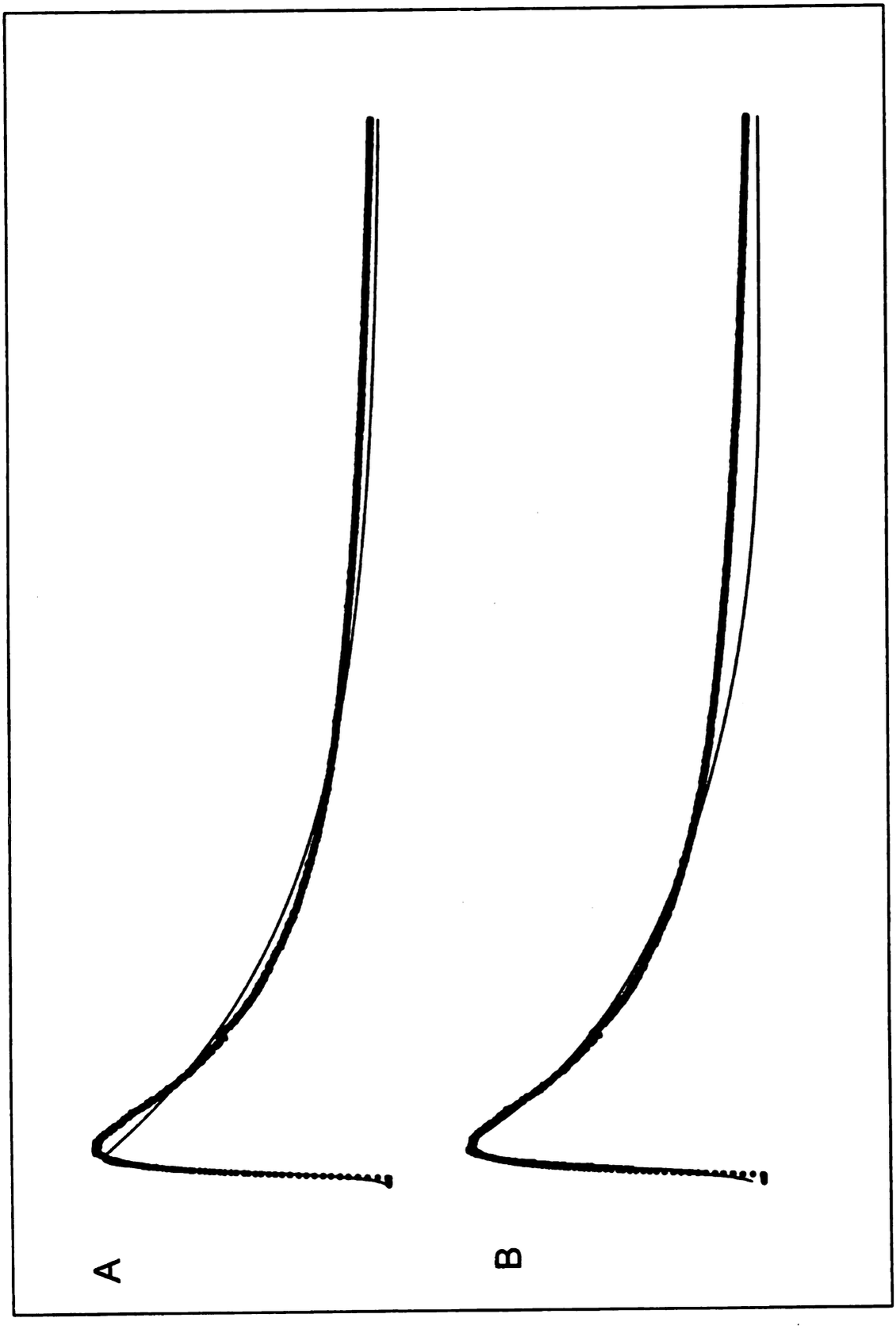

Figure 6.3

along the entirety of the peak. Numerically, the statistics of fit for both models are large: EMG (R^2 = 0.985, F = 52500), NLC (R^2 = 0.960, F = 18900). However, a comparison of Figure 6.3 and the statistics of fit demonstrate the danger in relying upon the statistics alone when analyzing peak profiles with either of these models.

6.3.2 Methanol Mobile Phase

6.3.2.1 Thermodynamic Behavior

6.3.2.1.1 Retention Factor

Representative values of the retention factor for the NPAHs in methanol are summarized in Table 6.1. The retention factors for the NPAHs are smaller than the parent PAHs [23]. At 303 K, 1-azapyrene and 4-azapyrene are eluted 38% and 44% faster than pyrene, respectively. Similarly, the retention of benz[*a*]acridine is 12% faster that benz[*a*]anthracene. This decreased retention in methanol is due to the increased solubility of the NPAHs relative to the PAHs. Since a partition mechanism is driven by differences in solubility [26], the more soluble NPAHs are less retained.

As demonstrated, the retention factor for all solutes decreases with increasing temperature. However, the retention factor increases with increasing pressure for benz[*a*]acridine and dibenz[*a,j*]acridine, but remains statistically invariant for the substituted pyrenes. The reasons for this behavior are discussed below in further detail.

Table 6.1: Retention factors for NPAHs in methanol

Solute [a]	k^a		k^b	
	288 K	303 K	585 psi	3585 psi
1-Aminopyrene	0.94	0.22	0.35	0.35
4-Azapyrene	0.78	0.47	0.79	0.78
1-Azapyrene	1.12	0.52	0.95	0.94
Benz[*a*]acridine	1.02	0.58	0.97	1.03
Dibenz[*a,j*]acridine	3.26	1.51	2.96	3.26

[a] Retention factor (k) calculated at 3585 psi

[b] Retention factor (k) calculated at 288 K

6.3.2.1.2 Molar Enthalpy

A representative graph of the logarithm of the retention factor versus the inverse temperature is shown in Figure 6.4. The data for methanol are depicted using solid lines. The graph for each solute is linear ($R^2 = 0.986 - 0.999$) and the slope is positive. A positive slope is indicative of a negative change in molar enthalpy and suggests that the transfer from mobile to stationary phase is enthalpically favorable. The change in molar enthalpy is calculated from the slope of Figure 6.4, according to Equation 1.5.

As shown in Table 6.2, the changes in molar enthalpy are the least negative for 1-aminopyrene. 1-Azapyrene and 4-azapyrene have changes in molar enthalpy that are similar, while benz[*a*]acidine is more negative than both. Dibenz[*a,j*]acridine, the NPAH with the most rings, demonstrates the most negative change in molar enthalpy. 1-Aminopyrene has the smallest change in molar enthalpy because it is more polar than the azapyrenes. This increased polarity increases the solubility in the mobile phase resulting in a smaller enthalpy. The changes in molar enthalpy for the other solutes follow the same trends as observed for the parent PAHs [23,24]. These tends indicate that the change in molar enthalpy becomes more negative with increasing ring number and decreasing condensation.

When compared to the parent PAHs, the changes in molar enthalpy are 1 to 2 kcal/mol more negative for the azapyrenes, and ~0.5 kcal/mol more negative for benz[*a*]acridine, even though the retention factors are smaller for the NPAHs. The more negative molar enthalpy for the NPAHs likely results from interactions

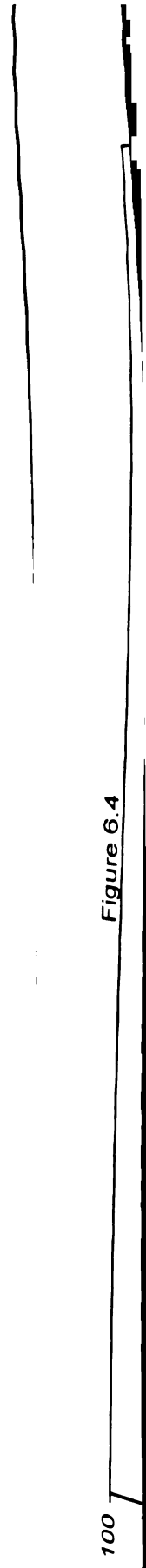

Figure 6.4: Representative graph of the retention factor versus inverse temperature used to calculate the change in molar enthalpy. Mobile phases: methanol, 2085 psi, 0.08 cm/s (——), acetonitrile, 2175 psi, 0.08 cm/s (– – –). Solutes: 1-aminopyrene (◇), 1-azapyrene (◆), 4-azapyrene (●), benz[*a*]acridine (■), dibenz[*a,j*]acridine (▲).

nverse

bile phases:

cm/s (---)

),

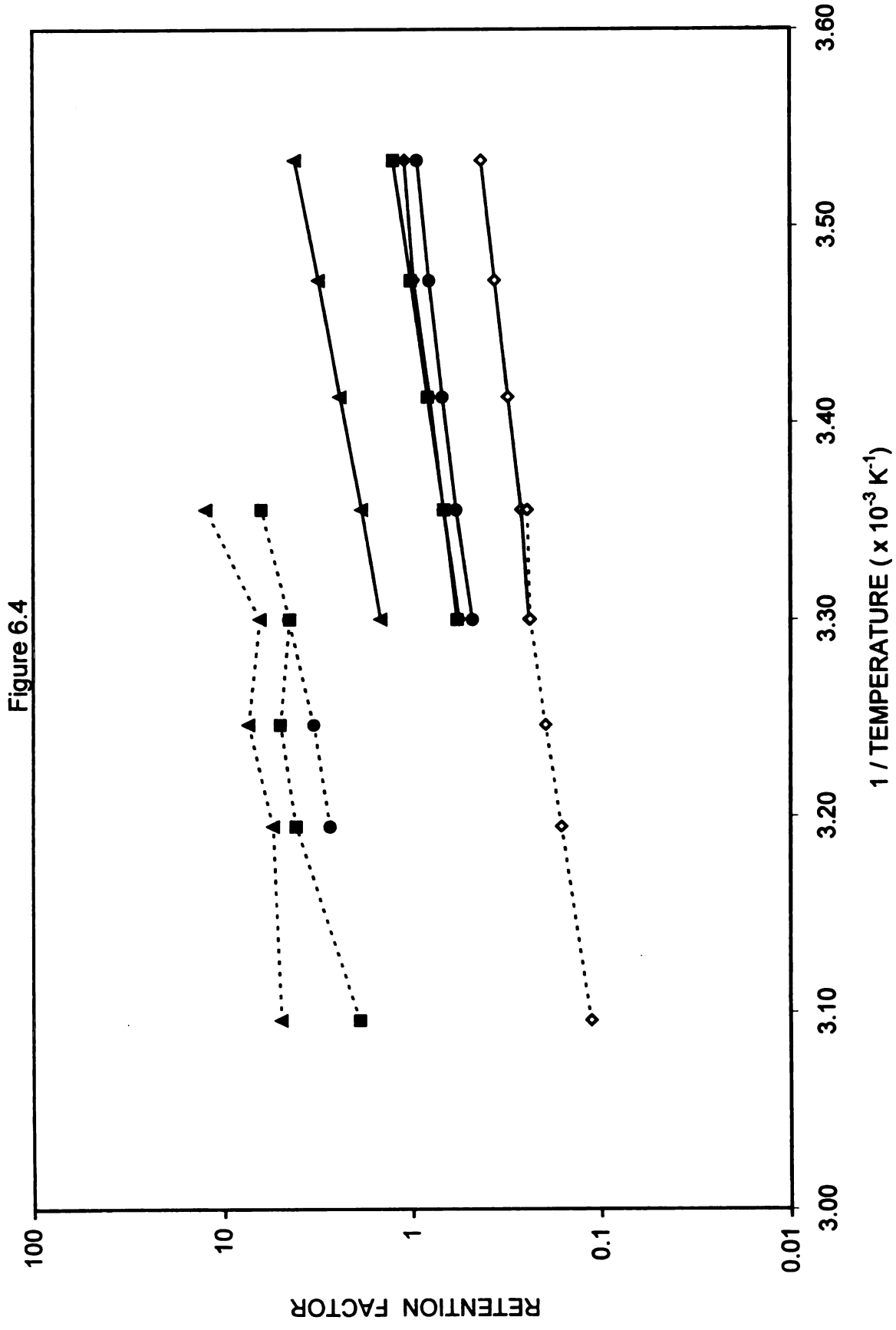

Figure 6.4

Table 6.2: Molar enthalpy and molar volume for NPAHs in methanol

Solute	ΔH_{sm} (kcal/mol) [a]	ΔV_{sm} (mL/mol) [b]
1-Aminopyrene	–5.0 ± 0.2	–1.7 ± 2[b]
4-Azapyrene	-5.6 ± 0.2	-1.5 ± 5[c]
1-Azapyrene	–5.7 ± 0.3	–1.0 ± 4[c]
Benz[a]acridine	–6.5 ± 0.1	–6.8 ± 1[c]
Dibenz[a,j]acridine	–8.9 ± 0.1	–10.7 ± 1[c]

[a] Molar enthalpy (ΔH_{sm}) calculated at 2085 psi

[b] Molar volume (ΔV_{sm}) calculated at 283 K

[c] Molar volume (ΔV_{sm}) calculated at 288 K

with the residual silanols [17]. The presence of the nitrogen within the NPAHs results in an increased basic character relative to the parent PAHs. This basicity allows the nitrogen to interact with silanols resulting in a more negative molar enthalpy.

The changes in molar enthalpy, and the retention factor at varying temperatures, are directly related to the depth to which a given solute penetrates. Highly condensed solutes, such as 1-azapyrene and 4-azapyrene, probe the regions of the octadecylsilica (ODS) that are closer to the distal terminus. As discussed previously, this region is characterized by a high degree of disorder and an increased density of gauche conformations [24,27,28]. Benz[*a*]acridine and dibenz[*a,j*]acridine, having a more linear structure, can probe the regions of the ODS closer to the proximal terminus, where the alkyl group is bound to the silica surface. These regions are highly ordered with all trans carbon-carbon bonds [27,28]. Since these regions are more ordered, the intermolecular distances between the solute and stationary phase are smaller, resulting in a more negative change in molar enthalpy. As temperature is increased, the ODS becomes more fluid. This increased fluidity allows the smaller solutes to penetrate further into the ODS, closer to the silanols.

Although there have been no published studies on the thermodynamics of NPAHs in RPLC, Woodrow and Dorsey studied the partitioning of acridine in micellar electrokinetic chromatography [29]. They report the enthalpy of transition as –6.75 kcal/mol for this solute. In addition, Shang et al. report the molar enthalpy of pyridine in supercritical fluid chromatography [30]. Varying the

density of the CO_2 mobile phase, they report values ranging from –6.17 to –7.41 kcal/mol. When compared to the data in Table 6.2, these values are similar, suggesting that the method employed herein is consistent with other experimental measurements of these solutes.

6.3.2.1.3 Molar Volume

A representative graph of the logarithm of the retention factor versus pressure is shown in Figure 6.5. For all solutes, the effect of pressure is small in methanol. Although the graph for each PAH is linear, the correlation coefficients are varied given the small influence that pressure has on retention (R^2 = 0.594 – 0.998). Similar to the molar enthalpy graph, the slope is positive for all solutes. A positive slope is indicative of a negative change in molar volume and suggests that the solute occupies less volume in the stationary phase than in the mobile phase. It should be noted that the smallest correlation coefficients correspond to the azapyrenes, the solutes that are affected by pressure changes the least. The change in molar volume is calculated from the slope of this graph, according to Equation 1.7. As shown in Table 6.2, 1-aminopyrene, 1-azapyrene, and 4-azapyrene have values that are statistically indistinguishable, and close to zero. In contrast, benz[*a*]acridine and dibenz[*a,j*]acridine demonstrate changes in molar volume that are statistically nonzero, with the five-ring NPAH demonstrating a more negative change in molar volume than the four ring analogue. The values for the azapyrenes and the benz[*a*]acridine are similar to those for the parent PAHs [24].

Figure 6.5: Representative graph of the retention factor versus pressure used to calculate the change in molar volume. Experimental conditions and symbols defined in Figure 6.4.

Figure 6.5

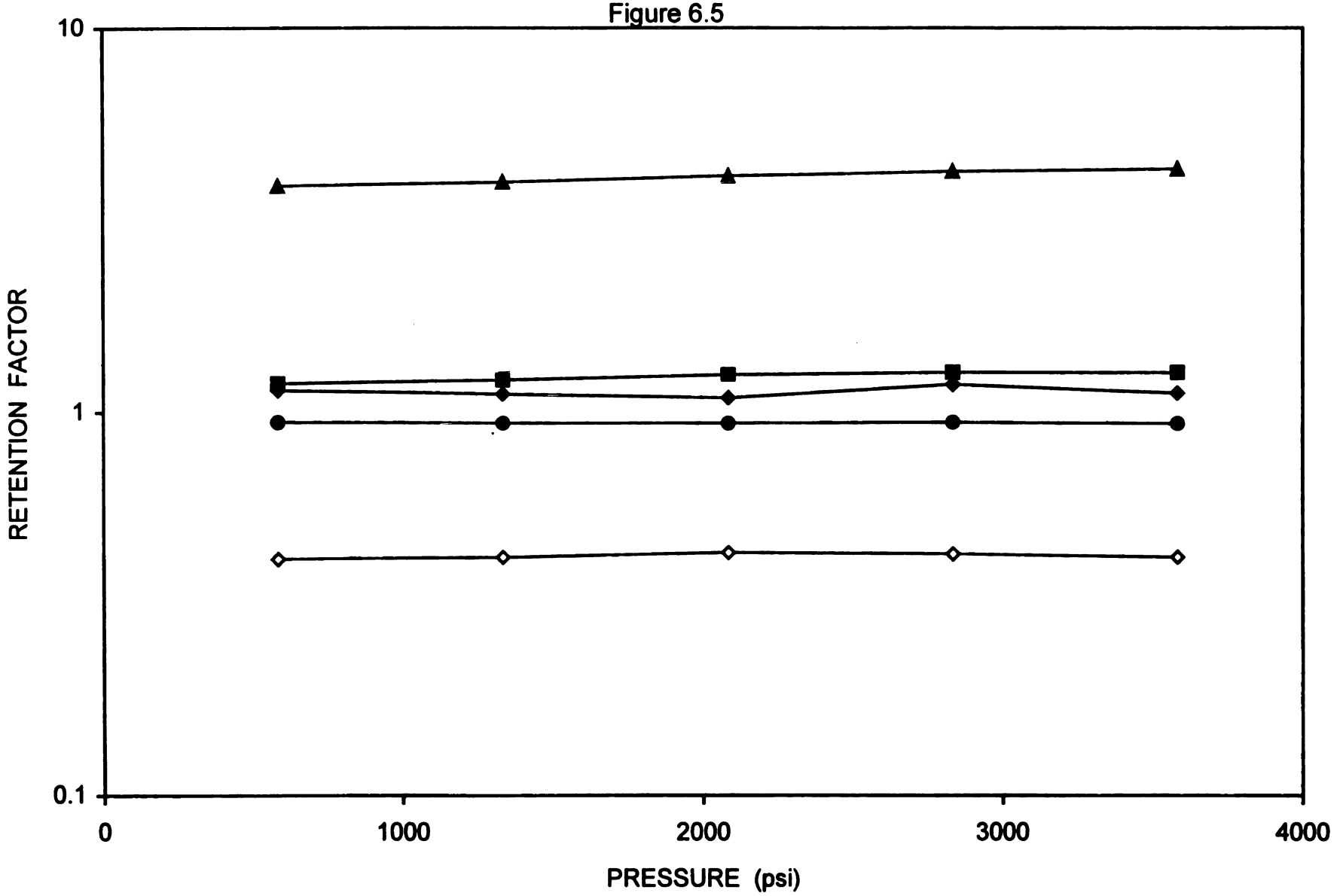

The differences in the molar volume are attributed to the depth that each NPAH penetrates into the stationary phase [23,24]. As pressure is increased, the ODS alkyl chains are forced closer together, increasing the overall order of the system. Highly condensed solutes, which probe the regions of the octadecylsilica that are closer to the distal terminus, demonstrate near-zero changes in molar volume because these regions remain fluid even at high pressure. However, those solutes that penetrate further into the stationary phase can probe regions that are more tightly packed, reducing the final volume that the solute occupies. This change in fluidity is analogous to the change imparted by temperature, except that an increase in pressure results in the same phenomena as a decrease in temperature.

6.3.2.2 Kinetic Behavior

6.3.2.2.1 Rate Constants

Although the thermodynamic data demonstrate the steady-state aspects of chromatographic behavior, they do not fully explain the retention mechanism. Using the equations and methods developed in Chapters 1 and 2, the pseudo-first-order rate constants, activation enthalpies, and activation volumes were calculated. These values help to quantify the kinetic aspects of mass transfer between the mobile and stationary phases as a function of solute structure. These data provide information about the retention that would be unavailable from thermodynamic data alone.

Representative values of the rate constants, calculated using Equations 1.16 and 1.17, are summarized in Table 6.3. At constant pressure, 1-

aminopyrene undergoes the fastest rates of transfer, followed by 4-azapyrene and benz[a]acridine. Dibenz[a,j]acridine undergoes slower rates of transfer, but 1-azapyrene is the slowest of all the solutes. The rate constants for the azapyrenes and benz[a]acridine are smaller than their parent PAHs [24]. It should be noted that at 288 K, the retention factor for benz[a]acridine is equal to unity (k = 1). Thus, the rate constants are equivalent.

For 1-aminopyrene, 1-azapyrene, 4-azapyrene, and benz[*a*]acridine the rate-limiting step is the transfer from mobile to stationary phase. By contrast, the rate-limiting step for dibenz[*a,j*]acridine is the transfer from stationary to mobile phase. The difference in the rate-limiting step is a consequence of the solubility of the solutes. As noted above, the polarity of the solutes make them less soluble in the ODS, thus increasing the rate of expulsion. Although dibenz[*a,j*]acridine is also polar, the larger number of rings decrease the localized electron density on the nitrogen. This delocalization of the lone pair of electrons causes the molecule to behave in an analogous manner to the parent PAH. These increased interactions lead to the slower rates of transfer out of the stationary phase.

Table 6.3: Rate constants for NPAHs in methanol as a function of temperature and pressure

Solute	k_{ms} (s^{-1}) [a]		k_{sm} (s^{-1}) [a]		k_{ms} (s^{-1}) [b]		k_{sm} (s^{-1}) [b]	
	288 K	303 K	288 K	303 K	585 psi	3585 psi	585 psi	3585 psi
1-Aminopyrene	148	675	52	154	351	148	123	52
4-Azapyrene	18	62	14	30	14	18	11	14
1-Azapyrene	0.7	4	0.6	2	0.8	0.7	0.7	0.7
Benz[*a*]acridine	14	81	14	47	18	14	17	14
Dibenz[*a,j*]acridine	6	49	21	75	9	6	28	21

[a] Rate constants from stationary to mobile phase (k_{ms}) and from mobile to stationary phase (k_{sm}) calculated at 3585 psi

[b] Rate constants calculated at 288 K

As shown in Table 6.3, the rate constants for all solutes increase with increasing temperature. This behavior is a consequence of the increased diffusion coefficients and the enhanced fluidity of the stationary phase. As more kinetic energy is imparted, the alkyl chains become more labile and can more readily undergo rotation of the carbon-carbon bonds from the trans to gauche conformation.

Also shown in Table 6.3, the rate constants decrease, or remain invariant, with increasing pressure for all solutes. This behavior is a consequence of the compression of the alkyl chains, which impedes solute diffusion into and out of the stationary phase. As the stationary phase is compressed, it becomes more hydrophobic, and thus excludes the polar NPAHs. The net increase in van der Waals forces that dibenz[*a,j*]acridine participates in overcomes this exclusion and allow the solute to behavior in a manner more similar to the parent PAHs.

It should be noted that the rate constants for 1-azapyrene and 4-azapyrene are statistically invariant with pressure. These data indicate that these solutes are not affected by the compression of the octadecylsilica chains. Rather, these solutes are interacting with adsorption sites within the stationary phase. These adsorption sites may be at the silica interface, or may result from the incomplete polymerization of the stationary phase. While it may be argued that the observed effect results from the depth to which these solutes penetrate the ODS, the likelihood that this is the only cause of the pressure independence is unlikely. As demonstrated for pyrene, pressure has little effect on the rates of transfer.[24] However, the rates are noticeably larger (~1000 s^{-1}) than those in

Table 6.3. The difference in the rate constants for these solutes indicates that the azapyrenes are accessing different sites, and that these sites are lower in energy than the partition 'sites' of the system (i.e. the molar enthalpies are more negative). These data support the assertion by Colin and co-workers [17]. Finally, the difference between the rate constants for 1-azapyrene and 4-azapyrene indicate that the location of the nitrogen is important when accessing these adsorption sites. This order of magnitude difference implies that the 1-azapyrene is configured preferentially to sorb at these sites.

6.3.2.2.2 Activation Energy

A representative graph of the logarithm of the rate constant versus the inverse temperature is shown in Figure 6.6. The data for methanol are depicted using solid lines. The graph for each solute is linear ($R^2 = 0.968 - 0.995$) and the slope is negative. A negative slope is indicative of a positive energy barrier. The activation energy is calculated from the slope of this graph, according to Equation 1.18. As shown in Table 6.4, the activation energies are positive for all solutes. The activation energy for the transfer between the stationary and transition state ($\Delta E_{\ddagger s}$) is larger than the activation energy for the transfer between the mobile and transition state ($\Delta E_{\ddagger m}$). These data indicate that it is easier for the solutes to exit the stationary phase than it is for them to enter it. Using a student t test to determine whether there are statistical differences, it was impossible to discern any definitive trend for these solutes.

Figure 6.6: Representative graph of the rate constant (k_{ms}) versus inverse temperature used to calculate the activation energy. Column: polymeric octadecylsilica. Mobile phases: methanol, 2085 psi, 0.08 cm/s (——), acetonitrile, 2175 psi, 0.08 cm/s (– – –). Symbols defined in Figure 6.4.

Figure 6.6

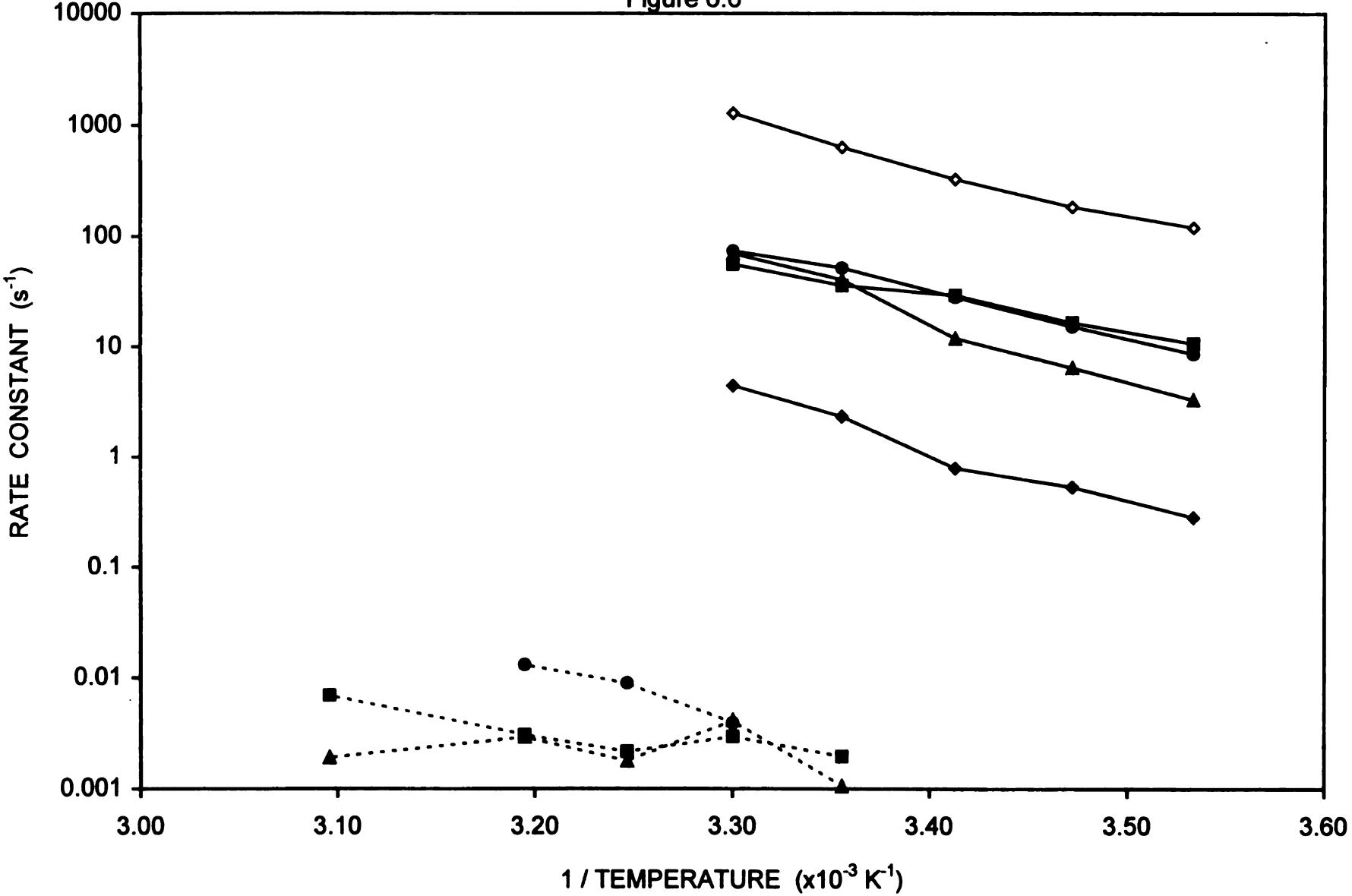
10000
1000
100
10
1
0.1
0.01
0.001
RATE CONSTANT (s^{-1})
3.00
3.10
3.20
3.30
3.40
3.50
3.60
1 / TEMPERATURE ($x10^{-3}$ K^{-1})

Table 6.4: Activation energies and activation volumes for NPAHs in methanol

Solute	$\Delta E_{\ddagger s}$ (kcal/mol) [a]	$\Delta E_{\ddagger m}$ (kcal/mol) [a]	$\Delta V_{\ddagger s}$ (mL/mol) [b]	$\Delta V_{\ddagger m}$ (mL/mol) [b]
1-Aminopyrene	21 ± 1	16 ± 1	97 ± 20	98 ± 18
4-Azapyrene	19 ± 1	14 ± 1	5 ± 6	6 ± 7
1-Azapyrene	24 ± 2	18 ± 2	47 ± 47	46 ± 44
Benz[*a*]acridine	21 ± 3	14 ± 3	58 ± 36	50 ± 36
Dibenz[*a,j*]acridine	25 ± 1	16 ± 1	48 ± 15	37 ± 15

[a] Activation energies from stationary phase to transition state ($\Delta E_{\ddagger s}$) and from mobile phase to transition state ($\Delta E_{\ddagger m}$) calculated at 2835 psi

[b] Activation volumes from stationary phase to transition state ($\Delta V_{\ddagger s}$) and from mobile phase to transition state ($\Delta V_{\ddagger m}$) calculated at 288 K

6.3.2.2.3 Activation Volume

A representative graph of the natural logarithm of the rate constant versus pressure is shown in Figure 6.7. The activation volume is calculated from the slope of this graph, according to Equations 8 and 9. As shown in Table 6.4, 1-aminopyrene has the largest activation volume while 1-azapyrene and 4-azapyrene have the smallest. Given the large standard deviation, the values for the azapyrenes are statistically indistinguishable and may in fact be zero. The values for the two azapyrenes are analogous to pyrene ($\Delta V_{\ddagger s} = 47 \pm 7$ mL/mol, $\Delta V_{\ddagger m} = 43 \pm 7$ mL/mol) [24]. Benz[*a*]acridine and dibenz[*a,j*]acrdine demonstrate activation volumes larger than the azapyrenes, but smaller than the aminopyrene. Given the large deviation abut the values, definitive correlation between the activation volumes and structure are currently unavailable. However, the activation volumes and the change in molar volume demonstrate the trend of $\Delta V_{\ddagger s} > \Delta V_{\ddagger m} >> \Delta V_{sm}$. Hence, the volumetric barrier for the transition is large, even though the overall change in molar volume is relatively small.

Figure 6.7: Representative graph of the rate constant (k_{ms}) versus pressure used to calculate the activation volume. Column: polymeric octadecylsilica. Mobile phase: methanol, 283 K, 0.08 cm/s. Symbols defined in Figure 6.3.

Figure 6.7

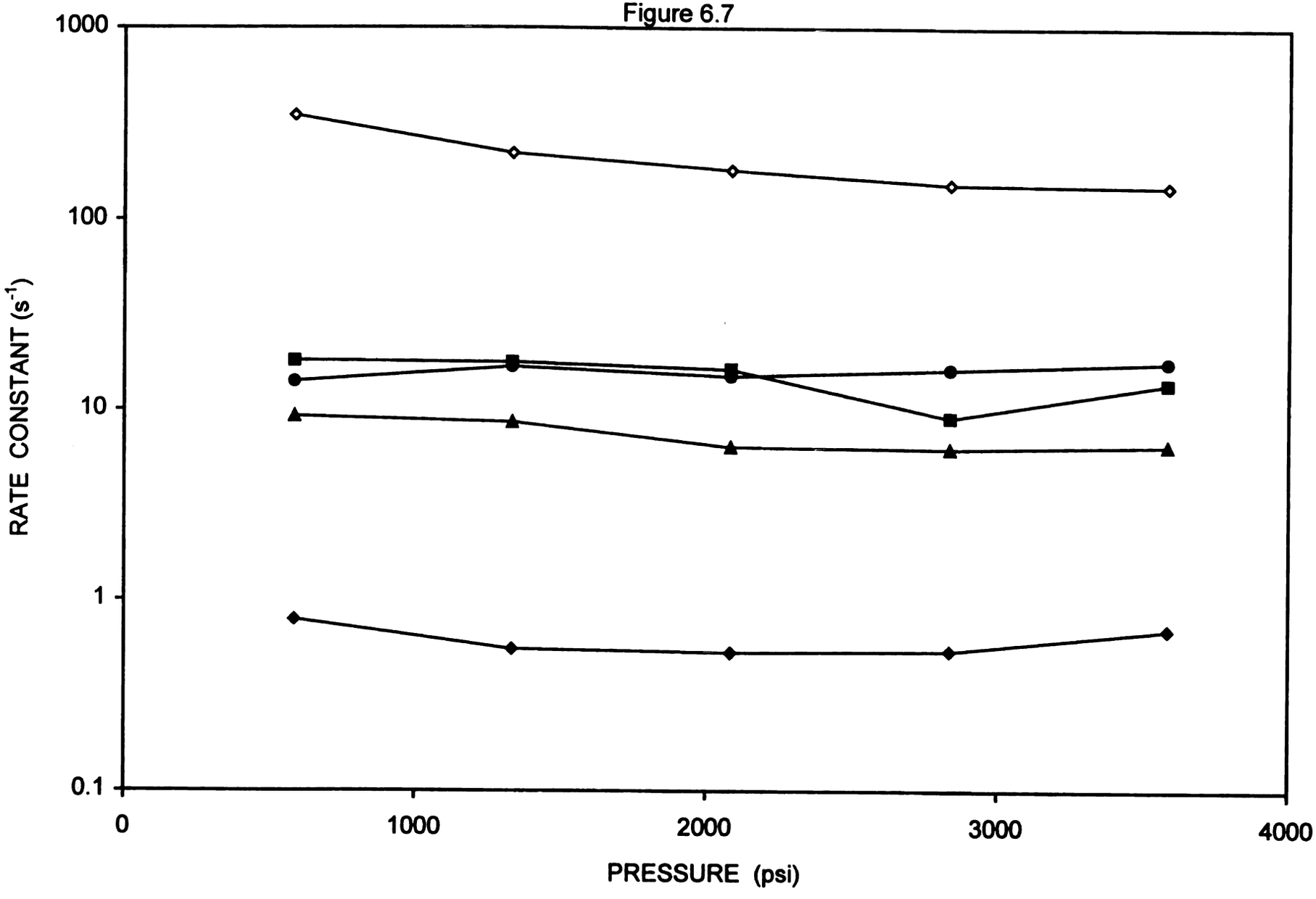
1000
100
10
1
0.1
RATE CONSTANT (s^{-1})
0
1000
2000
3000
4000
PRESSURE (psi)

6.3.3 Acetonitrile Mobile Phase

As noted above, Colin and co-workers postulate that the nitrogen in an NPAH can interact with the silica surface, leading to high degrees of asymmetry [17]. In order to test this hypothesis, acetonitrile was used to determine how an aprotic solvent would affect retention and the concomitant thermodynamic and kinetic parameters. Since acetonitrile is incapable of hydrogen bonding, it does not compete for adsorption sites that are capable of participating in such bonds. Although most solutes are retained via a partition mechanism in RPLC when acetonitrile is used, we hypothesized that the NPAHs could be retained either by a partition or adsorption mechanism.

Given that the data from the methanol studies exhibited small changes with pressure, the acetonitrile study was conducted at a single average pressure of 2175 psi. In contrast to the effect of pressure, the effect of temperature was significant in methanol. Thus, a large temperature range was also used for the acetonitrile (T = 293 to 333 K).

6.3.3.1 Thermodynamic Behavior

6.3.3.1.1 Retention Factor

Representative values of the retention factor are summarized in Table 6.5. As demonstrated, 1-aminopyrene is eluted first, followed by 4-azapyrene and benz[*a*]acridine. Dibenz[*a,j*]acridine is retained the most of the solutes. When compared to the retention factors in methanol (Table 1), all solutes except for 1-aminopyrene demonstrate an increase in retention. Given that acetonitrile is less

Table 6.5: Thermodynamic data for NPAHs in acetonitrile [a]

Solutes	k (303 K)	k (313 K)	ΔH_{sm} (kcal/mol)
1-Aminopyrene	0.23	0.16	–6.3 ± 0.7
4-Azapyrene	4.54	2.74	–9.5 ± 1.1
Benz[*a*]acridine	4.47	4.15	–8.3 ± 2.1
Dibenz[*a,j*]acridine	6.43	5.49	–6.1 ± 2.1

[a] All data calculated at 2185 psi

polar than methanol, the retention factor is expected to decrease if a partition mechanism is in effect. However, the increase in retention factor for four of the solutes implies that an adsorption mechanism is contributing to the observed behavior. By contrast, 1-aminopyrene exhibits behavior that is consistent with a partition mechanism. Similar to methanol, an increase in temperature results in a decrease in the retention factor for the reasons described above.

6.3.3.1.2 Molar Enthalpy

A representative graph of the logarithm of the retention factor versus the inverse temperature is shown in Figure 6.4. The data for acetonitrile are graphed using dashed lines. The graph for each solute is linear ($R^2 = 0.724 - 0.986$) and the slope is positive. A positive slope is indicative of a negative change in molar enthalpy and suggests that the transfer from mobile to stationary phase is enthalpically favorable. The change in molar enthalpy is calculated from the slope of Figure 6.4, according to Equation 1.5.

As shown in Table 6.5, the changes in molar enthalpy are the least negative for 1-aminopyrene and dibenz[*a,j*]acridine followed by benz[a]acridne and 4-azapyrene. When compared to the methanol data, the changes in molar enthalpy are similar for all solutes except 4-azapyrene. This difference as a function of mobile phase suggests that the 4-azapyrene is accessing sorption sites that are less available to the more linear solutes.

It should be noted that the changes in molar enthalpy are similar in both methanol and acetonitrile, even though the retention factors are different. These data imply that adsorption sites become available in the presence of an aprotic

solvent, but that the bonded ODS affects the accessibility of these sites. Since the NPAHs must diffuse through the ODS to reach the adsorption sites, the ODS acts as a barrier, preventing complete access to the surface. Thus, the effect of temperature on ODS plays an important role for these solutes in both the protic and aprotic mobile phases. 4-Azapyrene, being the most condensed solute, can diffuse more easily through the ODS chains, reaching the surface more quickly. Thus, the change in molar enthalpy for this solute is exaggerated. Since the other solutes are larger, it is energetically more difficult for them to reach the adsorption sites. Thus, their main mode of interaction still resides with the ODS.

6.3.3.2 Kinetic Behavior

6.3.3.2.1 Rate Constants

Representative values of the rate constants, calculated using Equations 1.16 and 1.17, are summarized in Table 6.6. At constant pressure, 1-aminopyrene undergoes the fastest rates of transfer, followed by dibenz[*a,j*]acridine, 4-azapyrene and benz[*a*]acridine. As with methanol, the rate-limiting step for 1-aminopyrene is the mobile to stationary phase transfer The other three solutes demonstrate the inverse trend, with the stationary to mobile phase transfer taking more time. When compared to the methanol data, the rate constants are two to four orders of magnitude smaller in acetonitrile.

Table 6.6 : Kinetic data for NPAHs in acetonitrile [a]

	k_{ms} (s^{-1})		k_{sm} (s^{-1})			
Solutes	303K	313 K	303 K	313 K	$\Delta E_{‡s}$ (kcal/mol)	$\Delta E_{‡m}$ (kcal/mol)
1-Aminopyrene	3.47	3.67	8.2×10^{-1}	5.9×10^{-1}	~ 0	~ 0
4-Azapyrene	3.9×10^{-3}	1.3×10^{-3}	1.8×10^{-2}	3.6×10^{-2}	9 ± 3	~ 0
Benz[*a*]acridine	2.9×10^{-3}	3.0×10^{-3}	1.3×10^{-2}	1.3×10^{-2}	2 ± 6	~ 0
Dibenz[*a,j*]acridine	4.1×10^{-3}	2.9×10^{-3}	2.6×10^{-2}	1.6×10^{-2}	23 ± 5	13 ± 3

[a] All data calculated at 2185 psi

The differences in the rate constants result from an increase in the ability of these solutes to interact with the silica support. Although very few molecules diffuse to the proximal terminus of the ODS, those that do bind strongly once they are within the minimum distance for interaction with the underlying silica support. This argument should hold true for dibenz[*a,j*]acridine as well. However, the nitrogen in dibenz[*a,j*]acridine is partially occluded by a phenyl unit. In addition, for the nitrogen to interact with the surface, dibenz[*a,j*]acridine must diffuse toward the surface with its longest axis parallel to the underlying silica support. Such diffusion is energetically less favorable than diffusion with its shortest axis parallel to the underlying support, and results in larger rate constants than might be predicted.

6.3.3.2.2 Activation Energy

A representative graph of the logarithm of the rate constant versus the inverse temperature is shown in Figure 6.6. The data for acetonitrile are depicted using dashed lines. It should be noted that the data for 1-aminopyrene are not represented. The zone profiles for 1-aminopyrene were nearly Gaussian, and as such had very small values of τ. The small values of τ result in calculated values of k_{ms} and k_{sm} that are highly scattered as a function of temperature.

As shown, the graph for the other three solutes is linear and the slope is negative. Unlike the methanol data, the correlation coefficients for the linear regression vary significantly (R^2 = 0.038 – 0.960). As such, the reported values should be used only to draw general conclusions.

The activation energy is calculated from the slope of this graph, according to Equation 1.18. As shown in Table 6.6, the activation energies are positive for all solutes. The activation energy for the transfer between the stationary and transition state ($\Delta E_{\ddagger s}$) is larger than the activation energy for the transfer between the mobile and transition state ($\Delta E_{\ddagger m}$). These data indicate that it is easier for the solutes to exit the stationary phase than it is for them to enter it. Given the standard deviations on the values, it is impossible to discern any definitive trend as a function of solute structure.

6.4 Conclusions

In this chapter, the thermodynamic and kinetic behavior of NPAHs was examined in reversed-phase liquid chromatography using a protic and aprotic mobile phase. The thermodynamic data indicate a noticeable effect of temperature for both mobile phases. An increase in temperature results in a decrease in the retention factor in both mobile phases. However, pressure was shown to have a small effect on the solutes in methanol, with the reported values being similar to those of the parent PAHs. As a result, a single pressure was examined for the acetonitrile data. The effect of mobile phase was more profound than that of pressure. The data demonstrate that the retention factors for all solutes, except 1-aminopyrene, increase in acetonitrile relative to methanol. Such an increase implies a change from a partition mechanism (methanol) to an adsorption mechanism (acetonitrile). However, the changes in molar enthalpy are similar, suggesting that the octadecylsilica may hinder the acess of the larger solutes to the silica support.

Similar to the thermodynamic data, the kinetic data indicate a noticeable effect of temperature for both mobile phases. Once again, pressure was shown to have a nominal effect on the solutes in methanol. More importantly, the aprotic nature of acetonitrile was shown to alter the rate constants by a factor of two to four orders of magnitude. However, the fluctuations imparted by the fitting process inhibit our ability to discern definitive correlations between the activation energies and structure in acetonitrile. Regardless of this deficiency, these data represent the first quantitative comparison of NPAH retention in reversed-phase liquid chromatography.

6.5 References

[1] C.-H. Ho, B.R. Clark, M.R. Guerin, B.D. Barkenbus, T.K. Rao, J.L. Epler, Mutat. Res. 85 (1981) 335-345.

[2] G.M. Seixas, B.M. Andon, P.G. Hollingshead, W.G. Thilly, Mutat. Res. 102 (1982) 201-212.

[3] A. Matsuoka, K. Shudo, Y. Saito, T. Sofuni, M. Ishidae, Jr., Mutat. Res. 102 (1982) 275-283.

[4] J.M. Schmitter, H. Colin, J.-L. Excoffier, P. Arpino, G. Guiochon, Anal. Chem. 54 (1982) 769-772.

[5] S.C. Ruckmick, R.J. Hurtubise, J. Chromatogr. 321 (1985) 343-352.

[6] C. Borra, D. Wiesler, M. Novotny, Anal. Chem. 59 (1987) 339-343.

[7] N. Motohashi, K. Kamata, R. Meyer, Environ. Sci. Technol. 25 (1991) 342-346.

[8] J.M. Schmitter, I. Ignatiadis, G. Guiochon, J. Chromatogr. 248 (1982) 203-216.

[9] M.R. Guerin, C.-H. Ho, T.K. Rao, B.R. Clark, J.L. Epler, Environ. Res. 23 (1980) 42-53.

[10] S.G. Wakeham, Environ. Sci. Technol. 13 (1979) 1118-1123.

[11] H.-Y. Chen, M.R. Preston, Environ. Sci. Technol. 32 (1998) 577-583.

[12] M. Wilhelm, G. Matuschek, A. Kettrup, J. Chromatogr. A 878 (2000) 171-181.

[13] K. Kamata, N. Motohashi, J. Chromatogr. 319 (1985) 331-340.

[14] K. Kamata, N. Motohashi, R. Meyer, Y. Yamamoto, J. Chromatogr. 596 (1992) 233-239.

[15] K. Kamata, N. Motohashi, J. Chromatogr. 396 (1987) 437-440.

[16] M. Ashraf-Khorassani, L.T. Taylor, J. Chromatogr. Sci. 26 (1988) 331-336.

[17] H. Colin, J.M. Schmitter, G. Guiochon, Anal. Chem. 53 (1981) 625-631.

[18] A.M. Siouffi, M. Righezza, G. Guiochon, J. Chromatogr. 368 (1986) 189-202.

[19] T.R. Steinheimer, M.G. Ondrus, Anal. Chem. 58 (1986) 1839-1844.

[20] J.W. Haas, III, W.F. Joyce, Y.-J. Shyu, P.C. Uden, J. Chromatogr. 457 (1988) 215-226.

[21] K. Kamata, N. Motohashi, J. Chromatogr. 498 (1990) 129-135.

[22] H. Carlsson, C. Östman, J. Chromatogr. A 715 (1995) 31-39.

[23] S.B. Howerton, V.L. McGuffin, Anal. Chem. 75 (2003) 3539-3548.

[24] S.B. Howerton, V.L. McGuffin, J. Chromatogr. A (2003) In press.

[25] V.L. McGuffin, S.-H. Chen, J. Chromatogr. A 762 (1997) 35-46.

[26] J.H. Hildebrand, R.L. Scott, The Solubility of Nonelectrolytes, Reinhold Publishing Corporation, New York, NY, USA, 1950.

[27] M.W. Ducey, Jr., C.J. Orendorff, J.E. Pemberton, L.C. Sander, Anal. Chem. 74 (2002) 5576-5584.

[28] M.W. Ducey, Jr., C.J. Orendorff, J.E. Pemberton, L.C. Sander, Anal. Chem. 74 (2002) 5585-5592.

[29] B.N. Woodrow, J.G. Dorsey, Environ. Sci. Technol. 31 (1997) 2812-2820.

[30] D.Y. Shang, J.L. Gransmaison, S. Kaliaguine, J. Chromatogr. A 672 (1994) 185-201.

Chapter 7: Retention Mechanisms in Whole Soil

7.1 Introduction

Using the techniques described in Chapters 1 through 4, an investigation into the molecular contributions to retention for a fraction of soil was conducted. Two polycyclic aromatic hydrocarbons, a series of nitroalkanes and a series of alkylbenzenes were used as test solutes. These experiments were designed to validate or refute the current theories of soil retention. This chapter contains a chemical description of soil, the current theories of soil retention, as well as the experimental methods used to study this complex material.

7.1.1 Composition of Soil

By its nature, soil is both physically and chemically heterogeneous. Physically, soil particles range from the sub-micrometer up to the millimeter, and sometimes centimeter sizes. The particles are composed of a wide range of materials that include plant, animal, and mineral matter. As a result, the chemical composition of soil can include plant and animal lipids, carbohydrates, humic and fulvic acids, as well as a large number of inorganic materials (i.e., iron and aluminum oxides, soluble salts, etc.). In addition, the environment in which the primary materials are deposited can greatly affect the final composition of the soil [1,2]. Despite the large amount of information regarding types of soils and the constituent elements, there is no exact structure for soil organic matter. This lack of information is due primarily to the large number of chemical moieties

found within soil (i.e. carboxylic acids, amines, etc.) and the environmental variables in which the soil is formed (i.e. temperature, humidity, flora, etc.) [1,2].

7.1.2 Retention Mechanisms in Soil

While the mechanism of retention in synthetic materials has been investigated using a wide range of experimental and theoretical techniques, the mechanism of soil retention has been probed using a smaller number of techniques. From the published literature, two theories of soil retention have come to the fore over the past twenty years. While the most recent focuses on soil organic matter, both recognize the importance of minerals in the sorption process.

7.1.2.1 Partition with Adsorption

The first investigation to postulate the retention mechanism of nonionic organic compounds (NOC) was published by Chiou et al. in 1979 [3]. In this seminal work, the isotherms of seven NOCs were measured. The investigators found that the isotherms were linear and exhibited no detectable level of curvature. The lack of curvature suggests that retention occurs via a partition mechanism. However, further experimentation was necessary in order to validate this hypothesis.

Chiou continued his investigations into the mechanism of retention by probing the effect of water on the sorption capacity [4,5], as well as the effect of dissolved organic matter (DOM) [6,7] and surfactants [8,9] on the solubility of NOCs. From these studies, water was found to alter the sorption capacity of the

soil. Above 90% relative humidity, Chiou and Shoup reported that the sorption capacities approached those found in completely aqueous systems [4]. Below this humidity, the soil exhibited an adsorptive mechanism. In addition, Chiou and coworkers noted that DOM, as well as surfactants, could increase the solubility of organic solutes in aqueous solutions. The authors also demonstrated that the source of the DOM was important, with commercially available materials increasing solubility by factors of four to twenty over that of samples from the field [7]. Using these data, Chiou and coworkers hypothesized that in the absence of water, the mineral matter in soil was the primary site of retention. This hypothesis has been supported by investigations of volatile organic compounds on silica, soils, and clays [10,11]. Furthermore, Chiou and coworkers postulated that in the presence of water, soil organic matter (SOM) becomes the primary site of retention. In contrast to the mineral matter, SOM is thought to exhibit a partition mechanism. Given that most naturally occurring soils are in water rich environments, Chiou and co-workers concluded that SOM was the most important factor for assessing the sorption capacity of soils.

Because of Chiou's work, the partition model was advanced as the primary mechanism of sorption for NOCs in water-rich environments. However, several investigators reported data that challenge the hypothesis of a partition mechanism. Significant differences in the sorption and desorption of organic compounds [12,13], competitive sorption [14,15], and nonlinear isotherms[16-18] were reported, suggesting that a partition mechanism was insufficient to fully explain retention in soil. The differences in the adsorption and desorption curves

for a series of PCBs reported by DiToro and Horzempa suggest that adsorption contributes to retention [13]. Similarly, Stuart et al. [14] and Abdul and Gibson [15] presented evidence of competitive sorption, which implies that soil has some adsorptive character. Since a partition mechanism is presumed to be a non-competitive, the reports of competitive sorption detract from Chiou's initial hypothesis. Lastly, the identification of nonlinear isotherms is also indicative of adsorption, since there are a limited number of sites for interaction. Once again, the partition mechanism is not predicated upon a limited number of sites, as is the adsorption mechanism [19].

7.1.2.2 Dual Reactivity Model (DRM)

Using the observed deviations as a stimulus, Weber and co-workers have hypothesized that the chemical nature of soil organic matter is not unlike a co-block polymer [20-33]. Dubbed the dual-reactivity model (DRM), Weber and co-workers postulate that many of the observed inconsistencies with Chiou's hypothesis are indicative of glassy and rubbery regions within soil organic matter. The glassy regions are typified by high structural rigidity due to aromatic moieties and cross-linking. These regions are hypothesized to result from longer periods of diagenesis. According to conventional polymer theory, glassy polymers are characterized by high glass transition temperatures and inflexibility. 'Rubbery' regions are said to be less rigid and likely composed of aliphatic moieties with minimal cross-linking. Rubbery regions are said to result from relatively small amounts of diagenesis and are characterized by low glass transition temperatures and higher degrees of molecular flexibility.

While Weber has been supported by other investigators [34,35], the only direct experimental evidence to demonstrate the possibility of two mechanistic sites come from differential scanning calorimetry data [27]. Although the authors demonstrate the presence of a glass transition temperature for a humic acid, the data are far from definitive, with some authors challenging the utility of the data [36].

Chiou and co-workers contend that the DRM is in fact erroneous and that the nonlinear effects arise from interactions with high-surface-area carbonaceous material (HSCAM). This material has been postulated to be a charcoal, or soot like material that is only a very tiny fraction of ordinary soil [37-39].

Given the discourse in the literature about the mechanism of retention in soil, a series of experiments were developed to probe the retention mechanism of a reference soil (CLN Soil-3 RTC Corp.).

7.2 Experimental Methods

7.2.1 Stationary Phase

Unlike the previous experiments that used a synthesized stationary phase, the stationary phase for these experiments was a reference soil (CLN Soil-3, Resource Technology Corp.). Since this material contains a large particle size distribution, it is unsuitable for packing within a fused-silica capillary as received. As a result, the soil was fractionated using a series of nylon mesh screens to yield a fraction from 5–125 μm. In order to confirm that the sorption of the characteristics of the material did not change with fractionation, batch isotherm

studies were carried out using naphthalene, phenanthrene, anthracene, fluoranthene, pyrene, and chrysene (Sigma) with equilibration times that ranged from 5 minutes to 48 hours and concentrations that ranged from1.4 to .75 μM. Each reaction vessel was filled with ~1.0 g of the soil and 4 mL of the PAH solution. The supernatant from each vessel was analyzed in triplicate.

Using the data from the batch isotherms as a guide, this fraction of soil was packed into a series of fused-silica capillaries (320 μm i.d., 1 m long, Polymicro Technologies) using the both the slurry pack method (Chapter 2) [40] and a manual procedure. The manual procedure involved filling a syringe with a small amount of slurry and introducing it into the fused-silica capillary in small aliquots. Once a sufficient amount had been injected, the soil was compressed at low pressures to remove any voids in the column.

7.2.2 System Parameters

Using the system described in Section 2.2.3.1 (Figure 2.1), the soil column was used to study the retention of two polycyclic aromatic hydrocarbons (PAHs), pyrene and benzo[*a*]pyrene (Sigma), which were dissolved in high purity methanol (Baxter Healthcare) at concentrations ranging from 10^{-6} to 10^{-3} M. In addition, a homologous series of nitroalkanes and alkylbenzenes was studied as a function of mobile phase (methanol/water, 90-100%). The nitroalkane series contained nitromethane, nitroethane, nitropropane, nitrobutane, and nitrohexane (Aldrich) dissolved to 2%, by volume, in a solution that matched the mobile phase. The series of alkylbenzenes contained toluene, ethylbenzene,

butylbenzene and hexylbenzene (Sigma) dissolved to 2%, by volume, in a solution that matched the mobile phase.

The separations were carried out at 298 K in pressure control mode at a nominal flow rate of 0.15 μL/min. Detection of the PAHs was achieved using laser-induced fluorescence as described in Chapter 2. Detection of the aliphatic compounds was achieved using the UV-Visible absorbance spectrometer at 210 nm for the alkylbenzenes and 260 nm for the nitroalkanes.

7.3 Results and Discussion

7.3.1 Batch Isotherms

Table 7.1 contains data from the batch isotherms of whole and fractionated soil. A minimum of twenty-four hours was necessary in order to reach equilibrium within the batch reactors. Using this equilibration time, the batch isotherms were studied using a range of concentrations that fell within the limits of detection for the UV-Visible absorbance spectrometer. The equilibrium constants were calculated by first determining the amount of each PAH in the supernatant. This was accomplished using a calibration curve. The equilibrium constants were calculated for both the whole and fractionated soil

$$K_{eq} = \frac{[X]_s}{[X]_m} = \frac{([X]_{con} - [X]_{sup})}{[X]_{sup} \times M_{soil}} \qquad (7.1)$$

Table 7.1: Concentrations and equilibrium constants for a series of polycyclic aromatic hydrocarbons on whole and fractionated soil.

Solute	Concentration Range (μM)	K_{whole} (× 10^{-2})	$K_{fraction}$ (× 10^{-2})
Naphthalene	18.7 – 75.1	12.4 ± 4.6	8.7 ± 2.8
Phenanthrene	1.4 – 5.5	33.6 ± 7.6	43.6 ± 4.7
Anthracene	1.4 – 5.6	55.3 ± 7.7	129.9 ± 4.0
Fluoranthene	2.4 – 9.7	58.9 ± 9.7	81.3 ± 20.0
Pyrene	1.3 – 5.1	139.8 ± 36.4	213.6 ± 38.2
Chrysene	0.8 – 5.0	385.6 ± 48.7	399.5 ± 16.9

where $[X]_s$ is the amount of solute X in the stationary phase and $[X]_m$ is the amount of solute X in the mobile phase. Since sorption to the reaction vessel was possible, control samples were examined concurrently with the soil samples. The difference between the concentration in the control vessel ($[X]_{con}$) and the supernatant ($[X]_{sup}$) is equivalent to the amount sorbed by the soil. Since the same mass of soil (M_{soil}) could not be accurately reproduced, the equilibrium constants were normalized to the amount for each reactor to compensate for any differences. The equilibrium constants were compared using a Smith-Satterthwaite test [41], which uses the t-statistic. Using a null hypothesis that the equilibrium constants in the whole soil and the fractionated soils are equivalent (i.e. $\Delta_0=0$), the test indicates that for all solutes, except naphthalene, there is a statistical difference between the whole and fractionated soil. However, these differences ranged only from a factor of ~0.3 to 2 for all solutes. Although the difference was measurable, the small degree of the difference suggests that the fractionated soil could be used without dramatically altering the retention characteristics.

7.3.2 Soil Column Characteristics

In order to study the retention characteristics of soil, the manufacture of a capillary soil column was necessary. As detailed in Chapter 2, the fractionated soil was packed into a fused-silica capillary via the slurry method and the manual method described above. A number of columns were packed and then characterized via visual inspection.

For both methods, the fractionated soil was found to pack in a nonuniform manner. The region closest to the quartz wool frit was found to have a large number of very small particles (< 5μm) that were densely packed. The remainder of the column was packed with larger particles (>75μm), which were loosely packed. In time, though, the voids between the larger particles were also filled in with small particles. When the soil columns were pressurized, they generated larger back pressures than their ODS counterparts. For example, a 25 cm soil column at 2500 psi evinced a 0.15 μL/min flow rate. By contrast, a 1m long ODS column at 800 psi evinced a 1 μL/min flow rate. This large backpressure in the soil columns prevented flow rates of 1 μL/min from being achieved.

7.3.3 Retention Mechanisms

Using a soil column packed via the slurry method, the investigation of soil retention began with a study of pyrene and benzo[*a*]pyrene. As demonstrated in previous chapters, these solutes are retained via a partition mechanism in octadecylsilica (ODS). Given that the experiments on ODS required only small injection volumes for detection, 10μL injections of 10^{-5} M solutions were used initially. However, this volume was undetectable even when the concentration was increased to 10^{-3} M. These results suggested that the sorption capacity of the soil was much greater than that of the ODS. However, the slow flow rates could also contribute to the inability to detect the solutes. At very slow flow rates, the zone profiles would eventually become very broad and shallow due to

diffusional processes. Thus, it is possible that the flow rate contributed to the lack of detection using the small injection volumes.

Given the difficulties with the smaller volumes, a larger injection loop was constructed (0.25 mL) so that the solutes could be studied via a breakthrough curve. Figure 7.1 is illustrative of the breakthrough curve for benzo[*a*]pyrene. As shown, the retention time for the solute is in excess of five hours at room temperature. This retention time is much larger than that observed for the solute on the synthetic phases (~1 h at comparable temperature and pressure) [42]. Note once again the flow rate is slower in the soil column. In order to compensate for the slow flow rates, an attempt was made to determine the retention factor for benzo[*a*]pyrene. However, the unretained marker (4-methylhydroxy-7-methoxycoumarin) that had been successfully employed in the ODS system was undetectable. Although several other solutes were used in an attempt to determine the true void time, no detectable solute was ever found. Regardless, pyrene was also injected at similar concentrations and volumes for a comparison. Unlike benzo[*a*]pyrene, the retention time of pyrene was found to be ~2 hours. These data suggest that the soil is retaining the solutes via a partition mechanism, and are consistent with investigations carried out on chemically immobilized humic and fulvic acids [43]. As shown in Chapter 4, an increase in ring number results in a logarithmic increase to the retention time when a partition mechanism is present. Thus, the observed behavior on the fractionated soil conforms to this observation, suggesting the presence of a partition mechanism.

Figure 7.1: Representative breakthrough curve of benzo[a]pyrene on a soil column. Mobile phase: methanol, 0.15uL/min.

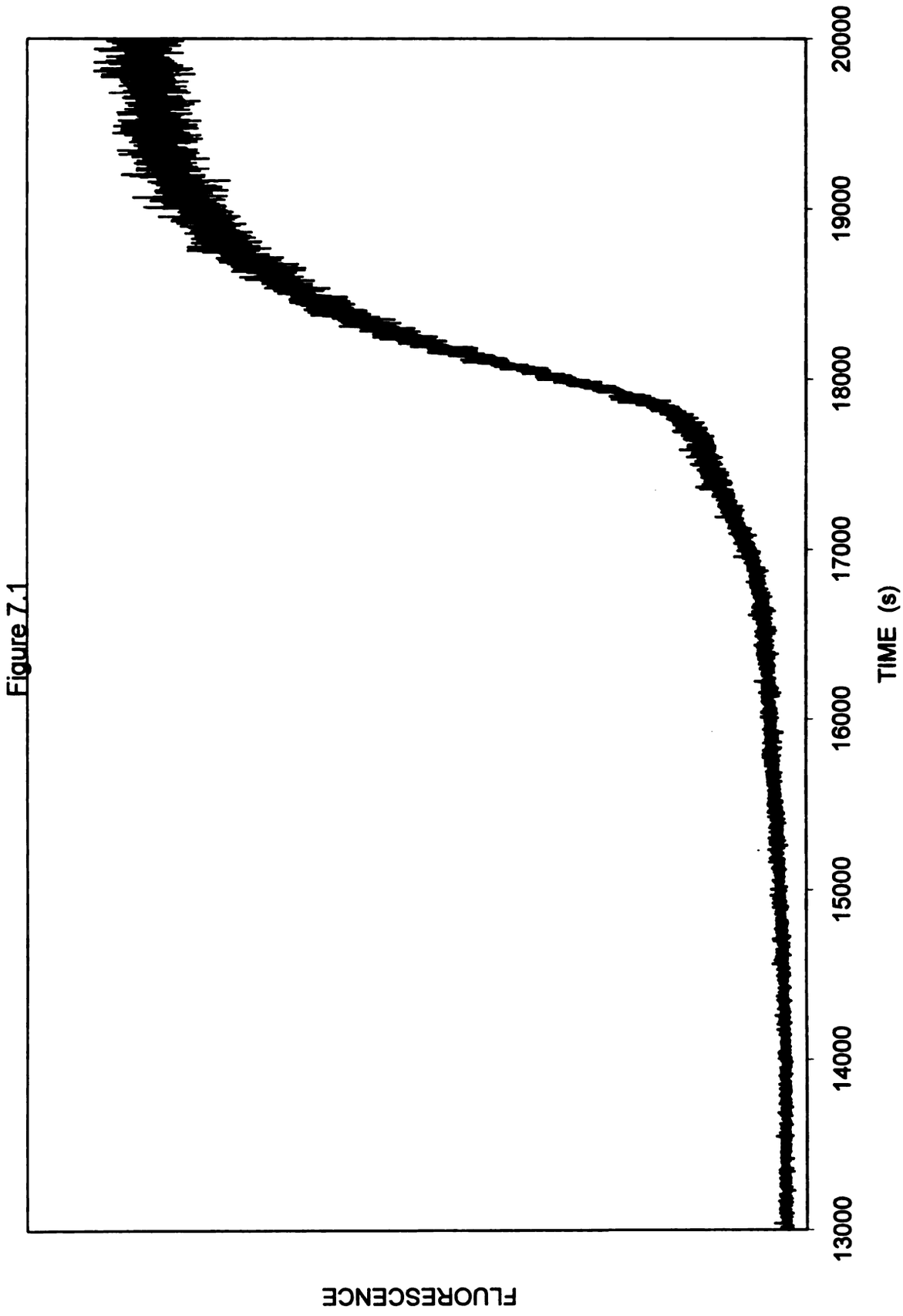
FLUORESCENCE
13000
14000
15000
16000
17000
18000
19000
20000
TIME (s)

Figure 7.1

mechanism in soil. Given the long retention times, the alkylated homologous series were used to better study retention since their elution time was shorter.

The nitroalkanes and the alkylbenzenes were separated under similar conditions as the two PAHs. If a partition mechanism were present, the solutes would be expected to elute in order from the shortest alkyl chain solute to the longest alkyl chain solute. This behavior has been demonstrated in previous investigations [44-46] . However, the alkylbenzenes eluted in order from the longest chain (hexylbenzene) to shortest (toluene) in methanol. Similarly, the nitroalkanes eluted in a reversed order (i.e. longest to shortest). These data imply that both series are separated based upon an exclusion mechanism.

In size exclusion chromatography, smaller solutes are able to access regions of the stationary phase (e.g. pores) that larger solutes cannot. As a result, smaller solutes spend a larger amount of time in these regions, away from the flowing mobile phase. Thus, the solutes elute in an inverse order.

In an effort to verify the presence of an exclusion mechanism, the mobile phase was altered to include 5 and 10% water. The presumption was that if any partition mechanism were present, it would be enhanced with increasing water concentration since the solutes would be less soluble in the mobile phase. Previous studies as a function of mobile phase for these solutes indicate an increase in retention factor with increasing water content [46-49]. Figures 7.2 and 7.3 illustrate the retention time of each series as a function of mobile phase composition. It should be noted that for these data there is a significant amount of scatter due to small changes in the linear velocity of the mobile phase. For

Figure 7.2: Graph of retention factor versus carbon number for a series of nitroalkanes as a function of methanol/water mobile phase. (◆) 100% methanol, (■) 95% methanol, (▲) 90% methanol.

Figure 7.2

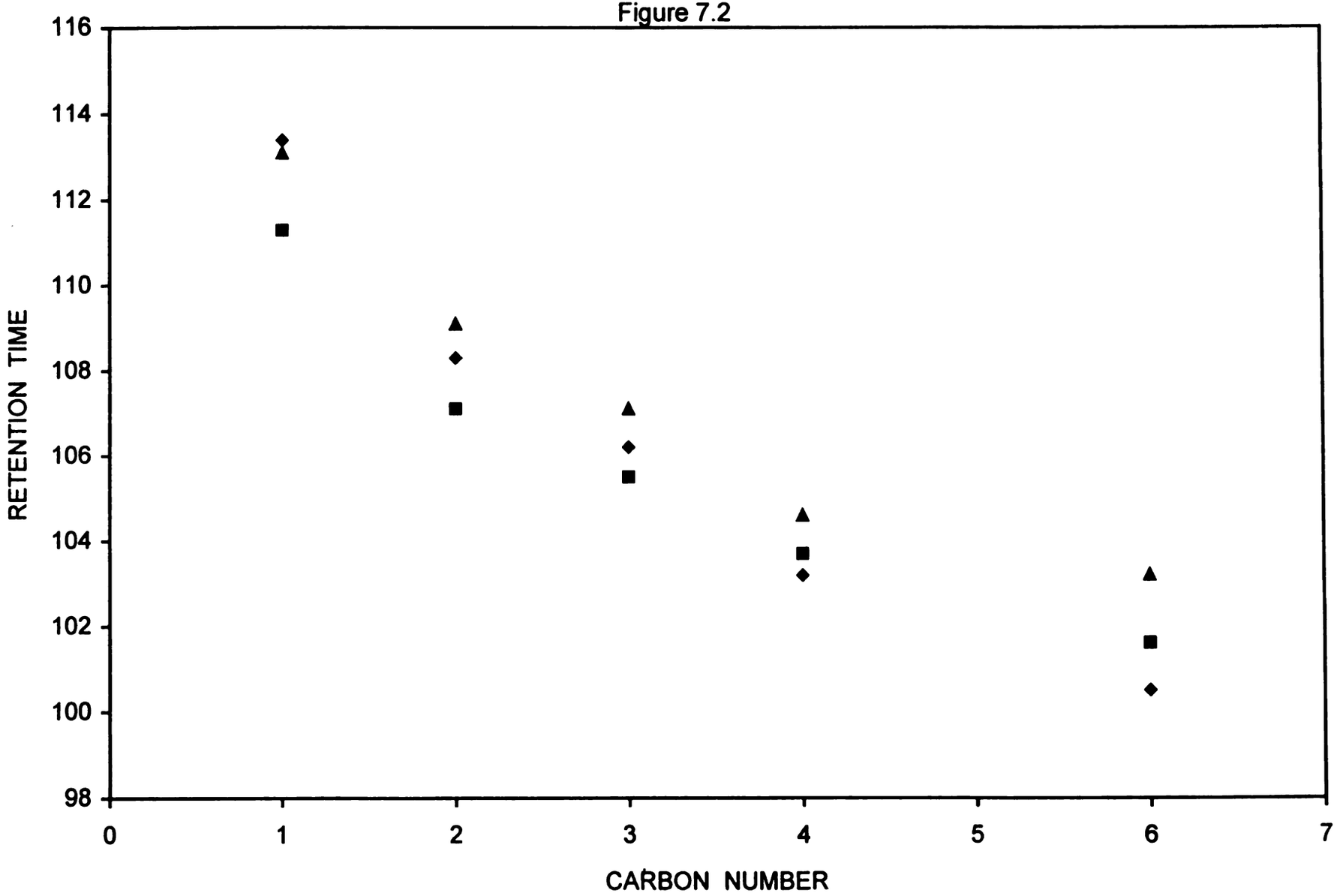
116
114
112
110
108
106
104
102
100
98
RETENTION TIME
0
1
2
3
4
5
6
7
CARBON NUMBER

Figure 7.3: Graph of retention factor versus carbon number for a series of alkylbenzenes as a function of methanol/water mobile phase. (◆) 100% methanol, (■) 95% methanol, (▲) 90% methanol.

Figure 7.3

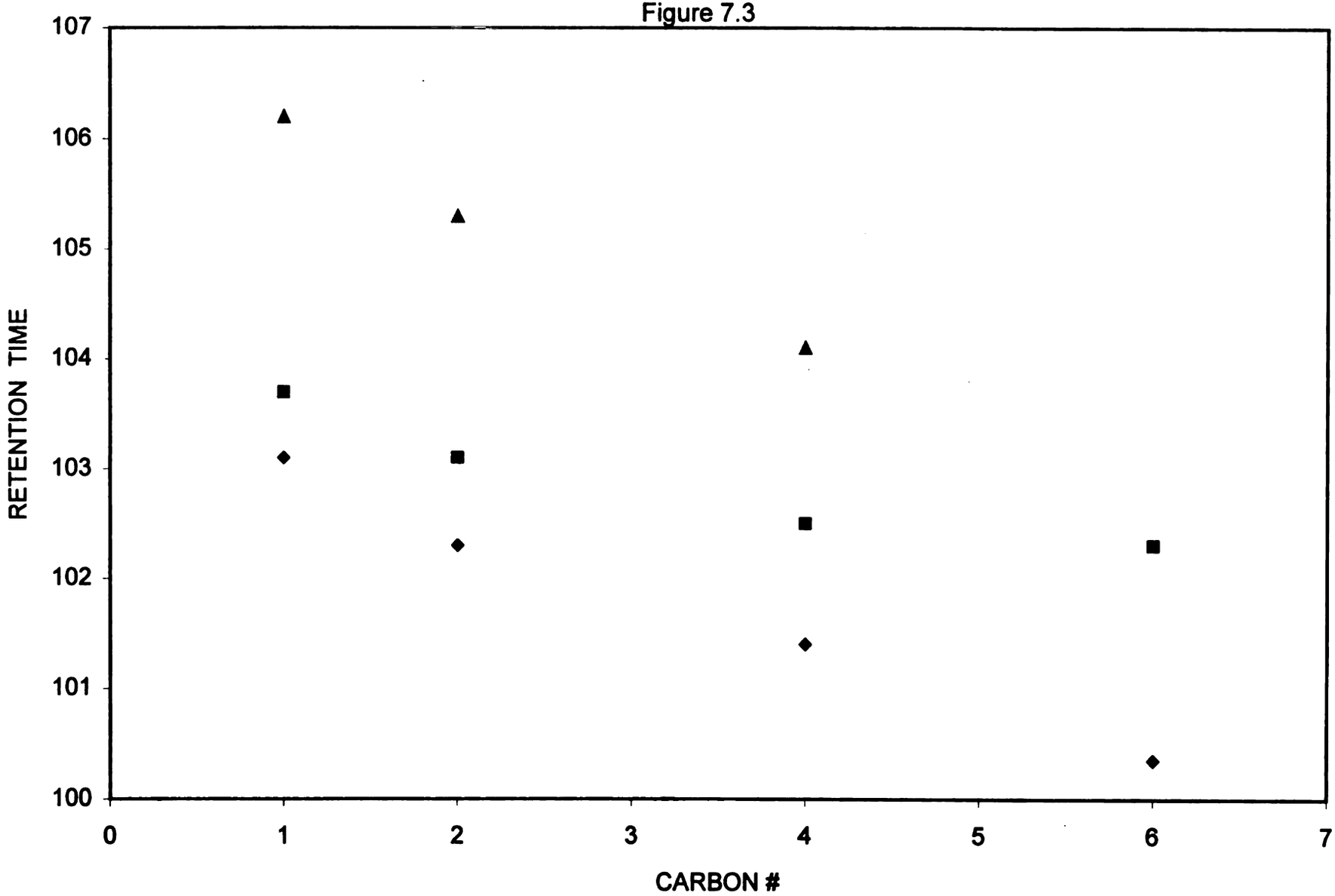
107
106
105
104
103
102
101
100
RETENTION TIME
0
1
2
3
4
5
6
7
CARBON #

example, multiple separations on the same day resulted in a variation of 5-7% in the retention time.

As shown, the data indicate that at all mobile phase compositions the solutes maintain the reversed elution order, indicative of an exclusion mechanism. However, the effect of water on the retention is not as obvious. For the nitroalkanes (Figure 7.2), the retention times are statistically indistinguishable as a function of mobile phase composition. For the alkylbenzenes (Figure 7.3) the retention time increases with increasing water concentration. It should be noted that the overall differences in retention time between the alkylbenzenes are very small. Using multiple injections at each mobile phase composition, the Student t-test results indicate that the retention times are statistically indistinguishable as a function of mobile phase composition. Thus, the alkylbenzene data that depicts the effect of mobile phase composition suggests the presence of a partition mechanism. However, the variance in the measurements prevents definitive identification of this mechanism. Regardless, the reversed elution order at all mobile phase compositions indicates the presence of an exclusion mechanism.

7.4 Conclusions

The experiments within this chapter demonstrate that the use of soil as a stationary phase presents some practical limitations that are not present with ODS. The large particle sizes and the large particle size distribution results in nonuniform packing of the capillary column. This nonuniform packing leads to very high pressures and very low flow rates. The retention of the PAHs suggests

a partition mechanism. The partition mechanism likely results from interactions with the organic carbon in the soil. The data from the alkylbenzenes could support this observation if the standard deviations for the retention times could be reduced. However, the data for the nitroalkanes and the alkylbenzenes demonstrates that size exclusion is more important for these solutes. The exclusion mechanisms likely results from the micro- and mesoporous structure of the mineral matter within the soil. This mechanism is not observed for the PAHs due to their large size. Although the molecular level contributions could not be studied as with ODS, the data contained in this chapter still provide a glimpse into the mechanism of soil retention, indicating that solute structure is an important variable in the retention mechanism.

7.5 References

[1] N.C. Brady, R.R. Weil, The Nature and Properties of Soil, Simon & Schuster, Upper Saddle River, NJ, USA, 1999.

[2] S.W. Buol, F.D. Hole, R.J. McCracken, Soil Genesis and Classification, Iowa State University Press, Ames, Iowa, USA, 1989.

[3] C.T. Chiou, L.J. Peters, V.H. Freed, Science (Washington, D. C., 1883-) 206 (1979) 831-832.

[4] C.T. Chiou, T.D. Shoup, Environ. Sci. Technol. 19 (1985) 1196-1200.

[5] C.T. Chiou, T.D. Shoup, P.E. Porter, Org. Geochem. 8 (1985) 9-14.

[6] C.T. Chiou, R.L. Malcolm, T.I. Brinton, D.E. Kile, Environ. Sci. Technol. 20 (1986) 502-208.

[7] C.T. Chiou, D.E. Kile, T.I. Brinton, R.L. Malcolm, J.A. Leenheer, Environ. Sci. Technol. 21 (1987) 1231-1234.

[8] D.E. Kile, C.T. Chiou, Environ. Sci. Technol. 23 (1989) 832-838.

[9] D.E. Kile, C.T. Chiou, R.S. Helburn, Environ. Sci. Technol. 24 (1990) 205-208.

[10] R.D. Rhue, P.S.C. Rao, R.E. Smith, Chemosphere 17 (1988) 727-741.

[11] R.D. Rhue, K.D. Pennell, P.S.C. Rao, W.H. Reve, Chemosphere 18 (1989) 1971-1986.

[12] S.W. Karickhoff, K.R. Morris, Environ. Toxicol. Chem. 4 (1985) 469-479.

[13] D.M. DiToro, L.M. Horzempa, Environ. Sci. Technol. 16 (1982) 594-602.

[14] B.J. Stuart, G.F. Bowlen, D.S. Kosson, Environ. Prog. 10 (1991) 104-109.

[15] A.S. Abdul, T.L. Gibson, Haz. Waste Haz. Mater. 3 (1986) 125-137.

[16] W.P. Ball, P.V. Roberts, Environ. Sci. Technol. 25 (1991) 1223-1237.

[17] G.P. Curtis, P.V. Roberts, M. Reinhard, Water Resour. Res. 22 (1986) 2059-2067.

[18] M.D. Piwoni, P. Banerjee, J. Contam. Hydrol. 4 (1989) 163-179.

[19] L. Snyder, in E. Heftmann (Editor), Chromatography, Van Nostrand Reinhold Company, New York, NY, USA, 1975, p. 46-76.

[20] W. Huang, M.A. Sclautman, W.J. Weber, Jr., Environ. Sci. Technol. 30 (1996) 2993-3000.

[21] W. Huang, T.M. Young, M.A. Sclautman, H. Yu, W.J. Weber, Jr., Environ. Sci. Technol. 31 (1997) 1703-1710.

[22] W. Huang, W.J. Weber, Jr., Environ. Sci. Technol. 31 (1997) 2562-2569.

[23] W. Huang, W.J. Weber, Jr., Environ. Sci. Technol. 32 (1998) 3549-3555.

[24] M.D. Johnson, W. Huang, Z. Dang, W.J. Weber, Jr., Environ. Sci. Technol. 33 (1999) 1657-1663.

[25] M.D. Johnson, W. Huang, W.J. Weber, Jr., Environ. Sci. Technol. 35 (2001) 1680-1687.

[26] M.D. Johnson, T.M. Keinath, II, W.J. Weber, Jr., Environ. Sci. Technol. 35 (2001) 1688-1695.

[27] E.J. LeBoeuf, W.J. Weber, Jr., Environmental Science and Technology 31 (1997) 1697-1702.

[28] P.M. McGinley, L.E. Katz, W.J. Weber, Jr., Environ. Sci. Technol. 27 (1993) 1524-1531.

[29] W.J. Weber, Jr., P.M. McGinley, L.E. Katz, Environ. Sci. Technol. 26 (1992) 1955-1962.

[30] W.J. Weber, Jr., W. Huang, Environ. Sci. Technol. 30 (1996) 3130-3131.

[31] W.J. Weber, Jr., T.M. Young, Environ. Sci. Technol. 31 (1997) 1686-1691.

[32] T.M. Young, W.J. Weber, Jr., Environ. Sci. Technol. 29 (1995) 92-97.

[33] T.M. Young, W.J. Weber, Jr., Environ. Sci. Technol. 31 (1997) 1692-1696.

[34] J.J. Pignatello, B. Xing, Environ. Sci. Technol. 30 (1996) 1-11.

[35] G. Xia, J.J. Pignatello, Environ. Sci. Technol. 35 (2001) 84-94.

[36] E.R. Graber, M.D. Borisover, Environ. Sci. Technol. 32 (1998) 3286-3292.

[37] C.T. Chiou, D.E. Kile, Environ. Sci. Technol. 32 (1998) 338-343.

[38] C.T. Chiou, D.E. Kile, D.W. Rutherford, G. Sheng, S.A. Boyd, Environ. Sci. Technol. 34 (2000).

[39] Ö. Gustafsson, F. Haghseta, C. Chan, J. Macfarlane, P.M. Gschwend, Environ. Sci. Technol. 31 (1997) 203-209.

[40] J.C. Gluckman, A. Hirose, V.L. McGuffin, M. Novotny, Chromatographia 17 (1983) 303-309.

[41] J.L. Devore, Probability and Statistics for Engineering and the Sciences, 4th ed., Duxbury Press, New York, NY, USA, 1995.

[42] S.B. Howerton, V.L. McGuffin, Anal. Chem. 75 (2003) 3539-3548.

[43] K. Kollist-Siigur, T. Nielsen, C. Gron, P.E. Hansen, C. Helweg, K.E. Jonassen, O. Jorgensen, U. Kirso, J. Environ. Qual. 30 (2001) 526-537.

[44] H. Colin, G. Guiochon, J. Chromatogr. Sci. 18 (1980) 54-63.

[45] G.E. Berendsen, L. de Galan, J. Chromatogr. 196 (1980) 21-37.

[46] E. Grushka, H. Colin, G. Guiochon, J. Chromatogr. 248 (1982) 325-339.

[47] W.R. Melander, C.A. Mannan, C. Horvath, Chromatographia 15 (1982) 611-615.

[48] R.B. Sleight, J. Chromatogr. 83 (1973) 31-38.

[49] R.P. Ranatunga, P.W. Carr, Anal. Chem. 72 (2000) 5679-5692.

Chapter 8: Characterization of Polycyclic Aromatic Hydrocarbons in Environmental Samples by Selective Fluorescence Quenching

8.1 Introduction

Given the ubiquitous nature of polycyclic aromatic hydrocarbons (PAHs) in the environment (Chapter 1), a new technique is employed to study these molecules from natural sources. This new technique takes advantage of selective fluorescence quenching for the qualitative characterization of alternant and nonalternant PAHs. Using a novel experimental design (Figure 2.3), three standard reference materials were analyzed and correlated using statistical methodology. This treatment allows environmental samples to be fingerprinted in a new way, providing a method for analyzing samples from contaminated waste sites and oil spills.

8.1.1 Fluorescence and Fluorescence Quenching

Fluorescence is the process by which molecules absorb radiation and are promoted to a higher energy excited state, then return to the ground state via the emission of a photon. Most PAHs are natively fluorescent because the electrons within the aromatic rings are delocalized and can be readily excited. The planar structure of PAHs restricts vibrational relaxation from the excited state, thus increasing the probability of relaxation through emission of a photon. Depending on the number and arrangement of the aromatic rings, the resulting fluorescence spectrum is highly characteristic of the PAH. For example, many alternant PAHs exhibit fluorescence spectra with well-defined vibrational fine structure, whereas

most nonalternant PAHs have broad spectra with few structural features (Figure 8.1) [1,2].

Fluorescence quenching can be defined simply as any process that causes a reduction in the observed fluorescence power [3-5]. This reduction can be the result of trivial processes, such as primary or secondary absorption, refractive index effects, etc. These trivial processes can be minimized by using a cell with a small optical path length, such as a capillary flow cell [6]. Of more interest for environmental applications are the quenching processes that involve specific interactions between the fluorophore and another molecule known as the quencher. Such quenching can occur by two mechanisms: static and dynamic. Static quenching occurs when the ground-state fluorophore and ground-state quencher form a stable complex [3,4]. This new complex may exhibit different spectral characteristics than the fluorophore, resulting in a reduction in the fluorescence power at the selected excitation and emission wavelengths. Dynamic quenching occurs when an excited-state fluorophore collides with and transfers energy to a ground-state quencher [3,4]. The excited-state quencher subsequently returns to the ground state via a nonradiative path (i.e. vibrational relaxation). Dynamic quenching is quantified by the Stern-Volmer equation:

$$\frac{\Phi_f^o}{\Phi_f} \approx \frac{P_f^o}{P_f} = 1 + k_d \tau_f^o C_q = 1 + K_q C_q \qquad (8.1)$$

Figure 8.1: Fluorescence spectra of (A) pyrene and (B) fluoranthene, which demonstrates the spectroscopic differences between alternant and nonalternant polycyclic aromatic hydrocarbons

Figure 8.1

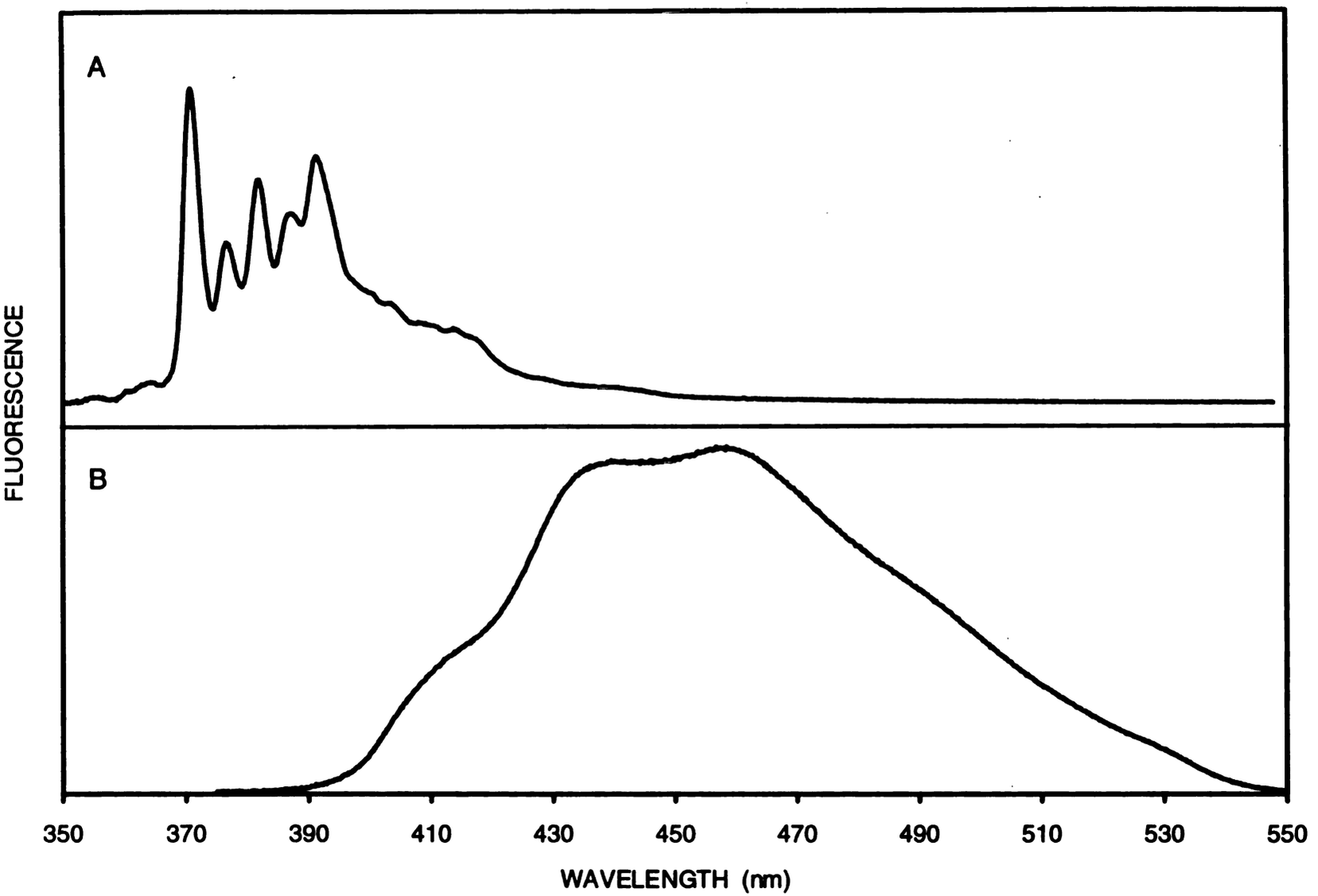
A
B
FLUORESCENCE
350
370
390
410
430
450
470
490
510
530
550
WAVELENGTH (nm)

where Φ_f^o and Φ_f are the quantum efficiencies of the fluorophore in the absence and presence of a quencher, respectively. The quantum efficiencies are directly proportional to the measured fluorescence powers (P_f^o and P_f, respectively) provided that the source power, efficiency of optical irradiation and collection, and fluorophore absorbance remain constant. Under these conditions, the ratio of the powers can be related to the molar concentration of the quencher (C_q), the bimolecular rate constant for dynamic quenching (k_d), the fluorescence lifetime of the unquenched fluorophore (τ_f^o), and the Stern-Volmer quenching constant (K_q). The Stern-Volmer quenching constant is characteristic of the fluorophore-quencher interactions and is a direct measure of the efficiency of the fluorescence quenching process. A graph of the ratio of powers versus the concentration of the quencher should yield a straight line with a slope equal to the quenching constant and an intercept of unity.

Although a large number of quenchers for PAHs have been identified, very few of them have been characterized in sufficient depth and detail to permit their routine use in environmental applications [5]. Initial studies by Sawicki et al. [7] showed that nitromethane, which acts as an electron acceptor, selectively quenches the fluorescence of alternant PAHs. Subsequent studies by Acree et al. [8-10] demonstrated that this so-called "nitromethane selective quenching rule" is broadly applicable with only a few exceptions. A quantitative study by Ogasawara et al. [11] revealed that the Stern-Volmer quenching constants of nitromethane are 33 to 100 times greater for alternant than for nonalternant isomers. In contrast, recent investigations by Goodpaster and McGuffin [12]

demonstrated that amines, which act as electron donors, are selective quenchers for nonalternant PAHs. The Stern-Volmer quenching constants of diisopropylamine are typically 15 to 45 times greater for nonalternant than for alternant isomers. In the present study, selective fluorescence quenching by nitromethane and diisopropylamine are combined with high-efficiency capillary liquid chromatography for detection of alternant and nonalternant PAHs in environmental samples. This approach is advantageous for the improvement of qualitative and quantitative analysis by removing potential interferences. In addition, PAH profiling may aid in the identification of sample origin, either for environmental and health-hazard documentation or for geological studies on soil sedimentation [13-15].

8.2 Experimental Methods

8.2.1 Materials

Three certified reference materials which contain a series of PAHs have been chosen for analysis (Table 8.1). The first sample is a standard (EPA 610, Supelco) that contains sixteen PAHs classified as priority pollutants by the United States Environmental Protection Agency (U.S. EPA). The second sample is an extract of Wheeling Pittsburgh medium crude coke oven tar (SRM 1647, National Institute of Standards and Technology), which is a natural combustion-related mixture of PAHs [16]. Both of these samples were used as received.

The third sample is a contaminated soil/sediment from the southern branch of the Elizabeth River near Norfolk, VA (CRM104-100, Resource Technology Corporation). This sample required extraction of the PAHs

Table 8.1: Concentration of polycyclic aromatic hydrocarbons (PAHs) in certified reference materials.

PAH	Standard EPA 610 (μg/mL)	Coal-Derived Fluid SRM 1597 (μg/mL)	Contaminated Soil CRM104-100 (μg/g)
Anthracene	100.1	87.4	1.44
Fluoranthene	200.2	278	24.6
Pyrene	99.9	204	15.0
Benz[*a*]anthracene	100.0	85.3	7.98
Chrysene	100.0	62.0	8.60
Benzo[*b*]fluoranthene	200.0	(53.1)[a]	(9.69)
Benzo[*k*]fluoranthene	100.0	(33.6)	(5.10)
Benzo[*a*]pyrene	100.1	82.9	5.09
Dibenz[*a,h*]anthracene	200.0	NA[b]	(1.55)
Indeno[1,2,3-*cd*]pyrene	100.1	52.1	4.46
Benzo[*ghi*]perylene	200.0	46.5	3.58

[a] Concentrations given in parentheses are not certified values

[b] NA = not available

according to U.S. EPA Method 3540c (Soxhlet Extraction) prior to analysis. The solvents used in the Soxhlet apparatus were pesticide-grade acetone and hexane (Burdick and Jackson Division, Baxter Healthcare) mixed in a 1:1 (v/v) ratio. After reflux for 24 h, the yellow extract was transferred to a Kuderna-Danish evaporator (Kontes) and the volume was reduced from 400 to 8 mL over a 2 h period. The resulting sample was then transferred, via a Pasteur pipette, in small aliquots to a conical vial. The sample was evaporated to dryness with a nitrogen stream, resulting in 0.63 g of solid material from 10.23 g of soil. The solid was reconstituted in 1.0 mL of pesticide-grade methylene chloride (Burdick and Jackson Division, Baxter Healthcare).

Two quenchers were chosen for these studies based upon their previously reported selectivity for alternant and nonalternant PAHs. Nitromethane (EM Science) was volumetrically diluted with pesticide-grade methanol (Baxter Healthcare, Burdick and Jackson Division) to yield a 2% (v/v) solution. Diisopropylamine (Aldrich) was volumetrically diluted with pesticide-grade acetonitrile (Baxter Healthcare, Burdick and Jackson Division) to yield a 50% (v/v) solution.

8.2.2 Experimental System

Each of the samples was analyzed on the system shown in Figure 2.3, which was constructed and characterized in house [17]. For these experiments the sample was split 1:42 to provide an injection volume of approximately 24 nL. The sample constituents were then separated on a fused-silica capillary (Hewlett-Packard, 200 μm i.d., 320 μm o.d., 1.5 m length) that was packed with a 5 μm

octadecylsilica stationary phase (Shandon, Hypersil C18, 115,000 theoretical plates), as described previously [18]. The column was immersed within a water bath maintained at 24 °C to minimize the effect of temperature fluctuations on the separation. The column effluent was combined and thoroughly mixed with the quencher solution, which was delivered by a syringe pump (Model 140, PE/Applied Biosystems) at a nominal flow rate of 1.0 μL/min.

The PAHs were then detected by laser-induced fluorescence in a fused-silica capillary flow cell (75 μm i.d., 360 μm o.d, 1.0 m length, Polymicro Technologies) using the system described in Section 2.2.3.3.

8.2.3 Data Analysis

Data from the chromatographic separation of each sample were integrated over the wavelength range of 350 to 564 nm by using the Spectramax software (Spectramax for Windows, v3.1, Instruments SA). These chromatograms were used for visual display, for discernment of fluorescence quenching behavior and, where possible, for identification of the individual PAHs. For correlation, it was necessary to normalize the abscissa such that the known PAHs had the same retention times in each chromatogram. The resulting chromatograms were then exported as ASCII files into the statistical analysis software (SigmaStat, Version 1.02, SYSTAT). The chromatograms were correlated with one another, in a point-by-point manner, using the product-moment correlation method [19,20]. This method is useful to establish the extent of association or similarity between two chromatograms, both of which are regarded as independent variables. This parametric method assumes that the association (if any) is linear and that the

residuals are normally distributed with constant variance. The resulting scatter plot shows the relationship between the relative fluorescence power or concentration of the PAHs in the two samples. The correlation coefficient (r) quantifies the degree of similarity, and the corresponding P-value expresses the statistical reliability of the results. This same approach can be used to examine the correlation of fluorescence spectra in order to verify the identity and purity of PAHs.

8.3 Results and Discussion

This experimental approach described above provides a wide range of information that can be used to identify the individual PAHs, including chromatographic retention time, fluorescence emission spectra, and Stern–Volmer quenching constants. In addition, it provides many ways to uniquely profile the distribution of PAHs in the sample, including chromatograms at individual fluorescence wavelengths, chromatograms at integrated fluorescence wavelengths, chromatograms with fluorescence quenching of alternant PAHs by nitromethane, and chromatograms with fluorescence quenching of nonalternant PAHs by diisopropylamine. The results for each sample are discussed in detail in the following sections.

8.3.1 Standard (EPA 610)

A chromatogram of the standard (EPA 610) is shown in Figure 8.2A. The identity of each PAH was confirmed by comparison of the retention time and fluorescence spectrum with authentic standards [1,21]. Of the sixteen known

components in this sample, only eleven are fluorescent with excitation at 325 nm and emission at 350 – 564 nm. Several of the smaller PAHs, including naphthalene, acenaphthylene, acenaphthene, fluorene, and phenanthrene, are not excited efficiently by the helium-cadmium laser. The PAHs ranging from anthracene to benzo[*ghi*]perylene are readily detected in spite of the relatively small mass injected (2.4-4.8 ng). The fluorescence power of each PAH is a function of the concentration (Table 8.1), as well as the molar absorptivity and quantum efficiency at the selected wavelengths for excitation and emission. A chromatogram of the standard with fluorescence quenching by nitromethane is shown in Figure 8.2B. It is immediately evident that the nonalternant PAHs (fluoranthene, benzo[*b*]fluoranthene, benzo[*k*]fluoranthene, and indeno[1,2,3-*cd*]pyrene) substantially retain their original fluorescence power. In contrast, the alternant PAHs are significantly quenched. This observation is consistent with the previously reported Stern-Volmer constants of 0.07 and 0.64 M^{-1} for the representative nonalternant PAHs fluoranthene and benzo[*b*]fluoranthene, and 94 and 61 M^{-1} for the representative alternant PAHs pyrene and benzo[*a*]pyrene [17]. It is also noteworthy in Figure 8.1B that benzo[*k*]fluoranthene appears to be more highly quenched than the other nonalternant PAHs. This is consistent with differences in the electron-donating ability of the aromatic system to the nitromethane quencher [6,11]. The gas-phase ionization energy [22] of benzo[*k*]fluoranthene (8.167 eV) is substantially less than that of fluoranthene (8.466 eV) and benzo[*b*]fluoranthene (8.410 eV), which suggests that it is a better electron donor. It is, in fact, more similar to the alternant PAHs

Figure 8.2: Chromatogram of standard PAHs (EPA 610) without (A) and with fluorescence quenching by nitromethane (B) and diisopropylamine (C). Column: 1.5 m × 200 μm i.d. fused-silica capillary, packed with 5 μm Shandon Hypersil C18. Mobile phase: methanol, 1.0 μL/min, 24 °C, with post-column addition of (A) methanol, 1.0 μL/min, (B) 2% (v/v) nitromethane in methanol, 1.0 μL/min, (C) 50% (v/v) diisopropylamine in acetonitrile 1.0 μL/min. Laser-induced fluorescence detection: 325 nm excitation, 350–564 nm emission. Solutes: (1) anthracene, (2) fluoranthene, (3) pyrene, (4) benz[*a*]anthracene, (5) chrysene, (6) benzo[*b*]fluoranthene, (7) benzo[*k*]fluoranthene, (8) benzo[*a*]pyrene, (9) dibenz[*a,h*]anthracene, (10) indeno[1,2,3-*cd*]pyrene, (11) benzo[*ghi*]perylene.

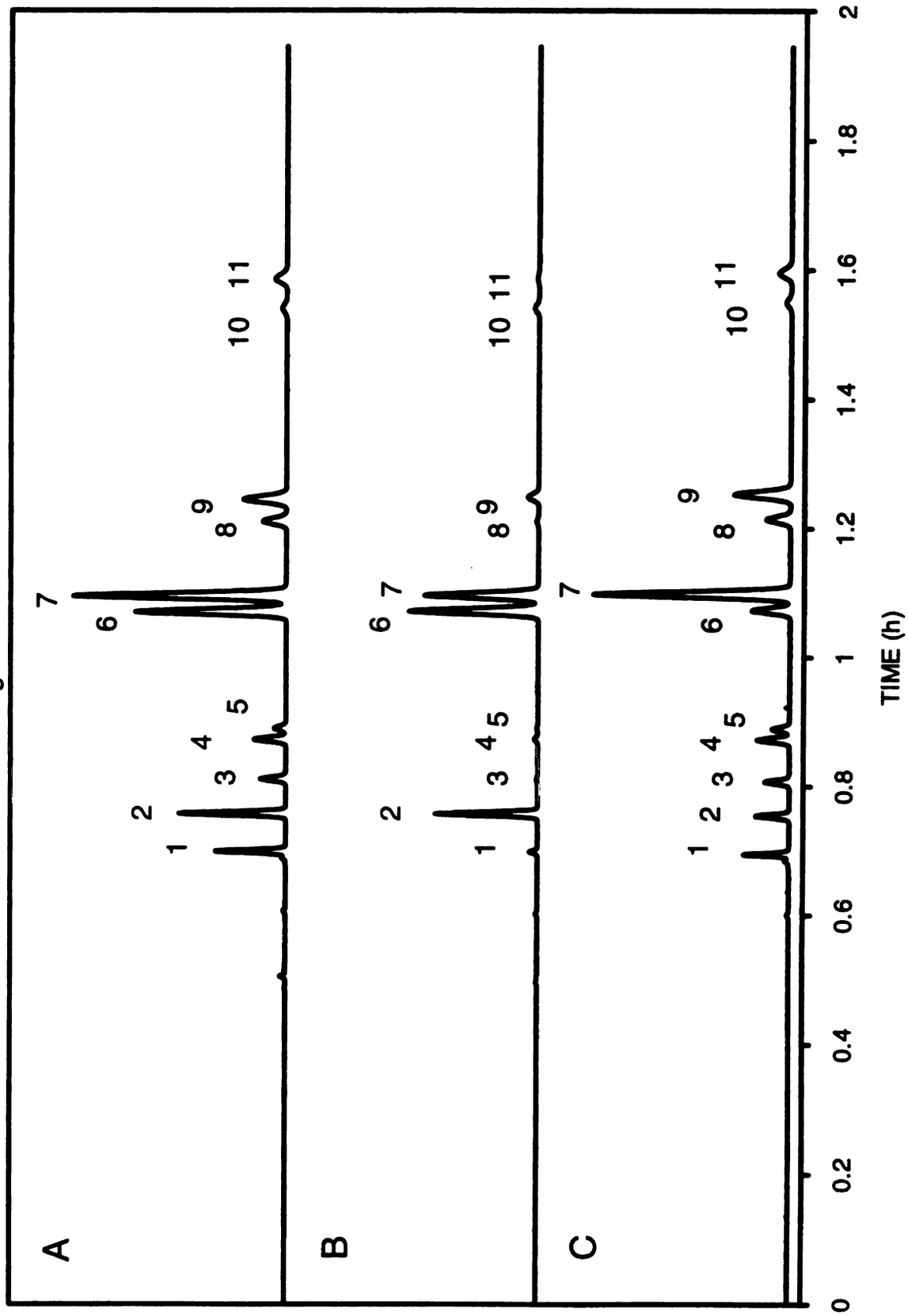

Figure 8.2

benz[*a*]anthracene (8.111 eV) and chrysene (8.261 eV). As a result, the fluorescence of benzo[k]fluoranthene is quenched better by nitromethane, than by diisopropylamine (vide infra).

A chromatogram of the standard with fluorescence quenching by diisopropylamine is shown in Figure 8.2C. In general, the nonalternant PAHs are moderately quenched and the alternant PAHs are unaffected. This observation is consistent with the previously reported Stern–Volmer constants of 17.1 and 21.2 M^{-1} for the representative nonalternant PAHs fluoranthene and benzo[*b*]fluoranthene, and 1.2 and 0.47 M^{-1} for the representative alternant PAHs pyrene and benzo[*a*]pyrene [12]. Benzo[*k*]fluoranthene is an interesting exception to this general trend, as it is relatively unquenched by diisopropylamine. Its behavior, again, is more similar to the alternant PAHs benz[*a*]anthracene and chrysene than to the other nonalternant PAHs fluoranthene and benzo[*b*]fluoranthene

8.3.2 Coal-Derived Fluid (SRM 1597)

A chromatogram of the coal-derived fluid (SRM 1597) is shown in Figure 8.3A. The identity of each PAH was again confirmed by comparison of the retention time and fluorescence spectrum with authentic standards [1,21]. The concentrations of the known PAHs are summarized in Table 8.1. In addition, there are a large number of unidentified PAHs that elute in the time range from 0.75 to 1.5 h. As the fluorescence spectra of many of these PAHs have vibrational fine structure similar to alternant PAHs, these may be methylated or other alkylated analogs. This is consistent with the combustion-related origin of

Figure 8.3: Chromatogram of PAHs in a coal-derived fluid (SRM 1597) without (A) and with fluorescence quenching by nitromethane (B) and diisopropylamine (C). Solutes: (12) unknown, possibly dibenzofluoranthene or naphthofluoranthene isomer, (13) dibenzo[*def,mno*]chrysene, (14) unknown, possibly dibenzofluoranthene or naphthofluoranthene isomer. Other experimental conditions and solutes as described in Figure 8.2.

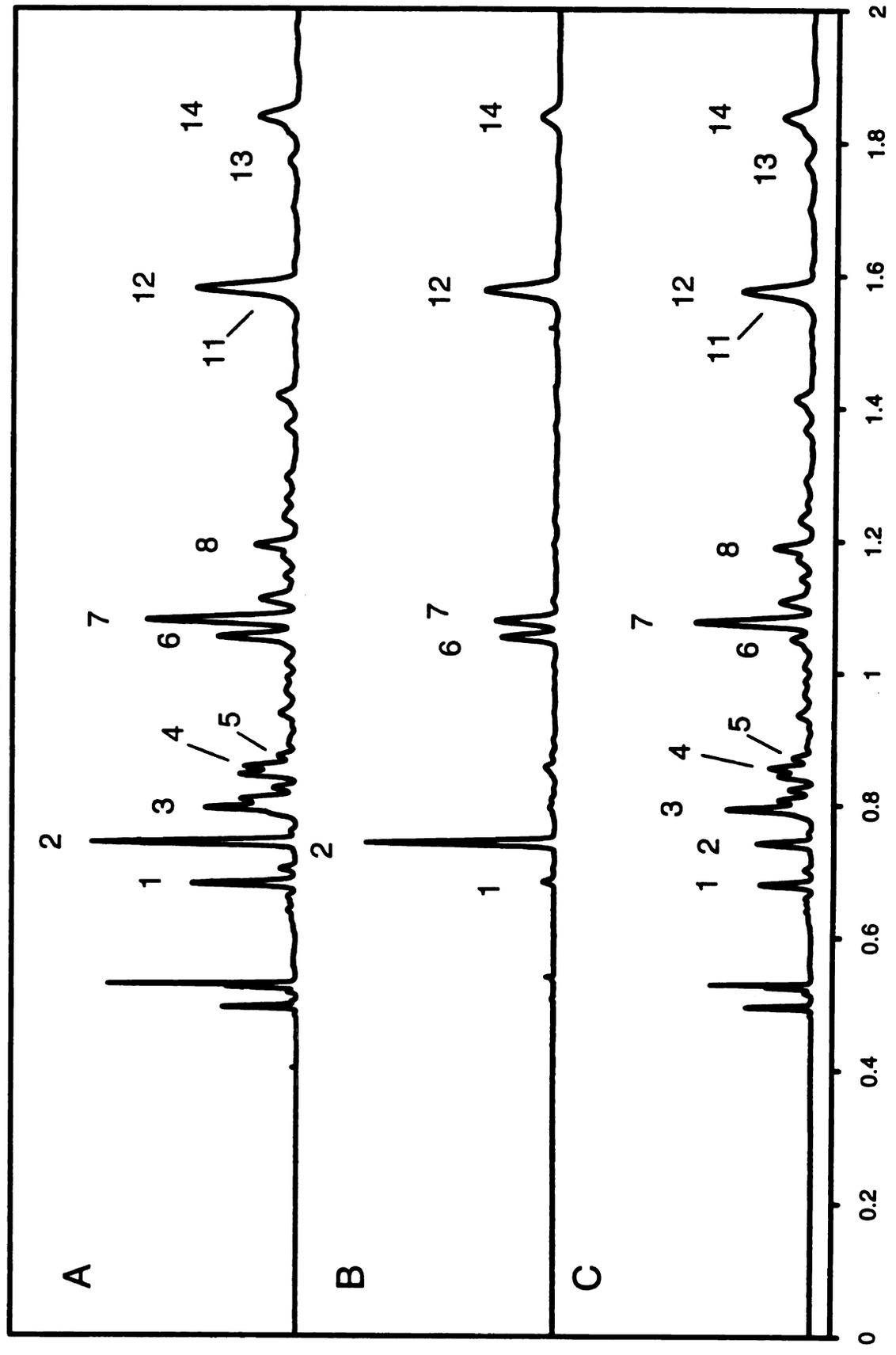

Figure 8.3

this sample and is supported by a prior detailed analysis by gas chromatography with mass spectrometric detection, which was able to identify many methylated PAH isomers [16]. There are two additional large peaks that can be observed between 1.5 and 2.0 h. On the basis of the fluorescence spectra and the prior analysis [16,23] these may be dibenzofluoranthene or naphthofluoranthene isomers. In addition, dibenzo[*def,mno*]chrysene (anthanthrene) can be identified unambiguously from the fluorescence spectrum [1].

A chromatogram of the coal-derived fluid with fluorescence quenching by nitromethane is shown in Figure 8.3B. All of the known nonalternant PAHs are relatively unaffected and the alternant PAHs are quenched in the same manner as for the standard sample in Figure 8.2B. The many unidentified PAHs are highly quenched by nitromethane, which is consistent with their tentative assignment as alkylated alternant isomers. Acree et al. [8,9] have reported that both alternant and nonalternant PAHs with alkyl substituents preserve the inherent quenching behavior of the parent PAHs. In addition, the fluorescence power of the two PAHs tentatively assigned as dibenzofluoranthene or naphthofluoranthene isomers is largely retained, as would be expected for nonalternant PAHs. However, the partial quenching by nitromethane indicates that these PAHs are more similar to benzo[*k*]fluoranthene, which has significant alternant character. This observation is in agreement with the previous results of Tucker and Acree [24] for selected naphthofluoranthenes. Finally, note that the qualitative and quantitative analysis for all of the alternant PAHs has been

substantially improved by fluorescence quenching with nitromethane in Figure 8.3B.

A chromatogram of the coal-derived fluid with fluorescence quenching by diisopropylamine is shown in Figure 8.3C. All of the known alternant PAHs are relatively unaffected and the nonalternant PAHs are quenched in the same manner as for the standard sample in Figure 8.2A. The unidentified PAHs that have been tentatively assigned as alkylated alternant isomers are not significantly quenched by diisopropylamine, as would be expected. The PAHs tentatively assigned as dibenzofluoranthene or naphthofluoranthene isomers are slightly quenched. Although this behavior is unexpected for nonalternant PAHs, it is fully consistent with the behavior of benzo[*k*]fluoranthene. Finally, because of the complexity of this sample with many alternant PAHs, the chromatogram is not greatly simplified by fluorescence quenching with diisopropylamine. However, some minor improvement in qualitative and quantitative analysis may be obtained.

8.3.3 Contaminated Soil (CRM104-100)

A chromatogram of the contaminated soil (CRM104-100) is shown in Figure 8.4A. The identity of each PAH was again confirmed by comparison of the retention time and fluorescence spectrum with authentic standards [1,21]. The concentrations of the known PAHs are summarized in Table 8.1. Like the coal-derived fluid, this sample has numerous PAHs in the time range of 0.75 to 1.5 h that appear to be alkylated alternant isomers. Moreover, the PAHs that

Figure 8.4: Chromatogram of PAHs in a contaminated soil (CRM104-100) without (A) and with fluorescence quenching by nitromethane (B) and diisopropylamine (C). Other experimental conditions and solutes as described in Figures 8.2 and 8.3

Figure 8.4

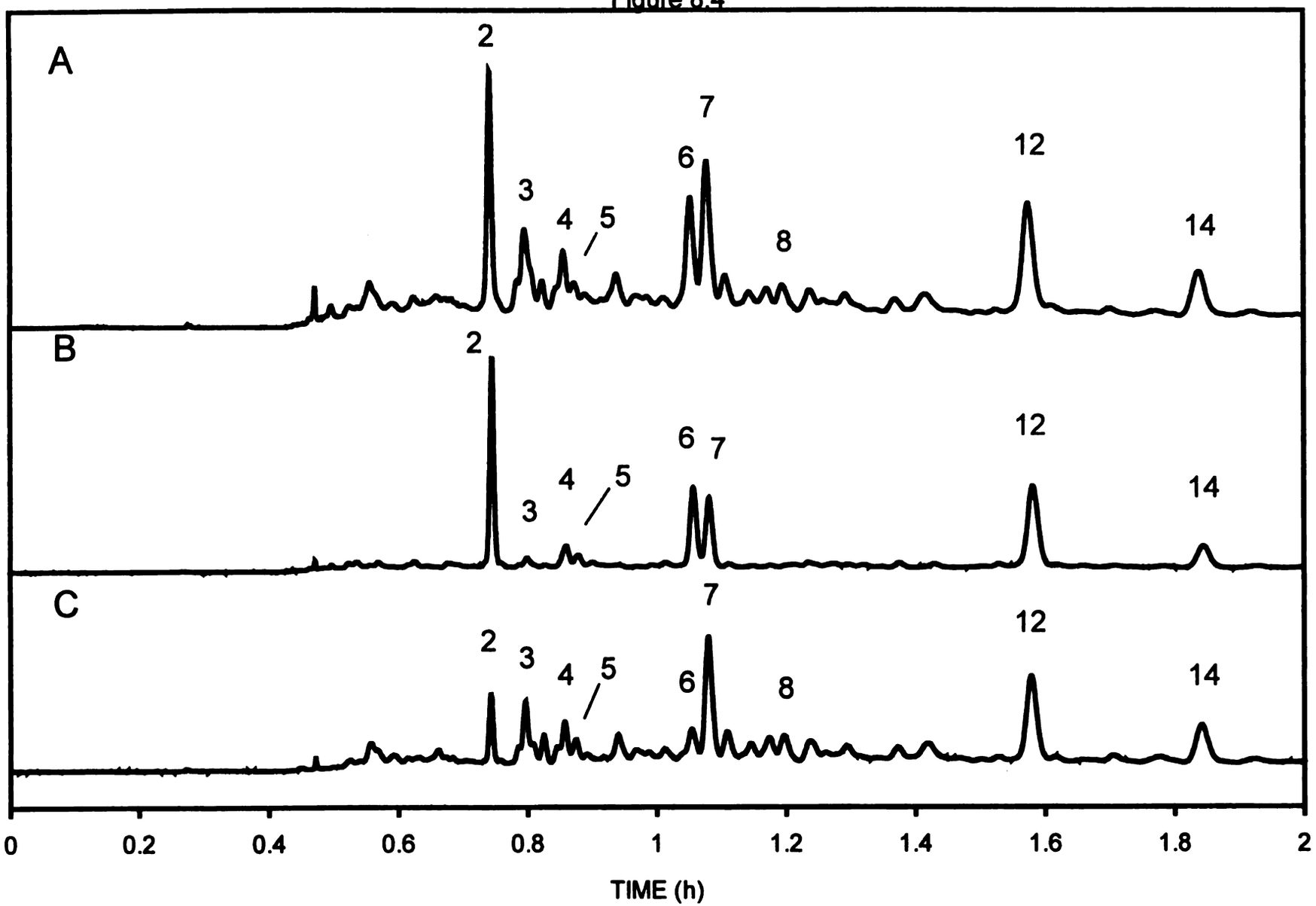

have been tentatively identified as dibenzofluoranthene or naphthofluoranthene isomers are also present.

Chromatograms of the contaminated soil with fluorescence quenching by nitromethane and diisopropylamine are shown in Figures 8.4B and 8.4C, respectively. The alternant and nonalternant PAHs are quenched in the expected manner, as described above for the standard and coal-derived fluid.

8.3.4 Statistical Correlation Analysis

In order to demonstrate the utility of fluorescence and fluorescence quenching for profiling PAHs in environmental samples, the chromatograms were correlated by using the product–moment method [19,20]. The complete chromatograms were correlated, point by point, which provides a more detailed comparison than the use of peak maxima or peak areas alone. The correlation graphs for three representative cases are shown in Figure 8.5. When samples are derived from exactly the same origin, the relative fluorescence power or concentration of PAHs in each sample is identical. The resulting scatter plot (Figure 8.5A) shows a high degree of correlation. Accordingly, the correlation coefficients (r) for identical or replicate samples are typically 0.99 or higher. When samples are of similar or related origin, many of the same PAHs may be present but at different concentrations. This results in an intermediate degree of correlation (Figure 8.5B), with typical values of r in the range of 0.90 to 0.50. Finally when samples are of distinctly unrelated origin, the disparate distribution of PAHs will result in little or no correlation (Figure 8.5C), with typical values of r less than 0.50. In all cases, valid conclusions can be drawn about the identity or

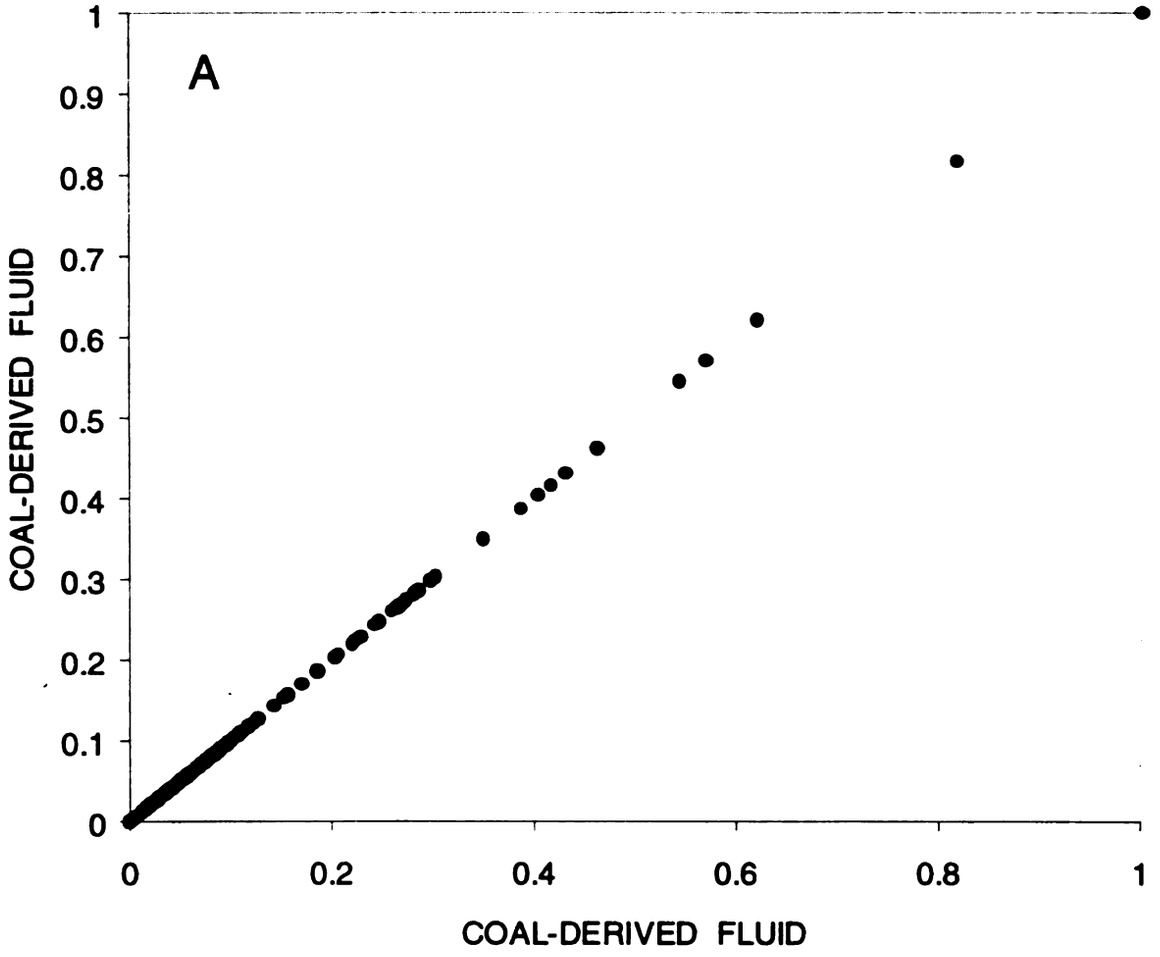

Figure 8.5A: Scatter plot demonstrating three differing degrees of product–moment correlation. (A) Coal-derived fluid (Figure 8.3A) *versus* coal-derived fluid (Figure 8.3A), r = 1.000, P = 0.00×10^{-4930}

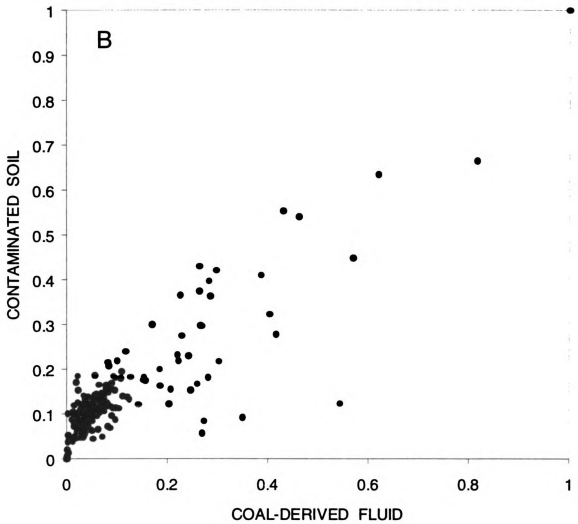

Figure 8.5B: Scatter plot demonstrating three differing degrees of product–moment correlation. (B) Contaminated soil (Figure 8.4A) versus coal-derived fluid (Figure 8.3A), $r = 0.877$, $P = 2.83 \times 10^{-113}$

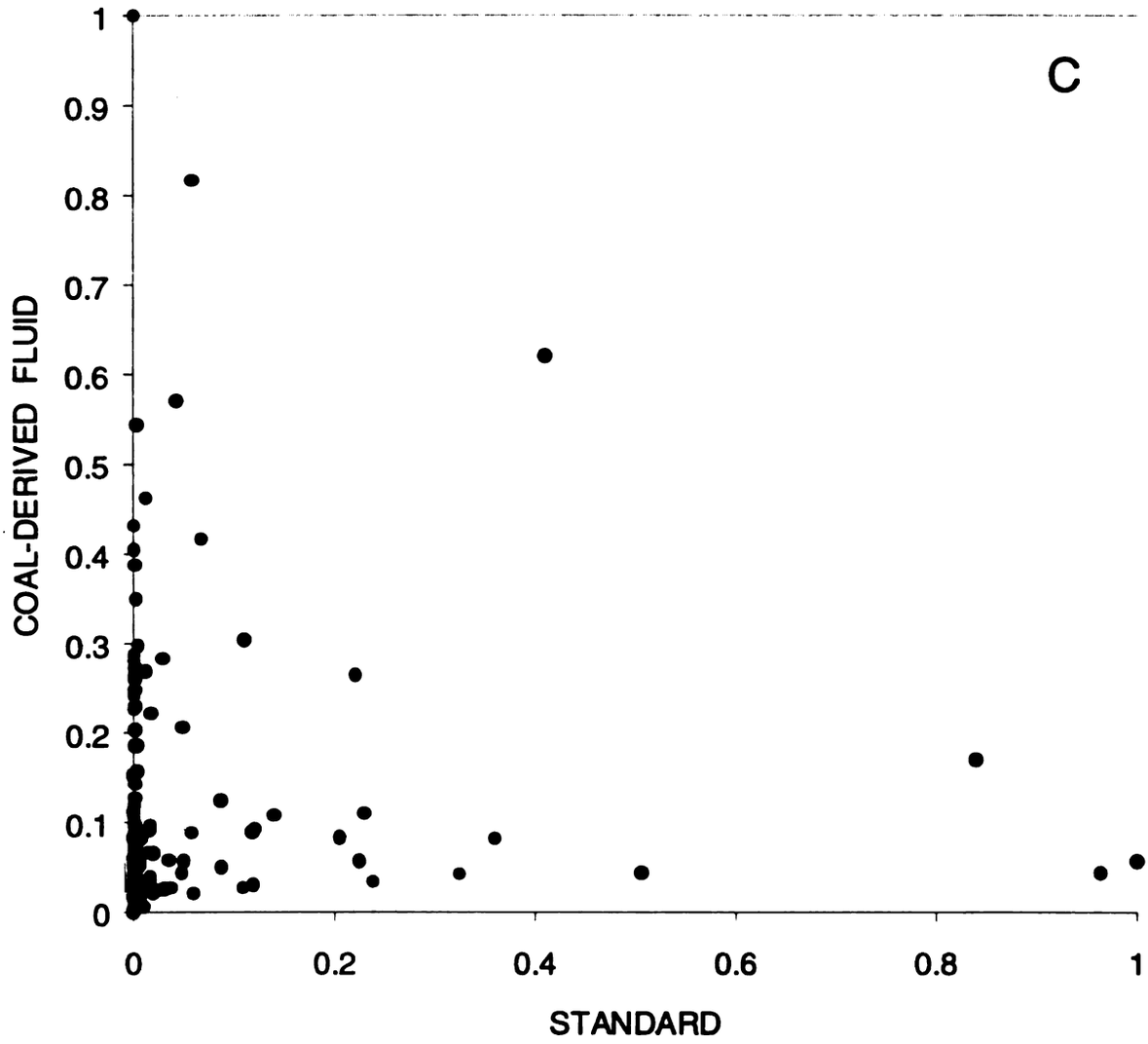

Figure 8.5C: Scatter plot demonstrating three differing degrees of product–moment correlation. (C) Coal-derived fluid (Figure 8.3A) versus standard (Figure 8.2A), r = 0.120, P = 0.0241

Table 8.2: Correlation coefficient (r) of the product–moment method for chromatograms obtained by using laser-induced fluorescence detection.

SAMPLE	Standard EPA 610	Coal-Derived Fluid SRM 1597	Contaminated Soil CRM104-100
Standard EPA 610	1.000	0.120	0.214
Coal-Derived Fluid SRM 1597	0.120	1.000	0.877
Contaminated Soil CRM104-100	0.214	0.877	1.000

Table 8.3: Correlation coefficient (r) of the product–moment method for chromatograms obtained by using laser-induced fluorescence detection with quenching by nitromethane.

SAMPLE	Standard EPA 610	Coal-Derived Fluid SRM 1597	Contaminated Soil CRM104-100
Standard EPA 610	1.000	0.111	0.144
Coal-Derived Fluid SRM 1597	0.111	1.000	0.977
Contaminated Soil CRM104-100	0.144	0.977	1.000

Table 8.4: Correlation coefficient (r) of the product–moment method for chromatograms obtained by using laser-induced fluorescence detection with quenching by diisopropylamine.

SAMPLE	Standard EPA 610	Coal-Derived Fluid SRM 1597	Contaminated Soil CRM104-100
Standard EPA 610	1.000	0.104	0.146
Coal-Derived Fluid SRM 1597	0.104	1.000	0.884
Contaminated Soil CRM104-100	0.146	0.884	1.000

origin of the samples when the P-value for the product moment correlation is less than 0.05 (95% C.L.). Table 8.2 summarizes the results of the product moment correlation for the three samples examined with fluorescence detection alone. It is apparent that there is little correlation between the standard and the coal-derived fluid or contaminated soil, despite the common PAHs found in each sample. As many of the PAHs in the more complex samples are not found in the standard sample, these samples present the unique challenge of profiling with limited information. This correlation method is well suited for such an analysis since no a prior information about the samples is necessary, allowing for specialists and non-specialists to employ the technique. The coal-derived fluid and contaminated soil show an intermediate degree of correlation ($r = 0.877$), which is consistent with their combustion-related origin and the similar appearance of their chromatograms in Figures 8.3A and 8.4A.

This approach for PAH profiling becomes even more versatile and powerful when combined with selective fluorescence quenching. The results of the product moment correlation for the three samples with fluorescence quenching by nitromethane are summarized in Table 8.3. As the alternant PAHs are selectively quenched, this correlation discriminates on the basis of the distribution of nonalternant PAHs in the samples. When viewed on this basis, the standard is still distinctly different from the coal-derived fluid or contaminated soil. However because of their common combustion-related origin [16], the coal-derived fluid and contaminated soil are highly correlated in nonalternant character ($r = 0.977$). The results of the product–moment correlation with

fluorescence quenching by diisopropylamine are summarized in Table 8.4. These results confirm that the dissimilarities between the coal-derived fluid and the contaminated soil lie in the distribution of alternant PAH isomers ($r = 0.884$). This approach has been successfully applied to a variety of other petroleum-based samples, including gasoline, motor oils, petrolatum jellies, etc. [25].

8.4 Conclusions

In summary, fluorescence and selective fluorescence quenching appear to provide complementary information for profiling PAHs in complex samples. The single wavelength or total fluorescence emission offers broad-based information about the PAH distribution. In contrast, fluorescence quenching by nitromethane allows selective discrimination of the nonalternant PAHs and quenching by diisopropylamine allows selective discrimination of the alternant PAHs. Only when all of these profiles indicate a high degree of correlation can it be confidently concluded that two environmental samples are of the same origin.

8.5 References

[1] W. Karcher, R.J. Fordham, J.J. Dubois, P.G.J.M. Glaude, J.A.M. Ligthart, Spectral Atlas of Polycyclic Aromatic Hydrocarbons, Reidel Publishing, Boston, MA, USA, 1985.

[2] J. Malkin, Photophysical and Photochemical Properties of Aromatic Compounds, CRC Press, Boca Raton, FL, USA, 1992.

[3] R. Badley, Fluorescence Spectroscopy, Plenum Press, New York, NY, USA, 1983.

[4] J.R. Lakowicz, Principles of Fluorescence Spectroscopy, Plenum Press, New York, NY, USA, 1983.

[5] V.L. McGuffin, J.V. Goodpaster, in R.A. Meyers (Editor), Encyclopedia of Environmental Analysis and Remediation, Wiley, New York, NY, USA, 1998, p. 3815-3831.

[6] S.-H. Chen, C.E. Evans, V.L. McGuffin, Anal. Chim. Acta 246 (1991) 65-74.

[7] E. Sawicki, T.W. Stanley, W.C. Elbert, Talanta 11 (1964) 1431-1439.

[8] S.A. Tucker, J.M. Griffin, W.E. Acree, Jr., J.C. Fetzer, M. Zander, O. Reiser, A. De Meijere, I. Murata, Polycyclic Aromat. Compd. 4 (1994) 141-161.

[9] S.A. Tucker, J.M. Griffin, W.E. Acree, Jr., M.J. Tanga, J.E. Bupp, T.K. Tochimoto, J. Lugtenburg, K. Van Haeringer, J. Cornelisse, P.C. Cheng, L.T. Scott, Polycyclic Aromat. Compd. 4 (1994) 161-172.

[10] W.E. Acree, Jr., S. Pandey, S.A. Tucker, J.C. Fetzer, Polycyclic Aromat. Compd. 12 (1997) 71-123.

[11] F.K. Ogasawara, Y. Wang, V.L. McGuffin, Appl. Spectrosc. 49 (1997) 1-7.

[12] J.V. Goodpaster, V.L. McGuffin, Anal. Chem. 72 (2000) 1072-1077.

[13] D. Broman, A. Colmsjö, B. Ganning, C. Näf, Y. Zebuhr, Environ. Sci. Technol. 22 (1988) 1219-1228.

[14] T. Vo-Dinh, Chemical Analysis of Polycyclic Aromatic Hydrocarbons, Wiley, New York, NY, USA, 1989.

[15] L. Nondek, M. Kuzliek, S. Krupicka, Chromatographia 37 (1993) 381-386.

[16] S.A. Wise, B.A. Benner, G.D. Byrd, S.N. Chesler, R.E. Rebbert, M.N. Schantz, Anal. Chem. 60 (1988) 887-894.

[17] J.V. Goodpaster, V.L. McGuffin, Appl. Spectrosc. 53 (1999) 1000-1008.

[18] J.C. Gluckman, A. Hirose, V.L. McGuffin, M. Novotny, Chromatographia 17 (1983) 303-309.

[19] J.L. Devore, Probability and Statistics for Engineering and the Sciences, 4th ed., Duxbury Press, Pacific Grove, CA, USA, 1995.

[20] R.M. Thorndike, Correlational Procedures for Research, Gardner Press, New York, NY, USA, 1978.

[21] L.C. Sander, S.A. Wise, J. High Resolut. Chromatogr. 8 (1985) 248-255.

[22] R.A. Hites, W.J. Simonsick, Calculated Molecular Properties of Polycyclic Aromatic Hydrocarbons, Elsevier, Amsterdam, The Netherlands, 1987.

[23] S.A. Wise, B.A. Benner, H. Liu, G.D. Byrd, A. Colmsjö, Anal. Chem. 60 (1988) 630-637.

[24] S.A. Tucker, W.E. Acree, Jr., Appl. Spectrosc. 46 (1992) 1388-1392.

[25] J.V. Goodpaster, S.B. Howerton, V.L. McGuffin, J. Forensic Sci. 46 (2001) 1358-1371.

Chapter 9: Conclusions and Future Directions

Over the past fifty years, liquid chromatography has been characterized via theoretical treatments, as well as empirical measurements. However, the molecular contributions to retention have been limited primarily to investigations of the molar enthalpy associated with retention. Virtually no experimentation has sought to characterize the change in molar volume. The change in molar volume is important because it provides insight into how molecules interact with the stationary phase. In addition to the molar volume, the kinetics of retention have also been largely overlooked. Although some investigators have sought to probe the kinetics of retention, the only author to publish extensively on the subject has been Guiochon. The kinetics of retention are important because they provide insight into the rate at which transitions occur, as well as the energy barriers that exist for a molecule to move from one phase to another. By quantitating both the thermodynamics and kinetics together, a better description of retention is possible, providing for a more accurate comparison of solutes and stationary phases to one another.

The research presented in this dissertation has attempted to overcome some of the past theoretical and experimental difficulties by studying the retention event in situ. Through the use of newly adapted mathematical analysis and experimental design, solute transfer in reversed-phased liquid chromatography has been studied as a function of several molecular variables for a series of polycyclic aromatic hydrocarbons and their nitrogenous derivatives.

9.1 Experimental Design and Theoretical Development

Chapters 2 and 3 detail the experimental design and the choice of mathematical functions necessary to study retention in reversed-phase liquid chromatography. The use of on-column detection at multiple locations allows measurements to be made in situ. Measurements made in this manner allow for the thermodynamics and kinetics to be studied without the error that arises from extra column effects.

As demonstrated in Chapter 3, the extraction of the peak profiles from the chromatogram can contribute to error during the fitting process. From the simulation studies, statistical moment analysis was shown to be more sensitive to the integration interval, number of points, and the noise when compared to the exponentially modified Gaussian (EMG) equation.

The most pressing limitation in the analysis of peak profiles is the lack of a multiple site model. In order for materials that have multiple retention sites to be characterized, a more robust mathematical model is necessary to distinguish one site from another. As illustrated in Chapter 5, the current form of a bi-exponentially modified Gaussian equation provides for an inadequate analysis of a two-site system. The primary cause for this limitation is the implicit assumption that the sites are equal in number. As shown, there is no weighting factor for the relative number of sites. As a result, the software used to fit the peak profiles fails to distinguish different exponential contributions. This failure manifests as an underflow or overflow error and ultimately leads to rate constants that are the same for both sites.

A user-defined function that convolutes the requisite functions in either Fourier or Laplacian space would be a straightforward method to circumvent this problem since current software relies completely on algebraic notation. Barring this approach, a second method to improve the analysis of multiple site data would be the development of a completely new mathematical function from first principles. Taking into account both the distribution of the sites (i.e. relative abundance) as well as the physical characteristics of these sites (i.e. energies of interaction, diffusion coefficients, etc.) could provide an improvement over the currently derived function.

9.2 Retention in Octadecylsilica

Chapters 4 through 6 detail the thermodynamics and kinetics of a series of polycyclic aromatic hydrocarbons (PAHs) and nitrogen containing PAHs (NPAHs) in monomeric and polymeric octadecylsilica (ODS) using methanol and acetonitrile mobile phases. As shown, the ring number, annelation, and planarity of the solutes influences the thermodynamic and kinetic values. In addition, the inclusion of a nitrogen into the PAH backbone allows for adsorption on the underlying support. These adsorptive contributions are exacerbated in acetonitrile, an aprotic mobile phase. The rate constants for four NPAHS are smaller by two to four orders of magnitude in acetonitrile than in methanol. In addition, the bonding density of the stationary phase was shown to alter the thermodynamics and kinetics of retention. As illustrated, polymeric ODS (5.4 $\mu mol/m^2$) causes the retention factors to increase up to a factor of six, relative to monomeric ODS (2.7 $\mu mol/m^2$). In addition, the changes in molar enthalpy and

volume are more negative for the planar PAHs in the polymeric ODS. Thus, these studies demonstrate how the solute structure, mobile phase, and stationary phase affect both the thermodynamics and kinetics of retention.

In order for a complete and quantitative description of retention to be presented, a series of experiments beyond those presented herein is still necessary. The first experiment should evaluate the effect of mobile phase velocity on the thermodynamics and kinetics of retention. Except in the case of the NPAHs, an implicit assumption in this dissertation is that a single kinetic site contributes to the tailing of peak profiles. When the kinetic events are slow, relative to the separation time, they contribute to asymmetric tailing. By systematically altering the velocity, and observing how the asymmetry changes, the assumption of a single kinetic site could be directly tested. If the rate constants change as a function of velocity, then the system likely contains multiple kinetics site, of which a limited number have been probed.

A second series of experiments that could lead to a more comprehensive explanation of retention would be a systematic study of the effect of mobile phase composition on the derived values. Methanol was used for the majority of experiments, but as demonstrated in Chapter 6, acetonitrile has a dramatic effect on the retention of the NPAHs. A series of alcohols with varying chain length could be used to make comparisons between mobile phases and study their effect on the stationary phase.

Similar to varying the mobile phase, a series of stationary phases could be used to study the effect of chain length, synthetic method, and polarity on the

derived parameters. While preliminary work by Berendsen and de Galan used a series of materials for a similar study [1], they focused on alkylated homologues as probes of a partition mechanism. A study with the NPAHs using the varying chain lengths for the alkyl-silica bonded phases could provide information about the depth to which these solutes penetrate. Such an investigation would help to identify the minimum length necessary to minimize adsorptive interactions for commercial separations.

In addition to changing the mobile or stationary phase, modifications to the instrument could also be undertaken. Such modifications would allow the retention event to be probed on an even finer scale. For example, the addition of near field optics or surface plasmon resonance could allow molecules to be studied as they interact with the surface. Such measurements would likely require the use of smaller grafted chains than octadecylsilica given the distance limitations of these techniques. In addition, an on-line Raman system could supplement the current fluorescence systems and expand upon the investigations conducted by Pemberton and co-workers [2-5].

9.3 Retention in Soil

. The study of pollutants, such as PAHs, in the environment is important since it can lead to better models for risk assessment. The goal of using soil as a stationary phase was to test whether current theories of retention are accurate, and to gather enough data to present a first approximation of the molecular parameters that lead to solute transport.

As shown in Chapter 7, the retention of two PAHs suggests that a partition mechanism is present in soil. However, the experiments were carried out in pure methanol with large concentrations (~10^{-3} M). These concentrations are well above what would be found in an aqueous environment and may not represent retention in a real world environment.

In addition, the data for the nitroalkanes supports the presence of a partition mechanism. However, the data for the nitroalkanes and the alkylbenzenes also indicate the presence of an exclusion mechanism. The data demonstrate that over the range of tested mobile phases the exclusion mechanism predominates. Although the systems could not be characterized in the same manner as the octadecylsilica phase, the data do provide a first glimpse into the molecular retention of these solutes in soil, demonstrating a difference in mechanism relative to synthetic phases.

The most promising direction for this research into soil retention would be an improvement in the sieving and packing method for capillary columns. Since many experimental difficulties arose from the heterogeneous nature of the soil, isolating a fraction with a smaller size distribution would allow columns to be more uniformly packed. For this improvement to be seen, though, swelling materials such as clays would need to be removed or controlled to prevent blockage of the quartz wool frit. However, the removal of the clay could significantly alter the retention characteristics and thus may need to be carefully analyzed through a more exhaustive series of batch isotherms.

A second approach to study retention in natural materials is to synthesize a stationary phase that mimics soil, but is not hindered by the heterogeneous size distribution. One approach that has been used involves tethering Aldrich humic acid to silica supports [6]. However, this material is still far from representative of most soils and may not yield information about younger soils. A more reasonable approach would be to tether natural humic and fulvic acids to silica supports. However, this method fails to truly represent the complex chemical nature of soil, and once again provides only a limited amount of information.

Perhaps the best method of synthesis would be to use organisms that contribute to the decomposition of animal and plant matter (i.e. white rot fungi). These organisms could be used to process mixtures of lipids, amino acids, and other naturally occurring materials. Using such mixtures as a food source, the by-products of degradation could be isolated and tethered to chromatographic supports, resulting in a material that is better than a truly synthetic phase, but easier to manipulate than soil. However, the reproducible synthesis and purification of such materials would be challenging. If identification of the materials were important before chemical immobilization, such a process would be laborious requiring significant mass spectral analysis.

9.4 Selective Fluorescence Quenching

A final use of capillary chromatography for environmentally relevant samples is the development of selective fluorescence quenching detection. As demonstrated in Chapter 8, qualitative information can be gathered about

unknown samples that contain PAHs based upon the choice of the quencher. As shown, several environmental samples were differentiated using post-column addition of the quencher with Pearson product moment correlation. The resulting data demonstrate how this method can be used to compare samples for similarities and differences. Such qualitative comparisons could help in identifying the source of a given mixture.

This method could be adapted to aid in the identification of solutes that are important to security experts (i.e. explosives, chemical weapons). In order to apply this technique to these solutes, though, selective quenchers would have be identified and characterized. To date, no reports of selective quenchers for pesticides or chemical weapons have been published. However, work by Goodpaster and McGuffin have investigated nitrated explosives for indirect detection [7].

9.5 References

[1] G.E. Berendsen, L. de Galan, J. Chromatogr. 196 (1980) 21-37.

[2] M.W. Ducey, Jr., C.J. Orendorff, J.E. Pemberton, L.C. Sander, Anal. Chem. 74 (2002) 5576-5584.

[3] M.W. Ducey, Jr., C.J. Orendorff, J.E. Pemberton, L.C. Sander, Anal. Chem. 74 (2002) 5585-5592.

[4] C.J. Orendorff, M.W. Ducey, Jr., J.E. Pemberton, L.C. Sander, Anal. Chem. 75 (2003) 3028-3036.

[5] C.J. Orendorff, M.W. Ducey, Jr., J.E. Pemberton, L.C. Sander, Anal. Chem. 75 (2003) 3037-3043.

[6] L.K. Koopal, Y. Yang, A.J. Minnaard, P.L.M. Theunissen, van Riemsdjik, W.H., Colloids Surf. A 141 (1998) 385-395.

[7] J.V. Goodpaster, V.L. McGuffin, Anal. Chem. 73 (2001) 2004-2011.